[American Journal of Science, Vol. 309, May, 2009, P. 333–396, DOI 10.2475/05.2009.01]

American Journal of Science

MAY 2009

EOCENE ARC-CONTINENT COLLISION AND CRUSTAL CONSOLIDATION IN KAMCHATKA, RUSSIAN FAR EAST

JEREMY K. HOURIGAN*†, MARK T. BRANDON**, ALEXEI V. SOLOVIEV***, ALEXEI B. KIRMASOV§, JOHN I. GARVER§§, JAMES STEVENSON**, and PETER W. REINERS§§§

ABSTRACT. The age and origin of high-grade metamorphic rocks of the Sredinnyi Range, Kamchatka have been the subject of a long and controversial debate. Based on geochronologic data and its association with a collage of accreted oceanic terranes, leading interpretations argue that the Sredinnyi Range metamorphic rocks represent an accreted Precambrian or Mesozoic microcontinent. In this contribution, we present new data that indicate that these metamorphic rocks were formed from the Cretaceous-Paleocene sedimentary margin of northeast Russia when it was overridden during Eocene obduction of the Olyutorsky arc, a far-travelled oceanic island arc. Our data include new mapping and structural observations along the northern and eastern flanks of the Sredinnyi Range, and SHRIMP zircon and monazite U-Th-Pb age data from 15 key samples. These new isotopic data demonstrate that paragneissic units were formed from sediments with depositional ages locally no older than Late Cretaceous to Paleocene. Furthermore, the statistical similarity of zircon U-Pb grain-ages from the Kamchatka Schist with very low-grade turbidite sandstones of the Ukelayat and Khozgon Groups indicate that metasediments of the Sredinnyi Range are upgraded stratigraphic equivalents of northeast Russian marginal strata. SHRIMP U-Pb ages of zircon overgrowths and metamorphic monazite extracted from migmatite and gneiss indicate that peak metamorphism occurred at 52 Ma, which is synchronous with the onset of the Olyutorsky arc-continent collision. Heating and cooling occurred rapidly, at rates approaching 80°C/m.y. Rapid heating is attributed to syn-collisional, subduction-related magmatism. Thermochronology and structural observations indicate that exhumation was due to a combination of ductile and brittle thinning of the crust. We speculate that this thinning was caused by diapiric ascent of a low-density low-viscosity continental material beneath a dense structural lid of the obducted island arc.

INTRODUCTION

The early Cenozoic collision of the Olyutorsky Island Arc (fig. 1) with the northeast Asian continental margin was coincident with a fundamental reorganization along the northern circum-Pacific margin that included the formation of back-arc basins and inception of island arc magmatism in the Aleutian Islands. Work over the past two decades has substantially refined the timing and kinematics of this arc-continent collision event, but the origin, age and tectonic setting of high-grade metamorphic rocks exposed within the collision zone are still vigorously debated.

* Department of Earth and Planetary Sciences, University of California, Santa Cruz, 1156 High Street, Santa Cruz, California, 95064, U.S.A.
** Geology and Geophysics, Yale University, P.O. Box 208109, New Haven, Connecticut, 06520-8109, U.S.A.
*** Geological Institute, Russian Academy of Sciences, Pyzhevski per. 7, Moscow, 119017, Russia
§ Geological Department, Moscow State University, Vorob'evy Gory, Moscow, 119992 Russia
§§ Department of Geology, Olin Center, Union College, Schenectady, New York, 12308-2311 U.S.A.
§§§ Department of Geosciences, University of Arizona, Tucson, Arizona, 85721 U.S.A.
† Corresponding author: hourigan@ucsc.edu

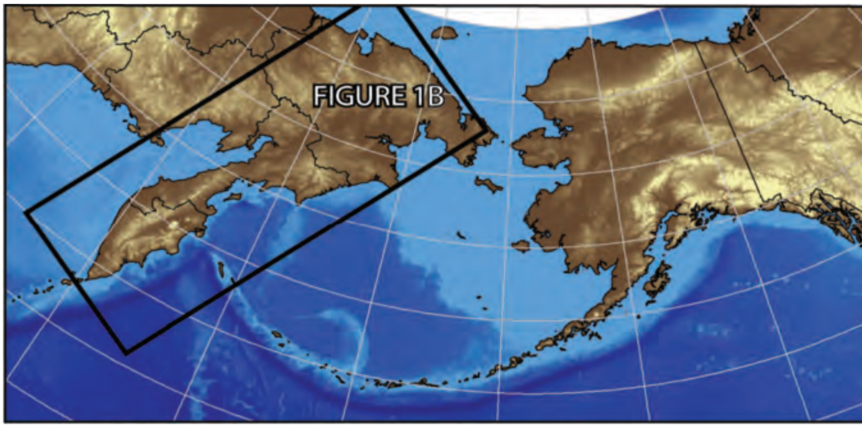

Fig. 1.(A) Index map. Shows the location of the geologic map area in figure 1B.

These questions are of fundamental importance for resolving the tectonic evolution of northeast Asia and also for understanding processes of continental growth at convergent margins.

The Sredinnyi Range (fig. 1), comprising high-grade gneiss and migmatite, is commonly referred to as the "metamorphic backbone" of the Kamchatka Peninsula (*Sredinnyi* is the Russian word for *middle,* as in Middle Range). Elsewhere, Kamchatka is principally made up of sedimentary and volcanic rocks of oceanic and island-arc affinity, which have experienced only limited metamorphism (Zonenshain and others, 1990; Geist and others, 1994). Based on its structural position within these low-grade terranes, the high-grade rocks of Sredinnyi Range have long been considered to be a Precambrian or Mesozoic microcontinent that was accreted onto the northeast Asian margin in Late Cretaceous or early Cenozoic time. This microcontinental interpretation figures prominently in nearly all models for the tectonic evolution of the northwest Pacific margin. Both of the two general forms of microntinental block model described in the literature require that the crust of the Sredinnyi Range was consolidated prior to accretion and thus heavily rely on extant geochronology data that indicate Mesozoic or older metamorphic and protolith ages. The primary differences in the models result from disparate interpretations of the composition, age and origin of the Okhotsk Sea basement.

The "Okhotomorsk" model postulates that the Sredinnyi Range is the exhumed eastern edge of a larger microcontinent that underlies most of the Sea of Okhotsk (see reviews in, Burk and Gnibidenko, 1977; Parfenov and Natal'in, 1977; Gnibidenko and Khvedchuk, 1982; Parfenov, 1984; Jolivet and others, 1988; Zonenshain and others, 1990; Sengor and Natalin, 1996; Nokleberg and others, 1998; Konstantinovskaia, 2000, 2001, 2002). The cessation of Andean-style subduction-related magmatism in the Okhotsk-Chukotka Volcanic Belt (fig. 1) is linked to the collision of this block with the northeast Russian margin in the Late Cretaceous (for example, Parfenov and Natal'in, 1977; Sengor and Natalin, 1996). In this model, exhumation of the Sredinnyi Range is attributed to basement-involved thrusting within the Olyutorsky island arc collision zone (Konstantinovskaia, 2000, 2001, 2002).

The alternative "Sredinnyi microcontinent" model grew out of the interpretation that the Sea of Okhotsk is underlain by an oceanic plateau that collided with northeastern Russia in the Late Cretaceous (Watson and Fujita, 1985; Bogdanov and Chekhovich, 2002; Bogdanov and Dobretsov, 2002). In this scenario, the Sredinnyi

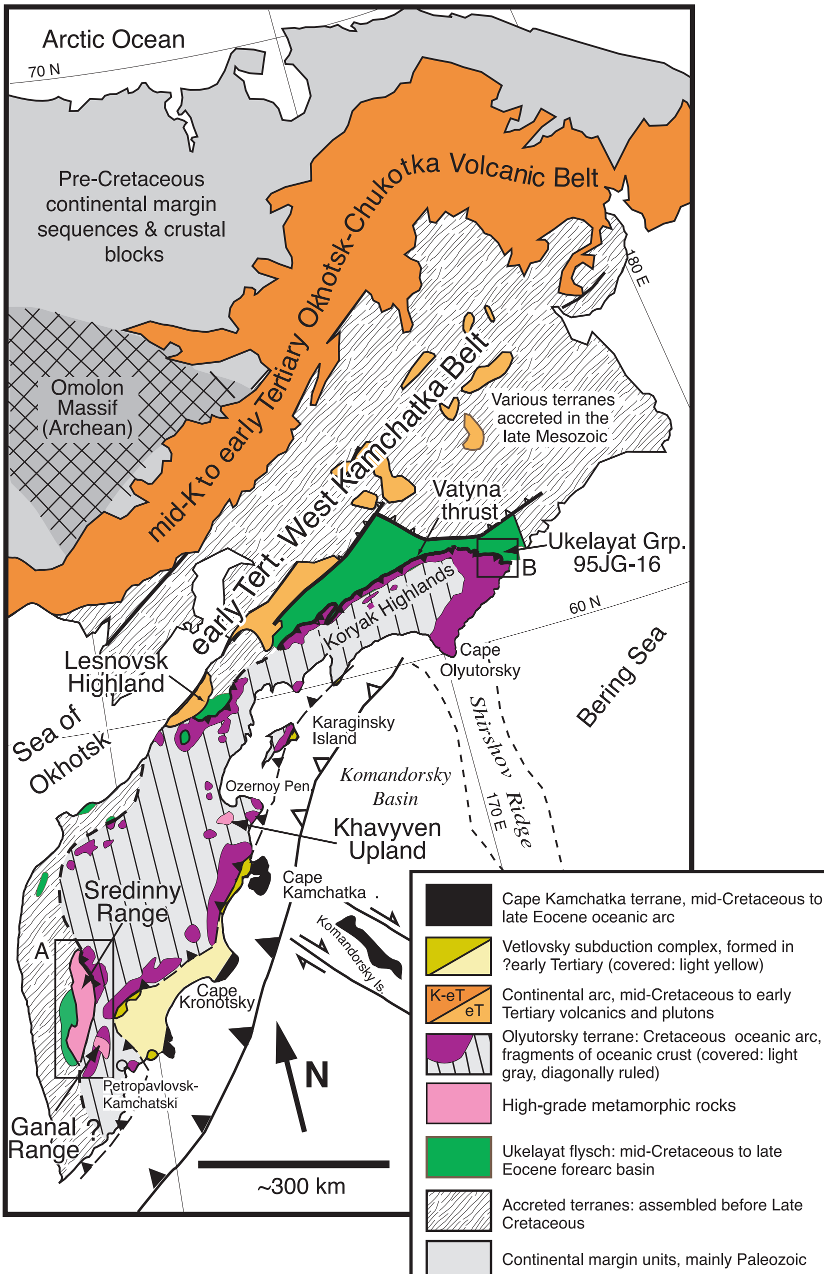

Fig. 1.(B) Generalized tectonic map of the Kamchatka Peninsula and Koryak Highlands. Medium to high-grade metamorphic rocks crop out in the Sredinnyi, Ganal, and Khavyven Ranges (Tilman and Bogdanov, 1992; Shapiro, 1995). The Sredinnyi Complex is exposed as domal uplift within a tectonic window into the lower plate beneath regionally extensive Olyutorsky or Achaivayam-Valagin arc thrust sheet. Boxes show: (A) Area of detailed map of the Sredinnyi Range (fig. 2) and (B) 1995 field area and sampling region for Ukelayat Group detrital zircon sample (95JG-16).

Range metamorphic rocks are a distinct far-travelled microcontinental terrane that was accreted during the early Cenozoic, along the outboard margin of the postulated Okhotsk oceanic plateau.

A common feature of the microcontinent models is that the crust of the Sredinny Range was consolidated *before* the Eocene arc-continent collision event. Prior to the availability of modern geochronologic techniques, high-grade gneisses were often assumed to result from multiple cycles of geosyncline development and thus be Precambrian basement (Marchenko, 1975; German, 1978; Khanchuk, 1985). Initial geochronologic efforts in the region appeared to confirm these interpretations. For instance, Pb-Pb zircon ages (Kuzmin and Chukhonin, 1980) and recent Sm-Nd whole-rock isochron and multigrain U-Pb ages (Kuzmin and others, 2003) suggest Precambrian ages. More recently, a combination of Rb-Sr whole-rock and mineral isochron ages were taken as evidence for Cretaceous metamorphism (Vinogradov and others, 1988, 1991; Bondarenko and others, 1993; Vinogradov and Grigor'yev, 1996). Bindeman and others (2002) presented the first modern single grain (ion microprobe) U-Pb zircon ages. They interpreted their grain-ages as a direct evidence for Cretaceous high-grade metamorphism.

In this paper, we evaluate the origin and evolution of the Sredinnyi Range based on new field mapping, structural analysis, thermobarometry, and U-Th-Pb geochronologic and low-temperature thermochronologic data. Our data demonstrate that the high-grade core of the southern Sredinnyi Range comprises metamorphosed Late Cretaceous to earliest Cenozoic continental margin sediments. Structural burial, metamorphism, and subsequent rapid exhumation occurred from 60 Ma to 48 Ma, coincident with the collision of a far-traveled intra-oceanic arc, the Olyutorsky terrane, with the northeast Russian margin.

Tectonic Overview

The central and western regions of the Kamchatka Peninsula record the Cenozoic collision of a Late Cretaceous-Paleocene island arc with the continental margin of northeast Asia (fig. 1). The Late Cretaceous-Eocene continental margin is composed of turbiditic sandstone and shale of the Ukelayat Group (Koryak Highlands, Shapiro and others, 2001), Lesnaya Group (Kamchatkan Isthmus area, Soloviev and others, 2002) and the Khozgon Group (southern Kamchatka, Marchenko, 1967). Allochthonous units are composed of Late Cretaceous to Paleocene basalt, chert, intermediate volcanic rocks, and associated volcanogenic sediments, and have been interpreted by Russian workers (for example, Zonenshain and others, 1990) as one or more island-arc terranes. Paleomagnetic studies (Levashova and others, 1997; Pechersky and others, 1997; Levashova and others, 2000) suggest that island-arc sequences exposed on the several capes along the east coast of Kamchatka probably represent fragments of another Cretaceous-Paleocene arc that was accreted during the Miocene (Cape Terranes in fig. 1). Geist and others (1994) concluded that much of this assemblage was related to a single island-arc terrane, which they called the Olyutorsky Arc. Although this view is not entirely correct, the concept of an Olyutorsky arc accounts for the stratigraphic and accretionary history of the bulk of the Late Cretaceous-Paleocene arc-volcanic units within the rest of Kamchatka.

The name Olyutorsky arc derives from its type locality in the Koryak Highlands. In the south, the arc terrane is referred to as the Achaivayam-Valagin arc (for example, Konstantinovskaia, 2000). Paleomagnetic data suggest that these Cretaceous rocks originated as far south as $49.7 \pm 5.6°$N, greater than 2000 km south of the expected paleolatitude range of 69 to 72°N (Levashova and others, 1998). Allochthonous island arc units and continental margin strata are juxtaposed along a ~1500 km-long suture zone (fig. 1). The northeast, central and southwest segments of this fault are referred to as the Vatyna thrust (Koryak Highlands), the Lesnovsk thrust (Lesnovsk Highlands in the Kamchatka Isthmus), and the Andrianov thrust (Sredinnyi Range), respectively. Lower-plate sediments are tight-to-isoclinally folded beneath the thrust, and shear-zone kinematics investigations indicate a highly-oblique north-northwest transport direction, compatible with a southerly origin for the Olyutorsky arc rocks (for example, Soloviev and others, 2001).

Detrital fission-track grain-age studies and biostratigraphic data from lower plate sedimentary rocks have significantly refined the timing constraints for arc-continent collision. Maximum stratigraphic age estimates given by young populations of unreset detrital zircon fission-track (FT) grain-ages from continentally derived strata in the lower plate of the suture zone indicate that collision began at 55 Ma and continued through 45 Ma (Garver and others, 2000a; Soloviev and others, 2002). Geochronologic constraints on the timing of arc emplacement are particularly good in the Kamchatka Isthmus area (fig. 1). There, a deformed section of the Lesnaya Group in the Lesnovsk Highlands contains continent-derived clastic rocks, which are tectonically interleaved with sedimentary mass-wasting deposits (broken formation and mélange) derived from the overriding Olyutorsky arc thrust sheet (Soloviev and others, 2002). Young (P1) FT grain-age peaks from the syn-orogenic part of this section range from ~55 Ma to ~44 Ma (Soloviev and others, 2002). The thrust sheet is unconformably overlain by Kinkil Group volcanic rocks and cross-cut by undeformed, comagmatic granitic intrusions of the Shamanka Massif, which yield 45.5 ± 2.9 Ma (2σ) and 45.3 ± 1.0 Ma (2σ) TIMS U-Pb zircon ages, respectively (Garver and others, 2000b; Soloviev and others, 2002). These data tightly bracket the timing of collision in the Kamchatka isthmus and Koryak region to the middle Eocene.

SREDINNYI RANGE METAMORPHIC ROCKS

The southern Sredinnyi Range exposes a 200 km-long by 40 km-wide domal culmination of metamorphic rocks (figs. 1 and 2) and is the largest of three high-grade exposures on the Kamchatka Peninsula. The other two are found in the Ganal (figs. 1 and 2) and Khavyven ranges (fig. 1). East of the suture zone, the basement of the Kamchatka Peninsula and Koryak Highlands are principally composed of low-grade terranes of oceanic and island-arc affinity that were accreted throughout the Cretaceous, continuing through the present (see review by Konstantinovskaia, 2000).

The Sredinnyi Range and much of the Kamchatka Peninsula were mapped in detail during major geologic campaigns in the late 1950s and early 1960s. These studies resulted in a series of 1:200,000 scale geologic maps for the Sredinnyi Range (Marchenko, 1967), which were compiled into regional geologic maps (Rotman, 1981; Litvinov and others, 1999). Tectonostratigraphic nomenclature in this area started with an initial classification by Marchenko (1967), and has evolved in subsequent publications by Khanchuk (1985), Bondarenko (ms 1992, 1997), and Rikhtyer (1995).

Overall, the detail and quality mapping studies in this region are impressive, especially given its remoteness. However, the published literature is very difficult to follow because of changes in stratigraphic names (figs. 3A-D), structural complexities, and disagreements about contact relationships and structural evolution. Furthermore, the most detailed geologic reports on the Sredinnyi Range are available only in Russian language publications. Figure 3 provides a summary of the evolution of tectonostratigraphic names for this area. Assignments and interpretations of Marchenko (1967) (fig. 3A) and Khanchuk (1985) (fig. 3B) were influenced strongly by ideas and terms from geosyncline theory. In contrast, Bondarenko (ms 1992) (fig. 3C) and Rikhtyer (1995) (fig. 3D) propose tectonostratigraphic interpretations that are more consistent with emerging evidence of accretion of far-travelled terranes. We favor the model of Rikhtyer (1995), because the terminology and tectonostratigraphic subdivisions are most compatible with our field observations.

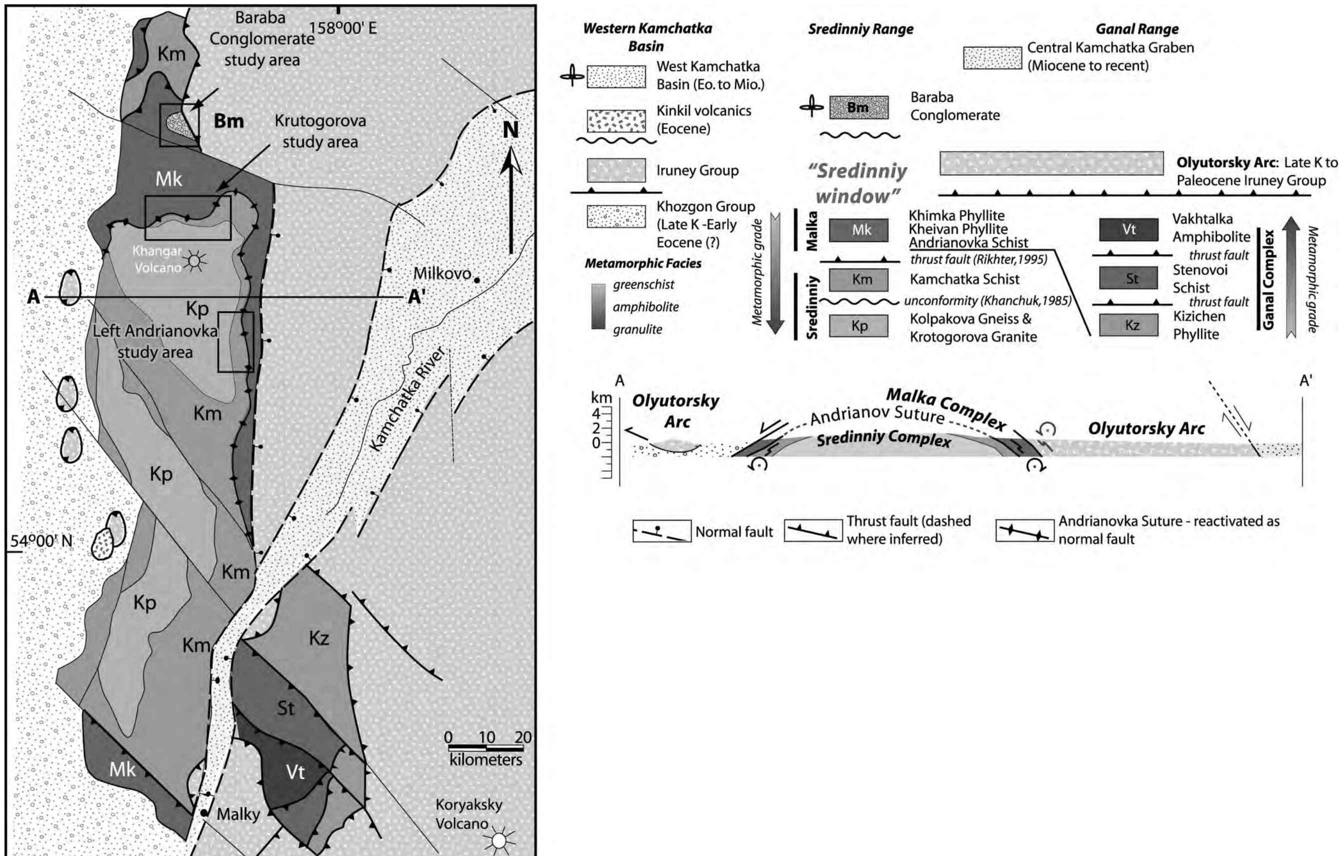

Fig. 2. Simplified geologic map of the Sredinnyi and Ganal Ranges with accompanying schematic tectonostragraphic legend (modified from Zinkevich and others, 1998). The locations of Krutogorova, Left Andrianovka and Baraba Mountain study areas are indicated by rectangles. Klippen of Irunei Group rocks and the overlapping West Kamchatka volcanic rocks are shown schematically. Line A-A′ defines the line of section.

Marchenko and others (1967)

Age	Rock Types	Stratigraphic Thickness (m)
J_3-K_1(?)	**Kvakhona Suite:** Schistose- plag-phyric volcanics, albite-epidote-chloriteschists, glaucophane schists, diabase, tuffaceous schists, and other associated volcanogenic sedimentary	2700
J_3-K_1(?)	**Stopol'nik Suite:** Sandstones, siltstones, polymictic meta-siltstones and phyllites with occcasional interbeds of metamorphosed tuffs	2600
$PZ_{2\text{-}3}$	**Khimka Suite:** Qtz-albite-chlorite schists with actinolite, metasandstones	1500
PZ_2	**Kheivan Suite:** Phyllites, metamorphosed oligoclase-bearing sandstones and siltstones	2000
PZ_1	**Andrianovka Suite:** Amphibole, amphibole-plagioclase, and albite-actinolite schists. Quartzites, metamorposed tuffaceous	700-1200
Pr?	**Kamchatka Series:** Mica schists with garnet, staurolite, kyanite, biotite and biotite-amphibole	3500
Pr?	**Kolpakova Series:** Biotite, biotite-garnet, biotite-amphibole, amphibole-pyroxene gneisses and migmatites, amphibolites and calciphyres	2000

Khanchuk (1985)

Age	Rock Types	Stratigraphic Thickness (m)
J	**Kvakhona Suite:** Weakly metamorphosed dacites and rare basalts, tuffs, and conglomerates	2000
$PZ_{2\text{-}3}$	**Alistor Suite:** Amphibole schists after ultramifc and mafic volcanics / **Khimka Suite:** Albite-actinolite schists after tuffs, sandstones and quartzites	800 / 600
	Kheivan Suite: Metamorphosed sandstones and rarer meta- siltstones, conglomerates (chiefly sericite-chlorite, biotite and staurolite metamorphic zone)	500-2000
PZ_2	**Andrianova Suite:** Amphibole, epidote-amphibole, and Cpx-amphibole crystalline schists. Amphibolite after mafic volcanics, rare occurrences of metaconglomerate	0-700
	Shikhta Series: Metamorphosed terrigenous deposits with basal conglomerates (chiefly straurolite-sillimanite and biotite-muscovite orthogneisses and migmatites	0-1500
Pr?	**Kolpakova Series:** Retrogressd kyanite, cordieite-hyperstherne gneisses and ortho-gneisses, rare garnet amphibolite and calciphyre	2500

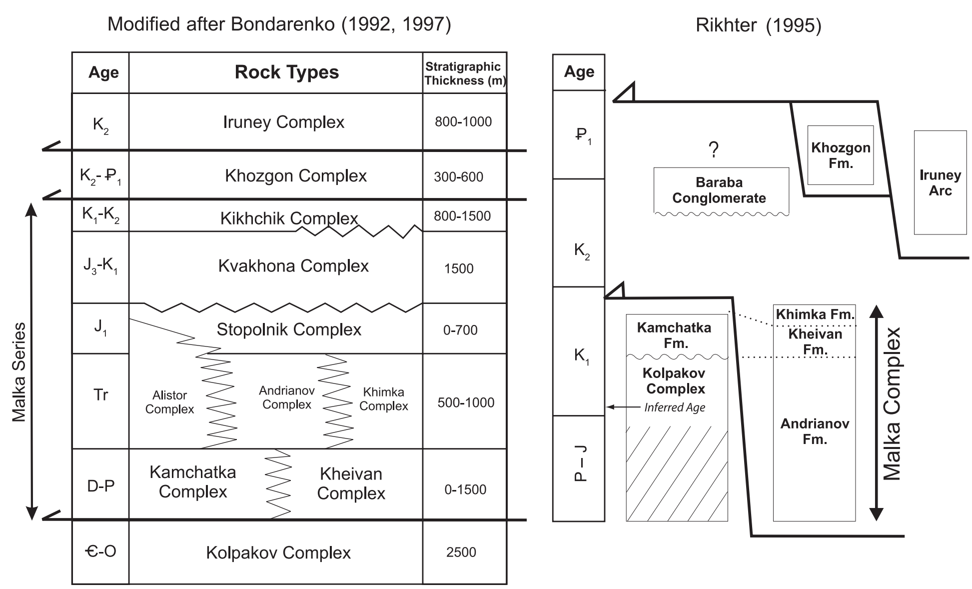

Fig. 3. Summary stratigraphic and tectonostratigraphic columns depicting the evolution of stratigraphic terminology and tectonostratigraphic interpretations for the Sredinnyi Range from the late 1960's to the mid 1990's. This figure is intended to familiarize the reader with the history of research in the Sredinnyi Range documented largely in Russian-only publications.

The published literature for the Sredinnyi Range is complicated by a mix of stratigraphic terms, as might be expected for a region underlain by poorly dated high-grade metamorphic rocks with complicated contact relationships. To provide consistent terminology and nomenclature for the rocks of the Sredinnyi Range, we have employed lithodemic naming framework laid out by the North American Stratigraphic Code (2005) and Salvador (1994). In particular, we use the terms *complex* defined as, "*an assemblage or mixture of rocks of two or more genetic classes, i.e., igneous, sedimentary or metamorphic, with or without highly complicated structure*" (North American

Stratigraphic Code, 2005). In practical terms, a complex is usually characterized by a distinctive geologic, metamorphic, and structural history, one that is sufficiently well defined that the complex can be mapped at a regional scale. The fundamental unit in this classification is a *lithodeme,* which includes type-locality and rock type (for example, *Krutogorova Granite*).

There seems to be widespread agreement in the published literature and also among current investigators that the Sredinnyi Range contains two mappable metamorphic units. We introduce the terms *Sredinnyi Metamorphic Complex* for the structurally lower and higher-grade unit, and *Malka Metamorphic Complex* for the structurally higher and lower-grade unit.

Sredinnyi Metamorphic Complex

The *Sredinnyi Complex* is exposed in the core of a north-south elongate domal uplift that underlies the southern half of the Sredinnyi Range. It contains three major lithodemic units (fig. 2). The structurally lowest unit, the *Kolpakova Gneiss*[1], is dominated by gneissic rocks and exhibits the highest metamorphic grade, including a local granulite-facies garnet-cordierite-hypersthene assemblage (Khanchuk, 1985; Tararin, 2008). The *Kamchatka Schist* is structurally higher and generally lower in metamorphic grade, consisting of amphibolite- to greenschist-facies schist with subordinate gneiss (Rikhtyer, 1995). The composition of the schist and gneiss indicates a pelitic to graywacke protolith (Rikhtyer, 1995), and the detrital zircon grain-age results presented below support this conclusion. The contact between the Kolpakova Gneiss and Kamchatka Schist has been interpreted as an unconformity, based on the reported presence of meta-conglomerates in the Krutogorova River region (Khanchuk, 1985; Rikhtyer, 1995) (fig. 3D). In contrast, Bondarenko (ms 1992) argued that the contact is a major thrust fault, marking a terrane boundary (fig. 3C).

The *Krutogorova Granite* (*sensu lato*) consists of foliated meta-aluminous to weakly peraluminous granitoids (Rikhtyer, 1995). Our field work at the type locality in the upper reaches of the Krutogorova River (fig. 4) indicates that the mapped boundaries encompass a composite igneous unit with variable cross-cutting relationships and textures. We recognize an older, foliated biotite granite that exhibits an apparent intrusive contact with Kolpakova Gneiss and does not cut the Kamchatka Schist. A second suite of predominantly equigranular granite intrusions cuts both the Kamchatka Schist and the Kolpakova Gneiss. In the Krutogorova drainage (fig. 4), small dikes of this equigranular granite form boudins subparallel to the dominant foliation along the contact between the Sredinnyi and Malka Complexes. In this paper, we restrict the definition of the Krutogorova Granite to the older orthogneiss.

Malka Metamorphic Complex

The *Malka Complex* lies structurally above the Sredinnyi Complex, and is primarily exposed along the northern and eastern flanks of the range (fig. 2). The association of mafic metavolcanic rocks and siliceous metasedimentary rocks indicates that the Malka Complex was formed in an oceanic setting. Lebedev and others (1967) argued that the Malka Complex represents a metamorphosed equivalent of the Irunei Group, the local name for the unmetamorphosed Olyutorsky arc rocks. This inference has been recently supported by the similarity of moderately well-preserved radiolaria found in both meta-chert of the Malka Complex and chert of the Irunei Group (Soloviev and Palechek, 2004).

[1] Transliteration note: Adjectival endings have been removed but the gender of type locality has been preserved. For example, the Kolpakovskaya Series of Marchenko (1967) is named for the type locality along the Kolpakova River, thus the unit is referred to as the Kolpakova Gneiss. For simplicity and continuity, adjectival endings have not been removed from units long-established in the western literature (for example, Olyutorsky Arc).

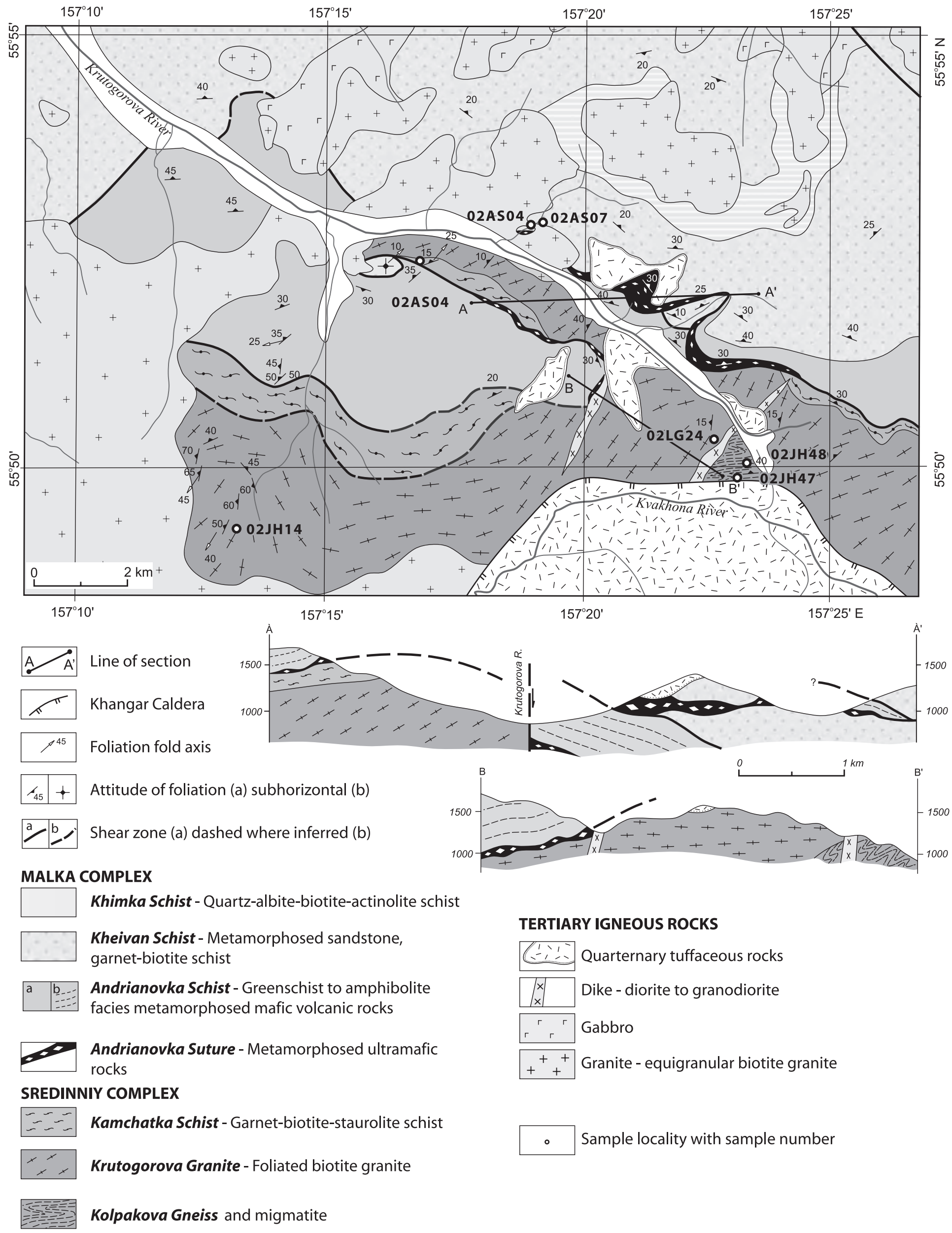

Fig. 4. Geologic and sample locality map and geologic cross sections for the upper Krutogorova River watershed study area (modified from Rikhtyer, 1995).

The lowest structural unit, the *Andrianovka Schist,* is composed mainly of metabasalt with subordinate meta-serpentinite (Rikhtyer, 1995). Structurally up-section in the Malka Complex, the *Kheivan Schist* and *Khimka Phyllite* comprise chert, mudstone, and sandstone, all metamorphosed to varying degrees (Khanchuk, 1985). Metamorphic grade at the base of the unit is as high as amphibolite facies, including garnet amphibolite, and decreases structurally upsection into low greenschist-facies metavolcanic rocks (Khanchuk, 1985).

The Andrianovka Schist is cut by several zoned ultramafic-mafic intrusions. Such zoned ultramafic-mafic complexes are a common feature of the Olyutorsky island-arc terrane (Fleorov and Koloskov, 1976; Ledneva and others, 2000; Batanova and others, 2005). The 1:200,000 geologic map of (Marchenko, 1967) shows that one of these intrusions, the Left Andrianovka massif, cuts the Kamchatka-Andrianovka contact. This relationship would be important if correct. Thus, we summarize evidence that this intrusion predates the contact and is similar to the other Olyutorsky zone intrusions (fig. 5).

The Malka Complex-Sredinnyi Complex contact was originally thought to be stratigraphic (Marchenko, 1975; Khanchuk, 1985). More recent mapping identified a sharp lithologic contrast across the contact, locally marked by blocks of ultramafic rocks in a meta-serpentinite matrix (Rikhtyer, 1995) (fig. 4). This contact is called the Andrianov suture in more recent literature (for example, Rikhtyer, 1995). Metamorphic grade increases progressively with structural depth throughout the Malka and Sredinnyi Complexes (Lebedev and others, 1967) indicating that peak metamorphic conditions post-dated the structural juxtaposition of these units.

Detailed mapping by M. Shapiro (2001, written communication), reproduced in figure 5, shows that the Left Andrianovka massif is restricted to the Andrianovka Schist, a relationship confirmed by our own observations in 2002. The massif is “normally zoned”, from dunite-clinopyroxenite in the core to gabbro around the margin, and is in turn cut by subordinate syenite intrusions. Belyatskii and others (2002) report a 65.8 ± 0.7 Ma Rb-Sr isochron age (MSWD =0.18) for the ultramafic part of the Left Andrianovka intrusion, defined by pyroxene and whole rock isotopic data. The low initial $^{87}Sr/^{86}Sr$ of 0.70354 ± 0.00006 (2σ) is consistent with the interpretation that these intrusions represent the magmatic roots of the island arc (Ledneva and others, 2000). Zircons from the syenite give U-Pb ages of 70.4 ± 0.7 Ma and 63.0 ± 0.6 Ma (Hourigan and others, 2004). Field relationships, including zones of mylonitization within the syenite, indicate that the Left Andrianovka massif was emplaced prior to deformation and metamorphism of the Andrianovka Schist (Kirmasov and others, 2004).

A more important aspect of Rikhtyer’s (1995) interpretation is that the Andrianovka Schist is a metamorphic equivalent of the Olyutorsky arc terrane. We have already noted the similarities between the Left Andrianovka massif and the zoned ultramafic-mafic intrusions widespread elsewhere in the Olyutorsky arc. Relatively low grade exposures of the Olyutorsky terrane (Irunei Group) are exposed to the west of the Sredinnyi uplift [for example, Vorovskaya River region in map by Marchenko (1967)], where they structurally overlie the Cretaceous Khozgon Group, which represent continentally derived turbidites deposited along the NE Asian continental margin. Rikhtyer (1995) views the Andrianovka suture as part of the boundary along which the Olyutorsky terrane was obducted on the NE Asian margin. The obducted arc rocks would have initially formed a continuous thrust sheet that covered the high-grade core of the range (fig. 2, cross section). Thus, the Sredinnyi Range represents a tectonic window through the Olyutorsky arc thrust sheet that exposes the deeply exhumed roots of the Eocene arc-continent collision zone.

Previous Age Estimates

The idea of a Precambrian microcontinent in Kamchatka was fuelled by reconnaissance dating of zircon from the Sredinnyi Complex and from the crystalline rocks of the Ganal Range (fig. 1). A 1.3 Ga age was proposed for the Kolpakova Gneiss based on Pb-Pb isotopic analysis of multi-grain zircon samples (Kuzmin and Chukhonin, 1980). An even older Archean age was inferred from Pb-Pb data from multi-grain zircon

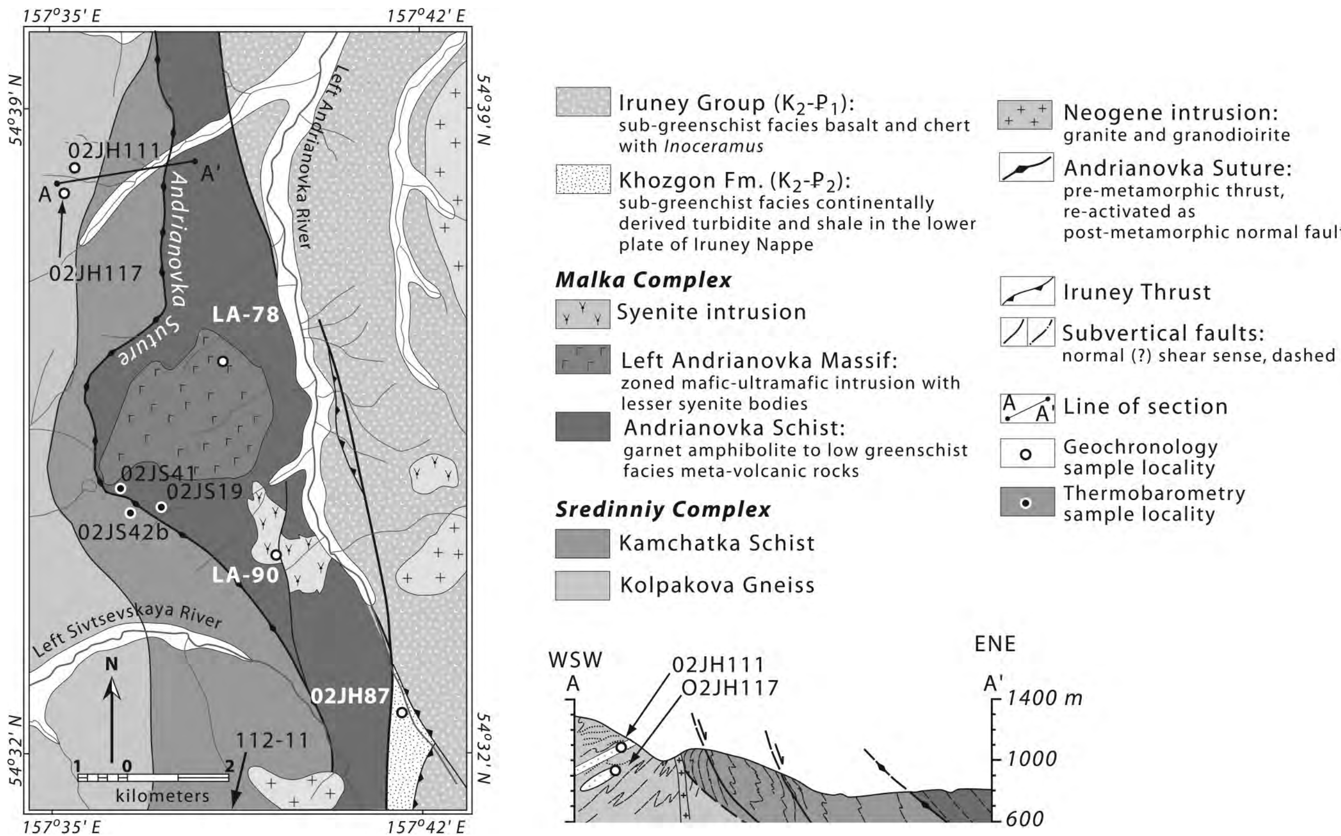

Fig. 5. Geologic and sample locality map and geologic cross sections for the upper Left Andrianovka River watershed study area (modified from Kirmasov and others, 2004 with data from Marchenko, 1967 and unpublished data of M. Shapiro).

samples from the Ganal Range (L'vov and others, 1985). Kuzmin and others (2003) report Sm-Nd whole rock isochron and multigrain U-Pb analyses. The Sm-Nd data suggest a wide range of Precambriam ages from 951 Ma to 2420 Ma, depending on which samples are used for isochron construction. U-Pb analyses yield discordant results from 3 multigrain fractions, which these authors interpret as a discordia line with a 106 $\pm$ 31 Ma lower intercept and a 2314 $\pm$ 325 Ma upper intercept (Kuzmin and others, 2003). These authors argue that the Sm-Nd and U-Pb data reflect isotopic disturbance of a Precambrian protolith during Cretaceous-Cenozoic active margin processes.

Vinogradov and coauthors (1988, 1991, 1996) report whole-rock Rb/Sr isochron ages from metamorphic rocks of the Sredinnyi and Malka Complexes that suggested two closure ages, in the Early Cretaceous and early Tertiary. Bondarenko and others (1993) report mineral and whole-rock Rb-Sr isochrons ranging from 67 $\pm$ 10 Ma to 48 $\pm$ 3 Ma from garnet-bearing plagiogranite in the Kamchatka Schist. K-Ar data for the Sredinnyi Range metamorphic rocks, summarized in Watson and Fujita (1985), cluster in peaks, one at ~100 Ma (n=4) and the other, at 50 to 60 Ma (n=7). Granitoids within the Sredinnyi Range yield K-Ar ages from 120 to ~10 Ma (n=43) with a peak at ~50 Ma (n=13). $^{40}Ar/^{39}Ar$ data from the Ganal and Khavyven Ranges suggest that post-metamorphic cooling occurred there between 51 and 47 Ma (Zinkevich and otehrs, 1993). Scattered $^{40}Ar/^{39}Ar$ dating has been done in the Sredinnyi Range, but has not yet been published (Paul Layer, personal communication 2008).

A Paleozoic protolith age is commonly cited for the Malka Complex, based on spores described by Sivertseva and Smirnova (1974). This assertion is a misrepresentation of the results of the original study where the authors report both Paleozoic and Mesozoic spores but limit their discussion to the more abundant Paleozoic taxa (Sivertseva and Smirnova, 1974). Furthermore, they note that shale of known Lower Tertiary age elsewhere in the Kamchatka region commonly contain "exotic" Paleozoic spores.

In the most recent work on the geochronology of the Sredinnyi Range, Bindeman and others (2002) report SHRIMP U-Pb ages of zircons from the Kolpakova Gneiss. Their study demonstrates a broad range of detrital grains-ages, ranging from Archean to Late Cretaceous, but their conclusions are compromised by an unusual sampling scheme involving mixing separates from multiple hand specimens collected over large areas. For instance, one "sample" comprises 15 hand specimens collected in three localities distributed over ~40 km^2, the other sample is made up of 39 hand specimens taken over the scale of an entire outcrop. Such mixing methods were intended to provide a broad look at Kamchatka metamorphic geochronology, but interpretations about the age of metamorphism are equivocal because the ability to correlate specific grains to their host lithology is lost in the mixing process. Despite this ambiguity, Bindeman and others (2002) conclude that peak metamorphism occurred in the Late Cretaceous based on the observation of multiple Late Cretaceous grain-ages from texturally distinct zircon rims. Appeals are made to the euhedral morphology and overgrowth relationships of the Late Cretaceous zircons to argue for "unconstrained growth in a leucosome." However, this conclusion is conjectural because the sampling method precludes a definitive link between the 77 Ma grains and leucosomal segregations. Bindeman and others (2002) acknowledge the presence of a detrital population of zircons with ages up to Late Cretaceous within these paragneisses. The assertion that the protolith is Archean (in their title) is therefore misleading. Our study supports an alternative conclusion: the zircons in the Kolpakova Gneiss are detrital in origin, and were derived from source regions that include Precambrian rocks.

The Baraba Conglomerate, located on the north side of the Sredinnyi Range (fig. 2) unconformably overlies the phyllitic rocks of the Malka Complex and thus provides an important stratigraphic constraint for the age of metamorphism. The unconformity is well exposed on Baraba Mountain, an observation that we were able to directly confirm in the field (Soloviev and others, 2004). At the base of the section, clasts are predominantly chert, derived from the Irunei Group (Olyutorsky terrane, exposed nearby), phyllite from the underlying Malka Complex. Granitic and higher-grade metamorphic clasts are present higher in the section (Shapiro and others, 1986; Soloviev and others, 2004; Shanster and Chelebaeva, 2005; Solov'ev and others, 2007), suggesting that the Baraba Conglomerate preserves an unroofing sequence for the Sredinnyi Range metamorphic core (figs. 2 and 3D).

There has been much interest in using the age of the Baraba Conglomerate to constrain the metamorphic age of the Malka Complex. Well-preserved and abundant plant fossils in the Baraba Conglomerate (Shapiro and others, 1986) were assigned to the latest Cretaceous (Campanian to Maastrichtian) (Shanster and Chelebaeva, 2004, 2005), but other workers argued that the possible age range of these flora might extend into the Paleocene (Slyadnev and others, 1997). We discount the Late Cretaceous phytostratigraphic age in favor of an Eocene age for three reasons: 1) our group has obtained SHRIMP zircon U-Pb age of 50.5 ± 1.5 Ma from a tuffaceous horizon at the base of the Baraba Conglomerate that indicates deposition in the early Eocene or younger (Soloviev and others, 2004, this study); 2) the biostratigraphic age is principally based on the presence of a Bennettitales flower (Williamsonia Kamtschatica Chelebaeva sp.), which is poorly preserved (Shanster and Chelebaeva, 2004, 2005); and 3) viewed as an assemblage, the fossil flora preserved within the Baraba Conglomerate are more consistent with a Paleocene or Eocene age (Ian Miller and Leo Hickey, personal communication, 2004).

field work and sampling

We targeted two field areas where previous work had already established the basic tectonostratigraphic framework. Our primary objectives were: 1) to constrain the nature and age of the protoliths; 2) to provide new geochronologic data on the timing and conditions of metamorphism within Sredinnyi Range; and 3) to establish the kinematics of major structures. The upper reaches of the Krutogorova River (fig. 4) expose the most readily accessible and well-studied sections of the Kolpakova Gneiss, as well as the contact between the Malka and Sredinnyi Complexes. The Left Andrianovka River region (fig. 5) provides access to well-studied intrusive relationships within the Malka Complex, as well as access to rocks for kinematic analysis of the eastern flank of the Sredinnyi Range. Detailed work in these study areas by Khanchuk (1985), Bondarenko (ms 1992), and Rikhter (1995), as well as unpublished mapping of M. Shapiro, provide structural and stratigraphic basis for our sampling.

At the headwaters of the Krutogorova drainage (figs. 2 and 4) the Kolpakova Gneiss is exposed in contact with Krutogorova Granite and amphibolite- to upper greenschist-facies rocks of the Kamchatka and Andrianovka Schists (fig. 4). This contact is the proposed "Andrianovka suture" of Rikhtyer (1995). Bondarenko (ms 1992) favors an alternative interpretation that the suture boundary is located at the Kamchatka Schist-Kolpakova Gneiss contact, based on their interpretation of top-west kinematic indicators present at that contact. Our own work indicates that faults are common throughout this region, and it is difficult to judge the relative importance of individual faults from kinematic indicators alone. Thus, we find Rikhter's (1995) interpretation more compelling, given his evidence for a metamorphosed serpentinite mélange localized along the Andrianovka-Kamchatka contact. Here, we collected samples of orthogneiss, migmatitic paragneiss and schist in order to constrain the nature and age of the protoliths of the Sredinnyi Complex. Furthermore we sampled intrusive units that cross-cut major structural boundaries to place minimum age constraints on the age of these boundaries.

The second field area is located in the upper reaches of the Left Andrianovka drainage (figs. 2 and 5). Our principal objective in this area was to understand the kinematics of major tectonic contacts and the nature of lithologic boundaries along the eastern flank of the range. Here, the metamorphic section appears attenuated. Over a horizontal distance of approximately 6 km, we observe migmatite of the Kolpakova Gneiss, garnet-biotite schist of the Kamchatka Schist, garnet amphibolite of the Andrianovka Schist, Cretaceous-Tertiary clastic sediments of the Khozgon Group and finally chert-basalt and tuff sequences of the Irunei Group. The units typically dip 30 to 50 degrees to the east, which indicates that this metamorphic gradient is presently only 3 to 4.5 km thick.

Detailed structural and microstructural analysis by Kirmasov and others (2004) suggests a two-stage evolution for the Andrianovka suture zone. The first stage involved west-directed thrusting of the Achaivayam-Valagin (Olyutorsky) arc rocks onto the continental margin interpreted from regional structural relationships and asymmetric, top-west folds in Irunei Group rocks in the Left Andrianovka study area. The second deformation is primarily preserved at deeper structural levels in Kamchatka Schist where ductile kinematic indicators give top-east normal shear sense. Kirmasov and others (2004) attribute the second stage to post-collisional extension and exhumation of the high-grade core of the Sredinnyi Range.

METAMORPHIC PETROLOGY AND THERMOBAROMETRY

Lebedev and others (1967), Khanchuk (1985), and Savostin and others (1994) established the metamorphic framework for the Sredinnyi Range. The memoir by Khanchuk (1985) provides the most detail, in terms of regional coverage, field and petrographic descriptions, and microprobe analyses, but it was circulated only as a limited Russian-language publication. Tararin (2008) provides a more focused study of the Kolpakova Gneiss, which includes both amphibolites and granulite facies assemblages.

Our summary here draws heavily on these sources, especially Khanchuk (1985) and Tararin (2008). In particular, we present recalculated PT estimates for 13 sites from Khanchuk (1985), which provides some coverage for the areas to the north (Kurtogorova, Zolotaya and Platonich) and northeast (Left and Central Andrianovka) of our detailed study areas. We also report PT results for 4 samples that we collected adjacent to the Kamchatka-Andrianovka contact. All P-T estimates (table 1) were calculated using Thermocalc v. 3.30 (Powell and Holland, 1988) which simultaneously solves pressure (P) and/or temperature (T) using all relevant experimentally calibrated phase equilibria. Details about analytical procedures are in the Appendix.

Our objective is to constrain, in a general manner, the metamorphic history of the Sredinnyi Range. This information is important for guiding our interpretation of the new geochronologic and thermochronologic data. The key issues are: 1) What were the maximum P-T conditions for each of the metamorphic units? 2) How do these P-T conditions correlate with the present structural order of the metamorphic units within the Sredinniy Range? And 3) are there significant discontinuities in the P-T conditions for adjacent metamorphic units?

Kolpakova Gneiss

The summary here is entirely based on Khancuk (1985) and Tararin (2008). Khancuk (1985) describes three low-variance metamorphic assemblages in the Kolpakov Gneiss, all of which are developed in the quartzo-feldspathic gneiss that characterizes the unit. The first two are upper amphibolites assemblages: kyanite-garnet-biotite-muscovite-plagioclase, and kyanite-sillimanite-orthoclase (± garnet, biotite, plagioclase). Recalculated P-T estimates (table 1) indicate 600 to 675°C and 0.5 GPa. The third assemblage indicates granulite facies, and is characterized by garnet-cordierite-

Table 1

Thermobarometric data from metamorphic rocks of the Malka and Sredinnyi Complexes

Sample	Locality	Rock Type	Assemblage	Temperature (ºC)		Pressure (kbar)		Source
			Andrianovka Schist					
02JS41	L. Andrianovka	Amphibolite	Grt-Hbl-Pl-Qtz-Bt	GH	533 ± 61	GHPQ	3.8 ± 1.4	1
02JS19	Krutogorova	Schist	Grt-Bt-Qtz	GB	535 ± 27	Ref.	4.0	1
			Kamchatka Schist					
02JS42b	L. Andrianovka	Schist	Grt-Bt-Ms-Pl-Qtz-	GB	525 ± 75	GBMP	4.0 ± 1.0	1
02AK06	Krutogorova	Schist	Grt-Bt-Qtz-Ms	GB	562 ± 24	Ref.	4.0	1
666/5A	Krutogorova	Staurolite schist	St-Grt-Bt-Ms-Pl-Qtz	GB	639 ± 96	GBMP	10.9 ± 1.7	2
734	Krutogorova	Staurolite schist	St-And-Grt-Bt-Ms-Pl-Qtz	GB	529 ± 76	Ref.†	<4.0	2
556	Kolpakova	Staurolite schist	St-Ky-Grt-Bt-Ms-Pl-Qtz	GB	571 ± 77	GASP	7.7 ± 0.7	2
257/1	Nemtik	Sillimanite schist	St-Sill-Grt-Bt-Ms-Pl-Qtz	GB	534 ± 77	GASP	5.7 ± 0.7	2
			Kolpakova Gneiss – amphibolite facies					
699	Zolotaya	Kyanite plagiogneiss	Ky-Grt-Bt-Ms-Pl-Qtz	GB	592 ± 87	Ref.	> 8.0	2
712	Zolotaya	Kyanite plagiogneiss	Ky-Grt-Bt-Pl-Qtz	GB	632 ± 91	Ref. ††	> 8.0	2
7121g	Zolotaya	Amphibolite	Grt-Hbl-Pl	GH	810 ± 104	GHPQ	7.7 ± 1.4	2
398/1	C. Andrianovka	Kyanite gneiss	Ky-Grt-Bt-Kfs-Pl-Qtz	GB	860 ± 156*	Ref.	5.5	2
213	L. Dukuk	Sillimanite gneiss	Sill-Grt-Bt-Kfs-Pl-Qtz	GB	679 ± 91	Ref.	5.5	2
629	Krutogorova	Cord gneiss	Grt-Crd-Bt-Kfs-Qtz	GCrd	798 ± 73	GCSQ	3.1 ± 0.6	2
601	Krutogorova	Gneiss	Grt-Bt-Kfs-Pl-Qtz	GB	750 ± 115*	Ref.	5.5	2
			Kolpakova Gneiss – granulite facies					
724	Platonich	Cord-Opx gneiss	Crd-Opx-Bt-Kfs-Pl-Qtz-Grt	GB	831 ± 115*	Ref.	5.5	2
				GCrd	807 ± 76			
706	Zolotaya	Granulite	Grt-Cpx-Pl-Hbl-Qtz	GCpx	584 ± 83	GADS	6.2 ± 1.4	2
				GH	745 ± 64	GHPQ	7.0 ± 1.2	

Mineral abbreviations are after Kretz (1983). All P-T conditions calculated using Thermocalc (v. 3.30) Fe-Mg exchange thermometers: GH—garnet-hornblende; GB—garnet-biotite; GCpx—garnet-clinopyroxene; GCrd—garnet-cordierite. Net transfer equilibrium barometers: GHPQ—garnet-hornblende-plagioclase-quartz; GBMP—garnet-biotite-muscovite-plagioclase; GASP—garnet-aluminosilicate-quartz-palgioclase; GADS—garnet-clinopyroxene-plagioclase-quartz; GCSQ—garnet-cordierite-sillimanite-quartz; Ref.—reference pressure for samples without sufficient data and/or assemblages for barometry.

* Overestimates likely related to Fe enrichment of matrix biotite caused by retrograde reactions (Kohn and Spear, 2000).

† GBMP determination of 7.4 ± 1.2 kbar outside of andalusite stability field.

†† GASP barometry of 6.1 ± 0.7 kbar outside of Ky-Grt-Bt stability field.

Sources: (1) This study; (2) Khanchuk (1985).

orthoclase (± biotite, orthopyroxene, plagioclase). Recalculated P-T estimates (table 1) indicate 750 to 850°C and 0.5 to 0.7 GPa for this metamorphic assemblage.

Recent work by Tararin (2008) indicates that the Kolpakova Gneiss was regionally metamorphosed to upper amphibolite facies, as indicated by the widespread occurrence of the kyanite-bioite-garnet assemblage. His P-T estimates are 560 to 660°C and 0.59 to 0.69 GPa. Local anatectic melts were formed at 620°C to 660°C and 0.19 to 0.30 GPa, which implies decompression melting, presumably associated with exhumation. Tararin (2008) also shows that granulite-facies metamorphism is localized around mafic intrusions of the Oligocene-Miocene Lavkinskii Instrusive Suite. The inference is that this event was due to contact metamorphism, and is younger and unrelated to the regional-scale amphibolites-facies event.

Kamchatka Schist

We analyzed two samples of the Kamchatka Schist, one from each of the two study areas. Sample 02JS42B was collected ~20 m below garnet amphibolites of the Andrianovka Schist, in the Left Andrianovka region (fig. 5). This sample contains garnet porphyroblasts (0.5-1.0 mm diameter) set in a biotite, muscovite, quartz assemblage, with subordinate Fe-Ti oxides. Garnet from this sample shows no significant zoning (fig. 6C). Sample 02AK06 was ~20 m below the contact with the Andrianovka schist, near the headwaters of the Krutogorova River (fig. 4). Rotated garnet porphyroblasts (0.5-1.0mm diameter) are set in a penetrative schistose matrix consisting of biotite, quartz, muscovite, and minor oxides. Garnet from this sample shows no significant zoning (fig. 6D). Garnet-biotite Fe-Mg exchange indicates temperatures of 550 to 650°C for these samples (table 1).

Andrianovka Schist

Sample 02JS19 contains garnet porphyroblasts (~1.0 mm diameter) set in a biotite-quartz matrix. Garnet from this sample is zoned, with the grossular mole fraction decreasing from 30 to 7 percent from core to rim (fig. 6A). Sample 02JS41 was collected from the upper reaches of the Left Andrianovka River (fig. 5). It consists of segregated layering of hornblende and quartz-plagioclase with garnet porphyroblasts (0.5-1.5mm diam.). Garnet shows only weak zoning in the almandine component. Our microprobe data indicate temperatures of 525 to 560°C (table 1), which is only slightly lower than metamorphic temperatures for the Kamchatka Schist. The garnet-hornblende-plagioclase-quartz barometer of Kohn and Spear (Kohn and Spear, 1990) indicates pressures of 0.64 to 0.68 GPa.

Interpretation

The available metamorphic data support the following conclusions: 1) metamorphic grade appears to increase smoothly with depth, with no obvious breaks in metamorphic section; 2) *regional* metamorphism reached the highest grade in the Kolpakova Gneiss, with P-T conditions of 560 to 660°C and 0.59 to 0.69 GPa (Tararin, 2008; this study); and 3) the granulite-facies metamorphism is local and significantly post-dates the regional-scale deformation and metamorphism of the Sredinniy Range (Tararin, 2008). Kirmasov and others (2004) found normal-shear-sense ductile shear zones in the region of Kamchatka-Malka complex contact. These observations, in concert with the continuous nature of metamorphic section across this contact, suggest that the metamorphic sequence has been ductily thinned, but this thinning may have occurred without the development of major structural breaks. We infer from these relationships and the apparent lack of duplication of metamorphic section at the Andrianovka Suture that peak metamorphic conditions occurred after the units were structurally assembled. In other words, metamorphism post-dated the obduction of the Olyutorsky Arc onto the continental margin.

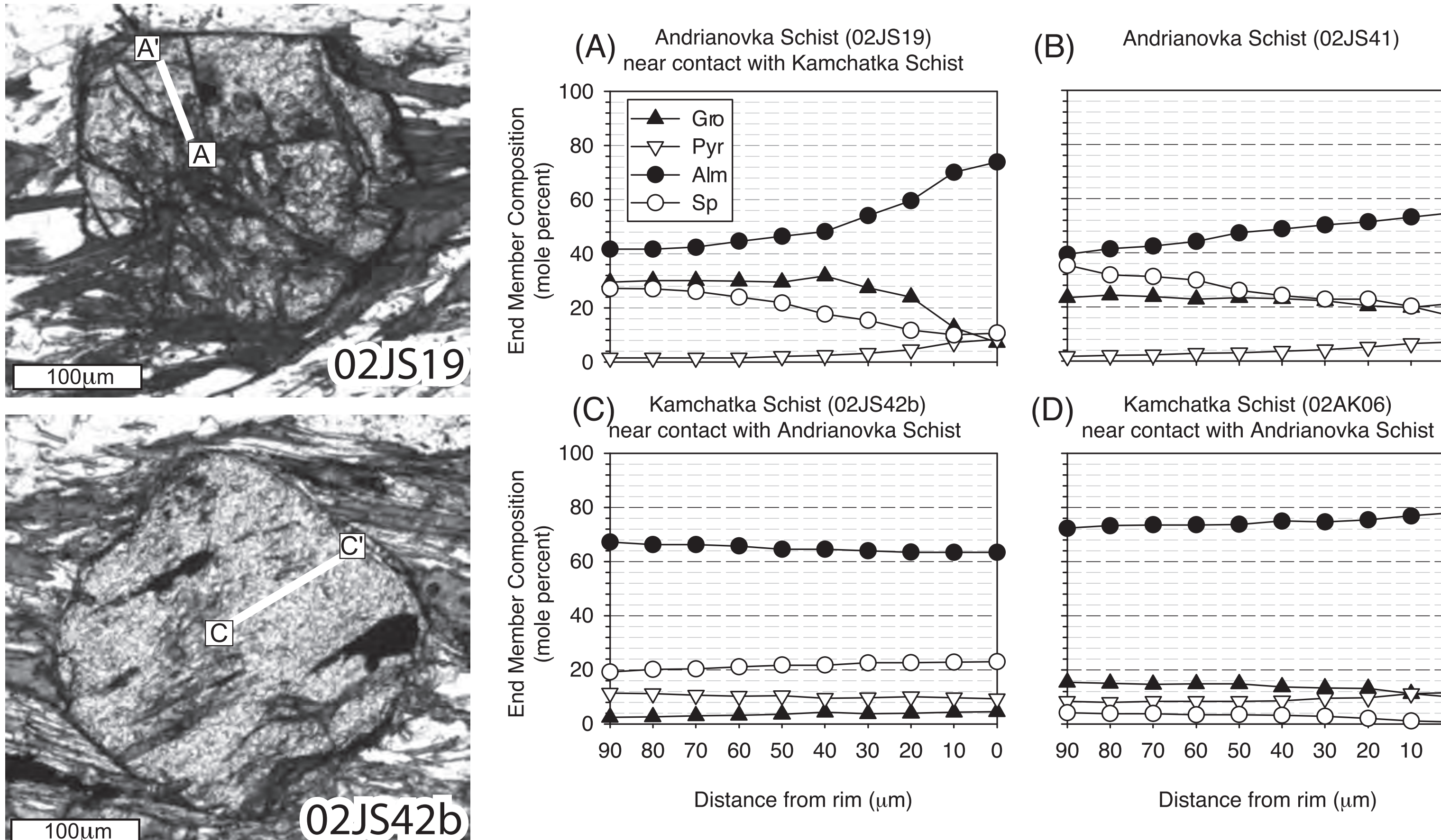

Fig. 6. Composition transects for garnets from the Andrainovka and Kamchatka schists. The photomicrographs show two of the analyzed grants and the transects for the analyses (white lines). End members were calculated from molar concentrations, with grossular (Gro) = Ca/(Ca+Mn+Fe+Mg), almandine (Alm) = Fe/(Ca+Mn+Fe+Mg), spessartine (Sp) = Mn/(Ca+Mn+Fe+Mg), and pyrope (Py) = Mg/(Ca+Mn+Fe+Mg).

GEOCHRONOLOGY AND THERMOCHRONOLOGY

Protolith Ages-Sredinnyi Complex

The following section contains a description of SHRIMP zircon U-Pb geochronometry from samples targeted to elucidate the pre-metamorphic history of the rocks that now constitute gneiss and schist of the Sredinnyi Complex. Zircon U-Pb grain-ages presented in this section are interpreted as primary crystallization ages in the case of igneous lithologies or concordant detrital ages in the case of metasedimentary rocks. The metasedimentary rocks are of particular interest because the distribution of the detrital grain ages can be used to constrain the maximum depositional age of the protolith and also to evaluate the source region from which the sediment was derived. A summary of all U-Th-Pb SHRIMP geochronologic data is presented in table 2. Detailed data tables are located in the Appendices A.1–A.14.

Zircons from several syn-tectonic granitoids were analyzed in the course of this investigation. While their ages are interpreted as primary crystallization, their geologic and structural settings indicate that their emplacement is broadly synchronous with high-grade metamorphism and deformation. Thus, presentation of these data is reserved for the section on the timing of peak metamorphism. All grain-ages were collected using the Stanford-USGS SHRIMP-RG ion microprobe using standard methodologies (see Appendix).

Kolpakova gneiss (sample 02JH47/2).—We sampled a melanosomal portion of migmatitic rocks of the Kolpakova gneiss exposed at the pass between the Kvakhona and Krutogorova Rivers (fig. 4). Thirteen grains including two with core-rim pairs produced a distribution of concordant ^{207}Pb-corrected ^{206}Pb*/^{238}U grain-ages that ranges from 85.1 Ma to 1859 Ma. A single grain lacking obvious growth domains (fig. 7A) yielded a grain-age of 54 Ma and a Th/U of 0.02 (Appendix A.1 #7). Another young analysis (80 Ma; Appendix A.1 #3) was excluded because of excessive U and Th. Distinct, enriched U rims measuring a few micrometers, are visible on most grains and are interpreted as metamorphic overgrowths based on lower cathodoluminescence (CL) intensity and zonation discordant to that of the apparent cores (fig. 7B). However, these domains were too small to analyze with the ion probe.

Kolpakova Gneiss (sample 02JH48).—Sample 02JH48 was collected from the melanosome of migmatitic paragneiss (fig. 8A) at the Krutogorova Pass (fig. 4). Analysis of 11 grains including two core-rim pairs produced a range of grain-ages from 64.0 ± 1.7 to 1859.0 ± 29.1 Ma (figs. 8A-C; Appendix A.2). The two rim analyses gave ages of 49.4 ± 1.2 and 45.9 ± 2.1 Ma with Th/U ratios significantly less than 0.1 (Appendix A.2) suggesting their possible origin as metamorphic overgrowths (fig. 8B). The youngest grain-age (64 Ma; Appendix A.2 #2) is younger than the cross-cutting Krutogorova granite (see below); however, the analyzed pit did not appear to intersect a metamorphic overgrowth domain. This relationship is best explained by partial lead loss during peak metamorphic conditions, thus the data point was discarded.

Krutogorova foliated granite (sample 02LG24).—We performed 12 analyses of 10 grains with two core-rim pairs (fig. 9; Appendix A.3). CL zonation of the imaged grains is predominantly oscillatory although some grains contain apparent cores exhibiting contrasting CL intensity and textures and resorbed margins (figs. 9C-D). One core analysis gave an age of 1049 Ma with a 77 Ma rim (figs. 9A, C-D; Appendix A.3 #8,8R). Nine of 12 analyses yield a weighted mean ^{207}Pb-corrected ^{206}Pb*/^{238}U age of 78.5 ± 1.5 Ma (2σ) (fig. 9). These zircon data suggest that a 78 Ma granitic intrusion assimilated crust that either includes a Precambrian crustal block or, more likely, cut young sediments containing Precambrian detrital zircons. The foliation likely formed during the high-grade metamorphism described below.

Kamchatka Schist (sample 02AS07).—Sample 02AS07, a garnet-biotite-albite-quartz schist, was collected from the northern side of the upper reaches of the Krutogorova

Table 2

Summary table for zircon and monazite U-Th-Pb geochronologic data

Sample	Rock Type	Mineral	Latitude	Longitude	Age	Type	n/N	MSWD
			Protolith ages					
02JH47/2	Kolpakova Gneiss, migmatite	detrital zircon	54º 50.120' N	157º 23.096' E	*85.1 ± 1.5*	U-Pb	*youngest grain-age*	
02JH48	Kolpakova Gneiss	detrital zircon	54º 50.128' N	157º 23.106' E	*82.1 ± 1.8*	U-Pb	*youngest grain-age*	
02LG24	Krutogorova Granite	zircon	54º 50.564' N	157º 22.754' E	78.5 ± 1.5	U-Pb	9/12	2.1
02AS07	Kamchatka Schist	detrital zircon	54º 53.160' N	157º 17.210' E	*106.2 ± 5.9*	U-Pb	*youngest grain-age*	
112-11	Kamchatka Schist	detrital zircon	54º 30.666' N	157º 38.833' E	*57.3 ± 4.0*	U-Pb	*youngest grain-age*	
LA-78	L. Andriankovka syenite	zircon	54º 35.900' N	157º 37.600' E	63.0 ± 1.2	U-Pb	14/15	0.86
LA-90	L. Andriankovka syenite	zircon	54º 34.200' N	157º 38.700' E	70.2 ± 1.4	U-Pb	15/15	0.60
			Metamorphic ages					
02JH47/1	Kolpakova Gneiss, migmatite	monazite	54º 50.120' N	157º 23.096' E	52.4 ± 0.7	Th-Pb	12/12	0.59
02JH47/2	Kolpakova Gneiss, migmatite	monazite	54º 50.120' N	157º 23.096' E	51.7 ± 0.7	Th-Pb	8/10	0.53
		zircon rim			51.2 ± 0.5	U-Pb	8/12	0.97
02JH14	Kolpakova Gneiss	monazite	54º 49.288' N	157º 13.258' E	50.5 ± 0.7	Th-Pb	11/12	0.89
02JH111	cross-cutting granite dike	monazite	54º 37.547' N	157º 35.049' E	51.9 ± 0.7	Th-Pb	8/8	0.25
		zircon			52.6 ± 1.2	U-Pb	12/12	6.0
02JH117	pegmatite	monazite	54º 37.017' N	157º 34.935' E	52.1 ± 0.6	Th-Pb	12/12	0.12
02AS04	biotite tonalite	zircon	54º 53.150' N	157º 17.200' E	51.5 ± 0.7	U-Pb	13/13	0.27
			Overlap sequence					
01JG11	tuff, Baraba conglomerate	zircon	55º 04.250' N	157º 18.583'E	50.5 ± 1.2	U-Pb	15/16	0.90
			Detrital zircon reference samples					
02JH87	Khozgon Group sandstone	detrital zircon	54º 32.178' N	157º 41.531' E	*59.2 ± 3.0*	U-Pb	*youngest grain-age*	
95JG-16	Ukelayat Group sandstone	detrital zircon	61º 41.947' N	171º 47.844' E	*54.2 ± 4.0*	U-Pb	*youngest grain-age*	

Data are divided in categories following description in the text. For igneous and metamorphic samples ages are weighted-mean Th-Pb (^{207}Pb-corrected ^{208}Pb/^{232}Th) or U-Pb (^{207}Pb-corrected ^{206}Pb/^{238}U). n/N shows the number of grain ages (n) of the total (N) used for weighted mean age calculation. MSWD is the mean square of the weighted deviates (Wendt and Carl, 1991). For detrital samples the youngest concordant grain-age with Th/U >0.01 is shown, although more conservative pooled ages are used to infer maximum stratigraphic age.

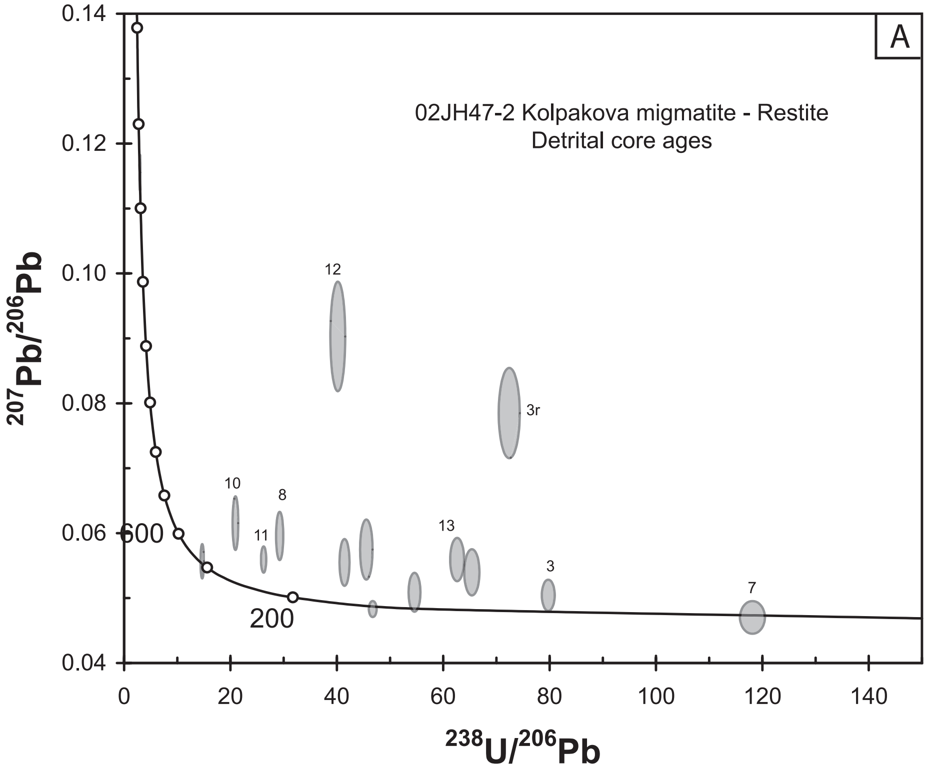

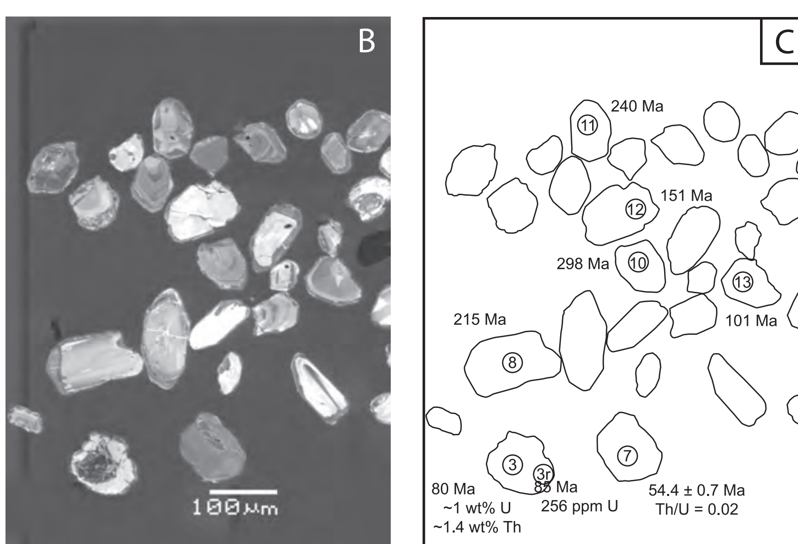

Fig. 7. (A) Tera-Wasserburg concordia plot of single-grain SHRIMP U-Pb analyses for sample 02JH47-2—a melanosome within migmatites of the Kolpakova Gneiss in the upper Krutogorova watershed (fig. 4). (B) Cathodoluminensce image of polished zircons in epoxy depicting the texturally heterogeneous nature of the zircon population. (C) Outlines of individual grains and the positions of spot analyses with corresponding ^{207}Pb-corrected $^{206}Pb^{*}/^{238}U$ ages. Encircled numbers refer to isotopic data in Appendix A.1.

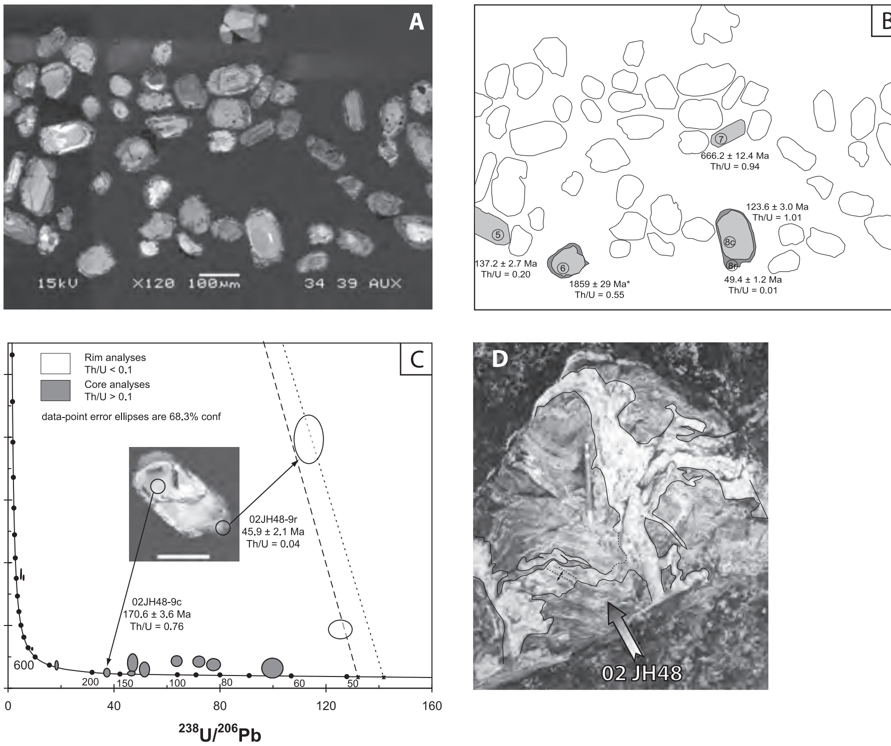

Fig. 8. Single-grain U-Pb data and CL images for zircons from a melanosome of the Kolpakova migmatites (Sample 02JH48) in the upper Krutogorova watershed. (A) Cathodoluminensce image of polished zircons. (B) Outlines of individual grains and position of spot analyses with corresponding ^{207}Pb-corrected ^{206}Pb*/^{238}U ages. Encircled numbers refer to data in Appendix A.2. Note that analyzed grains have been colored to indicate core and rim domains. Th/U ratios of individual analyses are shown because low Th/U ratios (<0.01) are thought to be a hallmark of zircon overgrowths formed in wet metamorphic conditions (for example, Ireland and Gibson, 1998) consistent with zircon overgrowth formation during migamtization. (C) Tera-Wasserburg concordia plot of all sample 02JH48 data. Filled ellipses are considered primary, detrital ages while open circles represent data from low Th/U relatively higher common Pb metamorphic zircons and zircon overgrowths. (D) Outcrop-scale photograph of migmatites of the Kolpakova Gneiss; sample 02JH48 was taken from the melanosome.

drainage (fig. 4). Zircons extracted from this sample are undoubtedly of detrital origin because the protolith is a clastic metasedimentary rock, and peak P-T conditions (table 1) within this section are below those at which metamorphic zircon typically grow (Vavra and others, 1999). The data set comprises 44 U-Pb analyses on 43 grains including one core-rim pair producing grain-ages ranging from 106 Ma to 2.65 Ga (figs. 10A-C; Appendix A.4). The largest peaks in the grain-age distribution are middle Cretaceous and Early Proterozoic in age. The youngest concordant grain-ages may be used as a proxy for the maximum stratigraphic age of the protolith. These data indicate that deposition of the Kamchatka Schist protolith occurred after 106 Ma (Albian) (Appendix A.4).

Kamchatka Schist (sample 112/11).—This sample was collected from a paragneiss in the Andrianovka drainage. CL images (figs. 11 C-D) reveal a population of zircons with simple internal zoning, but significant textural heterogeneity among grains. In cases where rims were identified using CL, exploratory SHRIMP analysis of core-rim pairs failed to demonstrate an age disparity between these textural domains. Grain-age and textural heterogeneity of the zircon population as a whole indicates a detrital origin

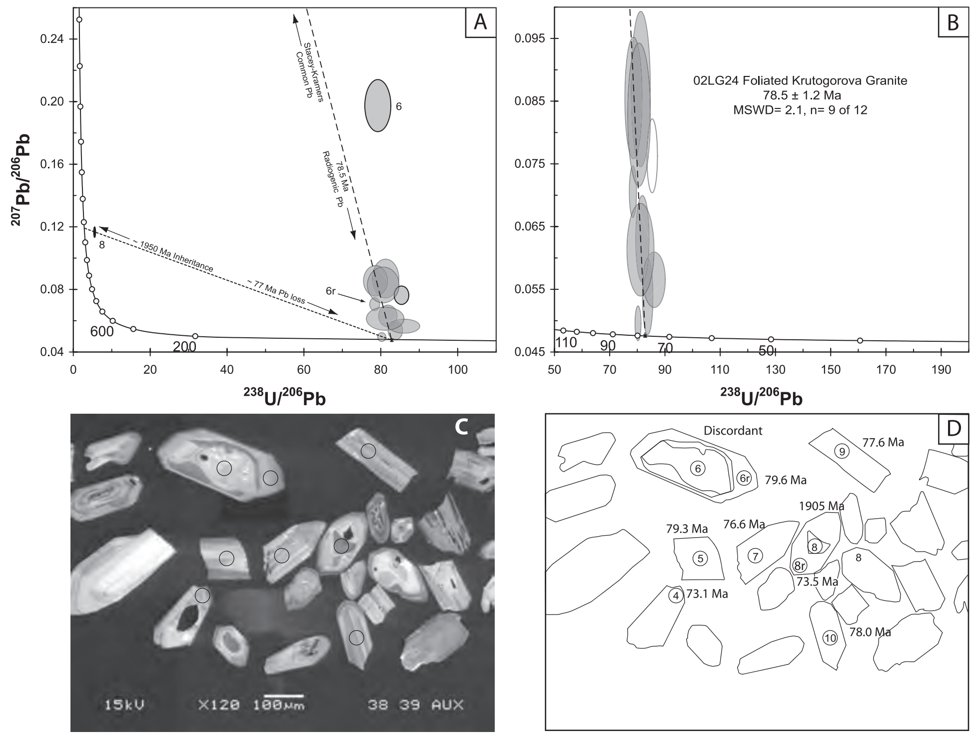

Fig. 9. Single-grain U-Pb data and CL images for zircons from the foliated Krutogorova Granite (sample 02LG24) in the upper Krutogorova watershed. Expanded (A) and focused (B) Tera-Wasserburg concordia diagrams show data defining a linear array of analyses from model common Pb (Stacey and Kramers, 1975) to radiogenic lead at 78.5 ± 1.2 Ma. CL images (C) display relative textural homogeneity, although a few grains do contain apparent inherited cores. Analysis of an apparent core in grain #8 (D) yields a ^{204}Pb-corrected $^{207}Pb/^{206}Pb$ age of 1905 Ma, while the corresponding rim gives a ^{207}Pb corrected $^{206}Pb/^{238}U$ age of 73.5 ± 2.3 Ma (Appendix A.3). The age data are consistent with partial assimilation of Kolpakova gneiss protolith, during pluton emplacement at 78 Ma. The 1.9 Ga grain-age component is well-represented among detrital zircons of the Kolpakova Gneiss and Kamchatka Schist.

(figs. 11 C-D). We performed 54 analyses yielding 47 concordant grain-ages (figs. 11 A, B, and D) from 55.2 ± 3.3 Ma to 2048 Ma, (Appendix A.5) reflecting a heterogeneous sedimentary source region for the protolith of the Kamchatka Schist. The youngest of these grain-ages is associated with low Th/U ratios and high common Pb and is likely metamorphic in origin (Watson and others, 1997). The inferred detrital origin of the next youngest population (~60 Ma; n =5) suggests that the detrital source region included a magmatic arc that was active into the Paleocene. We argue that the youngest concordant grain-ages constrain the maximum stratigraphic age of the sedimentary protolith of the Kamchatka Schist to the Paleocene. Because the age of metamorphism necessarily predates the stratigraphic age of the protolith, our data indicate a significantly younger age estimate for peak metamorphism than that of previous workers (Kuzmin and Chukhonin, 1980; Vinogradov and others, 1991; Vinogradov and Grigor'yev, 1996; Bindeman and others, 2002; Kuzmin and others, 2003).

Protolith Ages: Malka Complex

Left Andrianovka massif syenite intrusions (Samples LA-78, LA-90).—These intrusions represent a local example of zoned mafic-ultramafic intrusions that are found within the Oluytorsky arc terrane along its entire 800 km length (Fleorov and Koloskov,

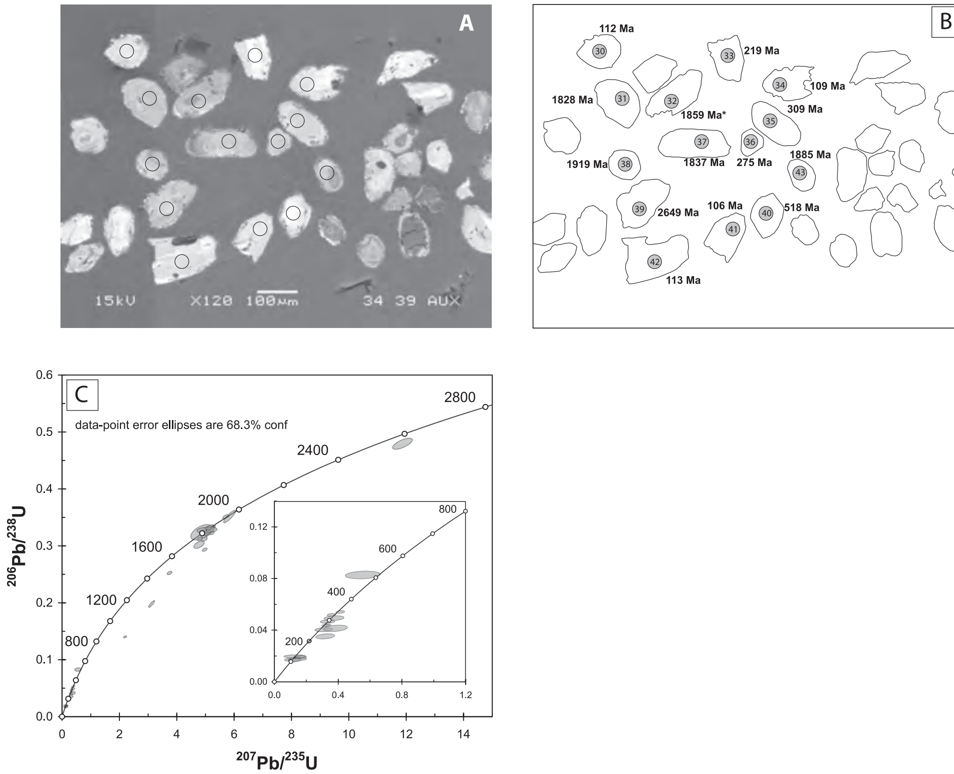

Fig. 10. Wetherill concordia, CL image and summary grain-age diagram for detrital zircons of the garnet-biotite Kamchatka Schist (sample 02AS07) from the upper Krutogorova watershed (fig. 5). (A) CL image showing location of spot analyses, age data are given in Appendix A.4. (B) Rounding is evident in these grains although the crenulate margins of some grains suggest minor dissolution prior to precipitation of zircon overgrowths. (C) Wetherill concordia diagram showing isotopic data. Zircons generally yield concordant grain-ages that range from mid-Cretaceous (106.2 Ma) to Archean (2649 Ma) (see table 5). An Albian maximum stratigraphic age is assigned to the protolith for this unit based on the youngest concordant grain-ages.

1976). Regionally, these intrusive rocks are observed only in the upper plate of the Vatyna and Lesnaya thrusts and thus are interpreted as allochthonous. These rocks are petrologically akin to Alaska-type zoned mafic-ultramafic intrusion on Duke Island, and are commonly interpreted as the magmatic plumbing system to the Olyutorsky Arc (Ledneva and others, 2000). We have already noted that local field relationships indicate that the Left Andrianovka Massif is confined to the Andrianovka schist (fig. 5).

Zircon ages reported here are from two small syenite bodies associated with the massif along the Left Andrianovka River (fig. 5). These data have been published elsewhere (Hourigan and others, 2004), and are summarized here for continuity. Sample LA-78 yielded zircons up to 500 µm in length that exhibit well-defined sector zoning under CL (figs. 12C and 12D). The spread of grain-ages is rather broad with a maximum of 70.4 ± 4.7 Ma and a minimum of 58.9 ± 2.8 Ma producing a weighted mean age of 63.0 ± 1.2 Ma (MSWD = 1.2) for 14 of 15 analyses (fig. 12C; Appendix A.6). Sample LA-90 yielded smaller ~100 µm prismatic zircons with oscillatory CL zoning (figs. 12A and 12B). The data produce a weighted mean ^{207}Pb-corrected ^{206}Pb*/^{238}U age of 70.2 ± 1.4 Ma (fig. 12A, Appendix A.6) for 15 of 15 single grain analyses.

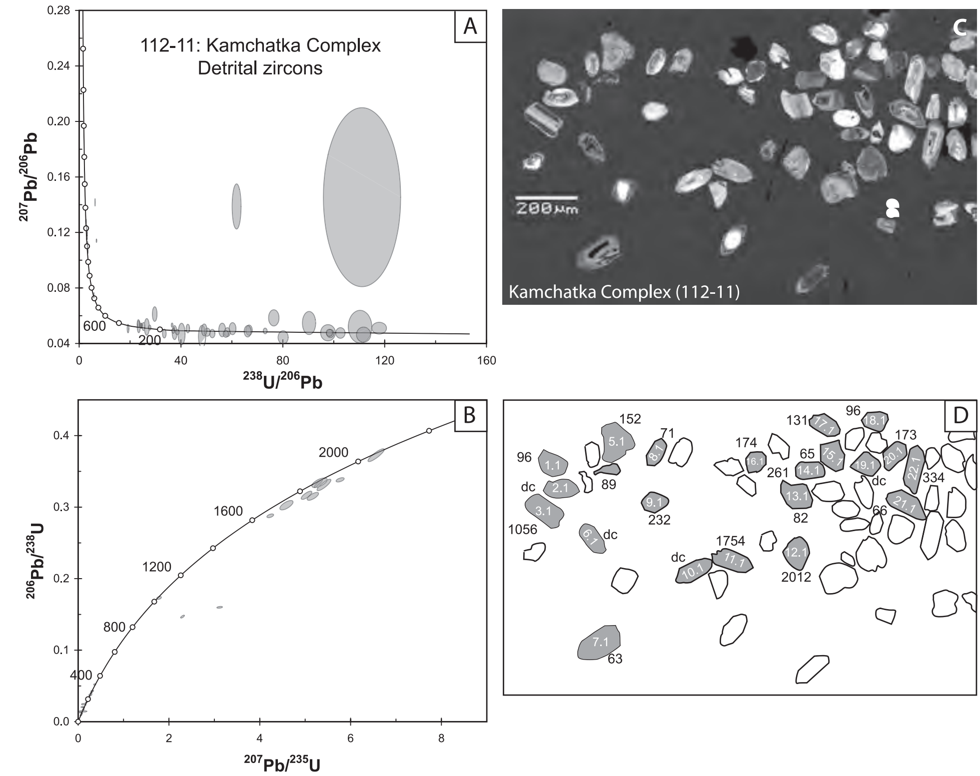

Fig. 11. Tera-Wasserburg (A) and Wetherill concordia (B) plots, CL images (C) and accompanying grain-age summary (D) for zircons from sample 112-11, Kamchatka schist in the Left Andrianovka River region. This sample yielded a texturally (C) and isotopically (Appendix A.5) heterogeneous suite of detrital zircons with concordant (A-B) grain-ages ranging from ~55 to 2048 Ma.

Metamorphic Chronology—Monazite

Monazite is a useful thermochronometer for constraining the thermal history of high-grade metamorphic rocks because of (1) its abundance as a newly formed metamorphic mineral in metasedimentary rocks of garnet-grade and higher (Overstreet, 1967; Smith and Barreiro, 1990; Harrison and others, 1997; Catlos and others, 2002; Harrison and others, 2002), (2) it concentrates Th and U and excludes common Pb (Parrish, 1990), (3) it lacks significant radiation damage (Meldrum and others, 1998) and (4) its high closure temperature (Smith and Giletti, 1997; Cherniak and others, 2004). The nominal closure temperature is a subject of considerable debate with estimates ranging from ~750°C (Smith and Giletti, 1997) to >1000°C (Cherniak and others, 2004) assuming a 10°C/m.y. cooling rate and common crystal sizes (~500µm). These temperatures are considerably higher than estimated peak metamorphic temperatures in the sampling area. As a result, U-Th-Pb ages provide a direct record of the age of metamorphism. In addition, monazite ages are used to constrain the minimum permissible detrital zircon grain-age for Kolpakova paragneiss given that zircons yielding ages concordant with or younger than monazite ages are either metamorphic in origin or have experienced Pb loss during peak metamorphism (for example, Ireland and Gibson, 1998).

Two monazite samples were selected from igneous rocks to date the timing of magma crystallization. The remaining three were taken from high-grade gneiss of the

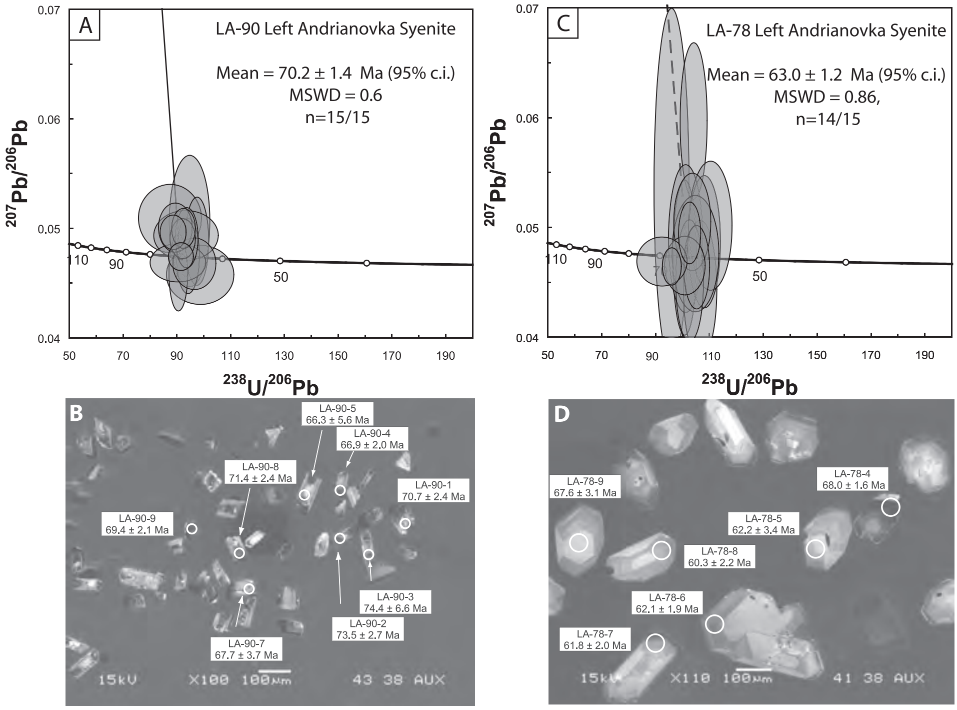

Fig. 12. Tera-Wasserburg concordia plots and CL images with ^{207}Pb-corrected ^{206}Pb/^{238}U grain-ages for texturally representative zircons from syenitic bodies (samples LA-78 and LA-90) within the Left Andrianovka massif, Left Andrianovka River region. Isotopic data are presented in Appendix A.6.

Kolpakova complex. For the migmatitic sample (02JH47), monazite aliquots were taken from both the mesosomal and leucosomal segregations to test for the presence of composite grains with detrital and/or low-grade metamorphic domains. High-gain back-scatter electron (BSE) imaging reveals simple, single-domain monazites with limited textural heterogeneity consistent with a single-stage growth history. The high degree of Th-Pb grain-age reproducibility corroborates this textural interpretation.

We show U-Pb system data in Tera-Wasserburg (^{207}Pb/^{206}Pb vs. ^{238}U/^{206}Pb) space to demonstrate that all samples are simple mixtures of radiogenic and common Pb. However, we cite ^{207}Pb-corrected ^{232}Th-^{208}Pb age data as our preferred ages because they are not complicated by excess ^{206}Pb (Parrish, 1990) and are less sensitive to common Pb corrections because of their high radiogenic ^{208}Pb content.

Kolpakova Gneiss (Samples 02JH47/1 and 02JH47/2).—A large sample (02JH47) of migmatite from the Kolpakova Gneiss was collected at the Krutogorova-Kvakhona Pass (fig. 4) and subsequently trimmed using a rock saw to provide individual separates of the leucosomal (02JH47/1) and melanosomal (02JH47/2) segregations. The melanosome sample (02JH47/2) produced a weighted mean Th-Pb age of 50.6 ± 1.8 Ma for 10 of 10 analyses with an MSWD of 6.0 (Appendix A.7, fig. 13C). Monazite from the leucosome (02JH47/1) yielded a weighted-mean Th-Pb age of 52.4 ± 0.7 Ma for 12 of 12 spot analyses with an MSWD of 0.59 (Appendix A.7, fig. 13B). The U-Pb ages for samples 02JH47/2 and 02JH47/1 are 53.6 ± 1.3 Ma and 54.1 ± 0.50 Ma (Appendix A.7). We favor the Th-Pb age because this system is insensitive to excess ^{206}Pb (see Appendix). In addition, Th-Pb ages are more consistent with the 51.2 ± 0.5 Ma low Th/U ratio, metamorphic zircon overgrowths from the same sample (see below). The

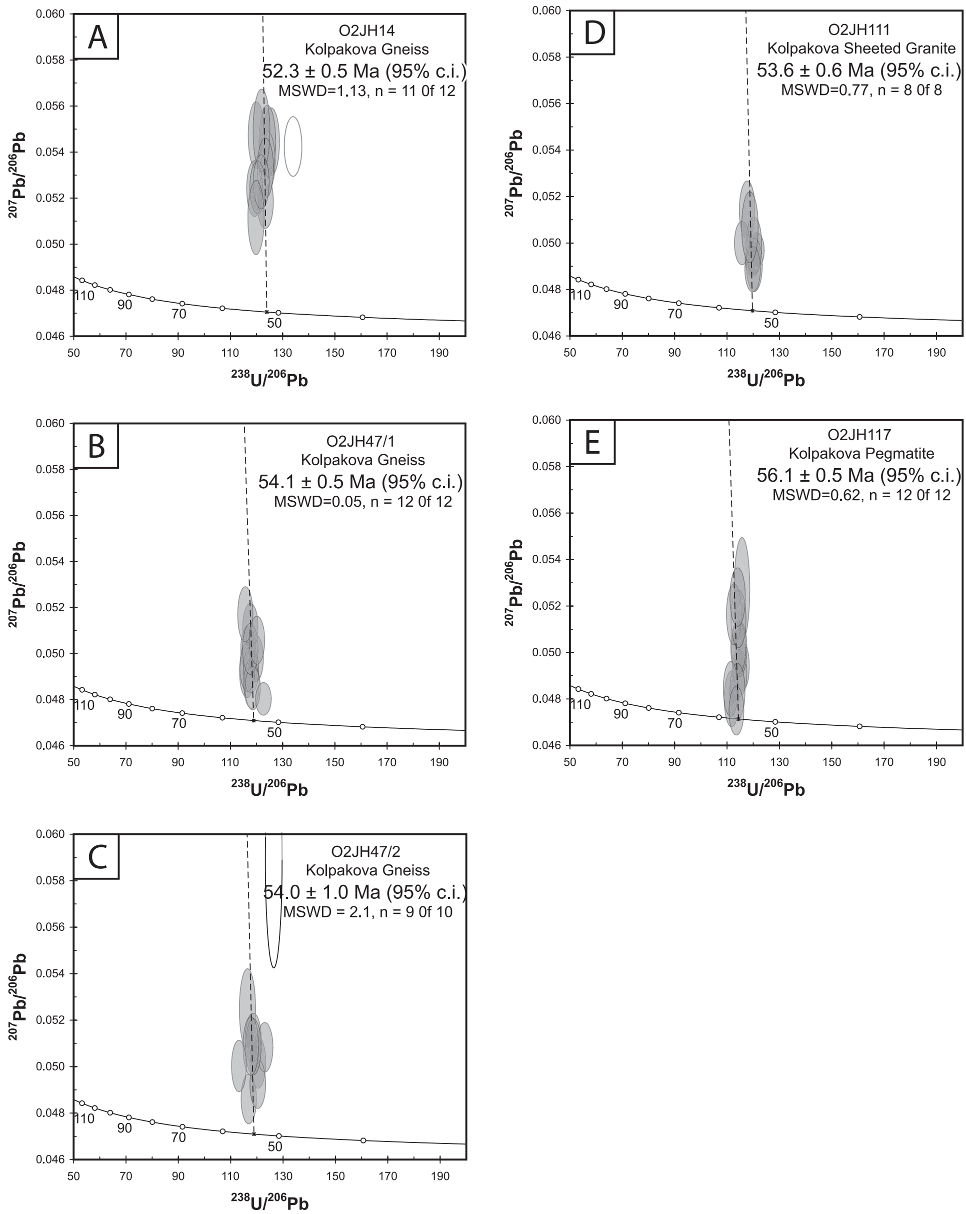

Fig. 13. Tera-Wasserburg concordia plots for 5 monazite samples from the Kolpakova Gneiss in the Krutogorova and Left Andrianovka study areas. Data for all individual analyses define near-concordant linear arrays dispersed along a mixing line from model common Pb (Stacey and Kramers, 1975) and concordia. The plots depict only U-Pb systematics; however, we cite Th-Pb ages in the text and in Appendix A.7. Further explanation of Th-Pb ages preference is given in the Appendix. Plots are shown to demonstrate that the data are best viewed as simple two component mixtures of common and radiogenic Pb with no evidence for inheritance.

Th-Pb ages indicate a geologically plausible thermal history where melt segregation and leucosome formation was synchronous with monazite crystallization and/or cooling from peak metamorphic conditions.

Kolpakova Gneiss, Krutogorova drainage.—Sample 02JH14 was collected from the Krutogorova River region within the Kolpakova Gneiss consisting of plagioclase-bioitite-quartz gneisses. The weighted mean ^{207}Pb-corrected ^{206}Pb*/^{238}U age for 11 of 12 analyses is 52.3 ± 0.5 Ma (2s; MSWD=1.13) (Appendix A.7; fig. 13A). These 11 spot analyses gave a weighted mean ^{207}Pb-corrected ^{208}Pb/^{232}Th age of 50.5 ± 0.7 Ma (Appendix A.7).

Kolpakova Gneiss, pegmatite.—Sample 02JH117 (fig. 5) from the Kolpakova Gneiss is a garnet-muscovite-kspar pegmatite that was slightly boudinaged, but is otherwise internally undeformed, suggesting late syn-kinematic emplacement. The sample yielded voluminous monazite up to 1 mm in diameter. Homogeneous back scatter intensity of individual grains suggests a simple growth history. The Kolpakova pegmatite sample yields a weighted mean age U-Pb of 56.1 ± 0.5 Ma for 12 of 12 individual analyses (Appendix A.7; fig. 13E). The data define a linear array between the Stacey-Kramer common Pb model composition at 56.1 Ma, suggesting that the Pb can be modeled as a simple two-component mixture (fig. 13E). ^{204}Pb-corrected data plot below concordia; the overcorrection is likely related to isobaric interference $^{232}Th^{122}Nd^{16}O_2^{\ 2+}$ at 204 m/e (T. Ireland, 2002, personal communication). Here, again we favor the Th-Pb age of 52.1 ± 0.6 Ma for 12 of 12 spot analyses yielding an MSWD of 0.12 (appendix A.7).

Kolpakova Gneiss, granitic dike.—Sample 02JH111 (fig. 13D) was collected from a shallowly west-dipping granitic dike that cross-cuts the Kolpakova Gneiss sub-parallel to dominant gneissic foliation. Eight spot analyses yield a weighted mean ^{207}Pb-corrected ^{208}Pb/^{232}Th of 51.9 ± 0.7 Ma (2σ, MSWD = 0.25) and a weighted mean ^{207}Pb-corrected ^{206}Pb/^{238}U age of 53.6 ± 0.6 Ma (2σ; MSWD = 0.77) for 8 of 8 analyses (Appendix A.7). This age is compatible with the monazite age from the nearby pegmatitic sample (02JH117).

Metamorphic Geochronology—Zircon

Kolpakova Gneiss, migmatitic paragneiss.—Sample 02JH47/1 was collected from a leucosome in a migmatite in the Kolpakova Gneiss at the same outcrop as sample 02JH47/2 described above. Both sample 02JH47/1 and sample 02JH47/2 exhibit overgrowth textures under CL. Zircon overgrowths in 02JH47/1 are large enough to analyze with a typical SHRIMP beam size of ~30μm without overlapping the core domain or epoxy substrate (figs. 14C-D). Grains are generally characterized by core domains that exhibit discordant CL and resorbed margins mantled by lower CL rims (figs. 14A-C). A few core-rim pair analyses corroborate the inherited nature of the cores (fig. 14A). For example, spots 3C and 3R yield ^{207}Pb-corrected ^{206}Pb*/^{238}U ages of 247.5 ± 7.3 Ma and 51.7 ± 1.6 Ma, respectively (Appendix A.8). Th/U ratios of ~0.01 for these zircon overgrowths is explained by increased U mobility relative to Th in a fluid-rich metamorphic environment and/or co-precipitation of monazite leading to Th partitioning into the phosphate phase. The weighted mean rim age is 51.2 ± 0.5 for 8 of 12 low Th/U rim analyses with an MSWD of 0.97 (fig. 14B). Four data points were rejected as outliers. If all rim analyses are considered the weighted mean age is 51.0 ± 1.7 with an MSWD of 3.0 (Appendix A.8).

Kolpakova Gneiss, Pegmatite (Sample 02JH117).—This sample was taken from a boudinaged garnet-muscovite-K-feldspar pegmatite that intrudes the Kolpakova Gneiss (fig. 5). The pegmatite is interpreted as late to syn-deformational because it occurs as boudins that are aligned parallel to the dominant foliation. The zircons have extremely high U contents (~2,000 ppm to >1 wt. %) and low Th/U ratios (Appendix A.9). The seven low Th/U (<0.1) single-grain analyses produce a weighted mean ^{207}Pb-corrected ^{206}Pb*/^{238}U age of 50.7 ± 1.3 (2σ, MSWD =8.4). The two remaining analyses yield either an older ~64 Ma grain-age (Appendix A.9, #7) or suffer from high common Pb content (#1, fig. 15A). Radiation damage for these grains was likely severe given their high U concentrations making fluid-mediated Pb loss a probable cause of

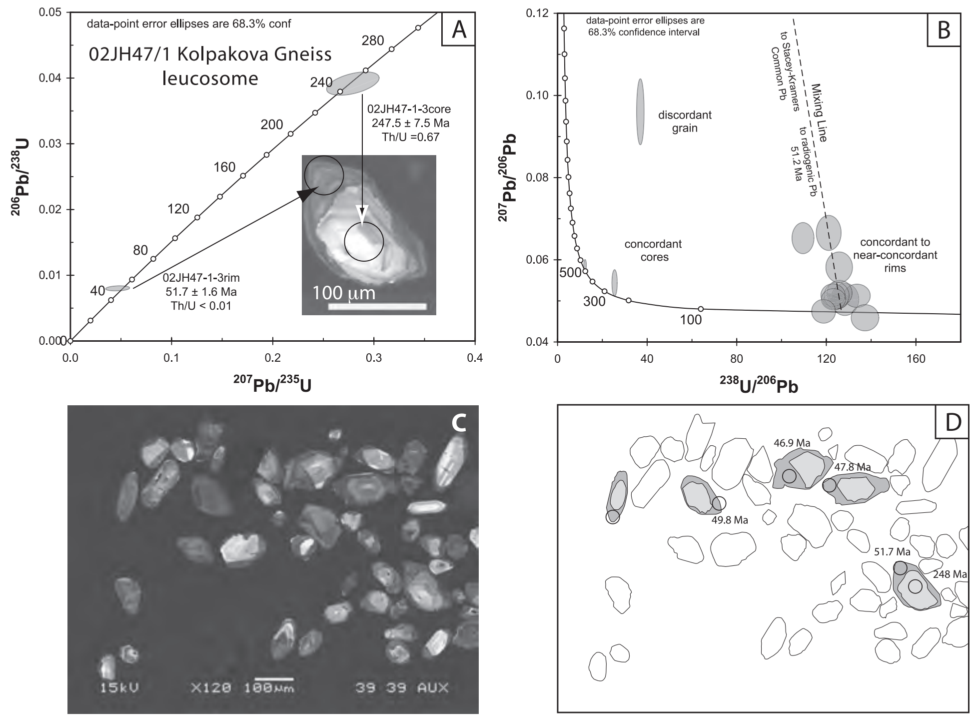

Fig. 14. Plots and CL images for zircons from a leucosomal segregation within the Kolpakova Gneiss (sample 02JH47/1). (A) Wetherill concordia diagram and CL image showing data from a core-rim pair analysis: the core has bright CL with moderate Th/U, crenulate margins and yields a 247 Ma grain-age indicating resorption of a zircon xenocryst; the rim has low CL, low Th/U, is euhedral and yields a 52 Ma grain-age indicating its origin as a metamorphic zircon overgrowth. (B) Analyses of multiple rims (panels C-D) produce a linear mixing array of common Pb and 51.2 ± 0.5 Ma radiogenic Pb. Isotopic data are presented in Appendix A.8.

grain-age scatter. Nonetheless, the pooled ages are consistent with monazite Th-Pb ages for the same sample.

Kolpakova Gneiss, granite dike (sample 02JH111).—We analyzed 14 zircons from the equigranular granite dike in the Left Andrainovka region that cuts the Kolpakova Gneiss subparallel to the dominant gneissic foliation (fig. 5). Unlike the pegmatite, boudinage was not observed at the outcrop scale. High common Pb and U concentrations impart significant complexity to the zircons and likely account for much of the grain-age scatter (fig. 16A, Appendix A.10). Two old grain-ages (93 Ma and 175Ma) indicate the presence of an inherited component, likely incorporated during assimilation. The remaining 12 analyses produce weighted mean ^{207}Pb-corrected ^{206}Pb*/^{238}U age of 52.6 ± 1.2 (2σ, MSWD=6.0). This zircon age is in agreement with both the pegmatite zircon data and monazite Th-Pb ages throughout the Kolpakova Gneiss.

Granite dike within the Kamchatka Schist.—Sample 02AS04 (Appendix A.11; figs. 17A-B) was collected from a granite dike at the contact between the Sredinnyi and Malka Complexes (fig. 4). The dike is composed of equigranular biotite granite with little evidence for deformation other than weak boudinage with maximum extension direction subparallel to mineral stretching lineations in the Kamchatka Schist. Xenoliths of foliated Kamchatka Schist are common. Thus we interpret the dikes to be syn-kinematic, but late with respect to the deformational and metamorphic history of the host rocks. Zircons are generally euhedral with oscillatory CL zonation typical of

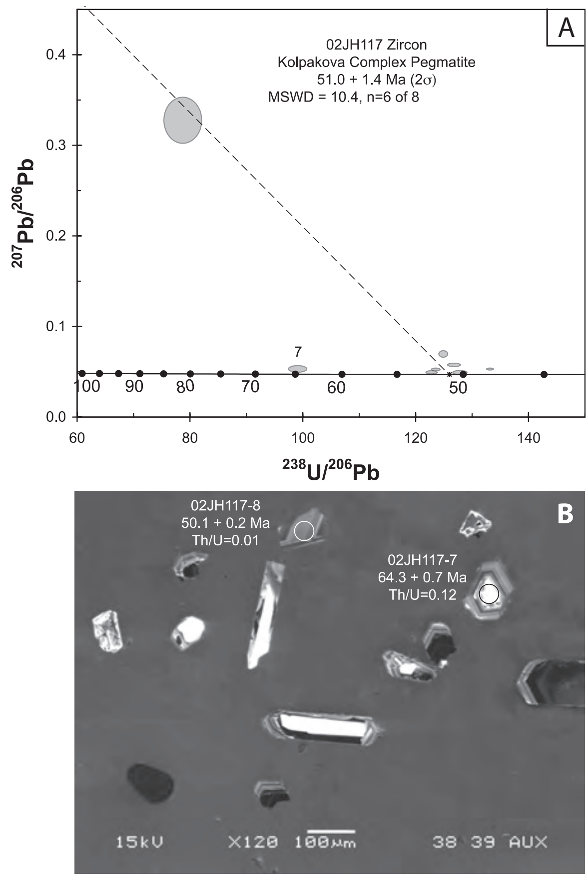

Fig. 15. Tera-Wasserburg concordia plot (panel A) and CL image (panel B) with ^{207}Pb-corrected ^{206}Pb/^{238}U grain-ages for analyzed representative zircons from a boudinaged garnet-muscovite-Kspar pegmatite (sample 02JH117) within the Kolpakova Gneiss in the Left Andrianovka region. The data exhibit considerable scatter despite textural heterogeneity, perhaps due to Pb loss caused by radiation damage in very high U zircons (Appendix A.9).

magmatic zircons (fig. 17B). Thirteen of 13 analyses produce a weighted mean ^{207}Pb-corrected ^{206}Pb*/^{238}U age of 51.5 ± 0.7 Ma with an MSWD of 0.27 (Appendix A.11). Despite high common Pb contents (up to 10.8 %) for several grains, the mean age is robust because the data produce a well-defined mixing array between model common Pb (Stacey and Kramers, 1975) and 51.5 Ma radiogenic Pb components.

Overlap Sequence—Zircon Geochronology

The Baraba Conglomerate unconformably overlies lower greenschist-facies metasedimentary rocks of the Malka Complex (Kheivan and Khimka units) (figs. 2 and 18). Above, we summarize previous work that inferred a Campanian-Maastrichtian depositional age (Shantser and Chelebaeva, 2004), which would imply that metamorphism of the Malka Complex was Cretaceous or older (Shapiro and others, 1986).

Tuffaceous member, Baraba Conglomerate.—Sample 01JG-11 was collected from a 10 m-thick tuffaceous horizon at the base of the Baraba unit at its type-locality on Baraba Mt. (figs. 2 and 18) where the unconformity is well-exposed. The separate contains euhedral, oscillatory-zoned zircons ranging from 75 to ~200 µm in length (fig. 19B).

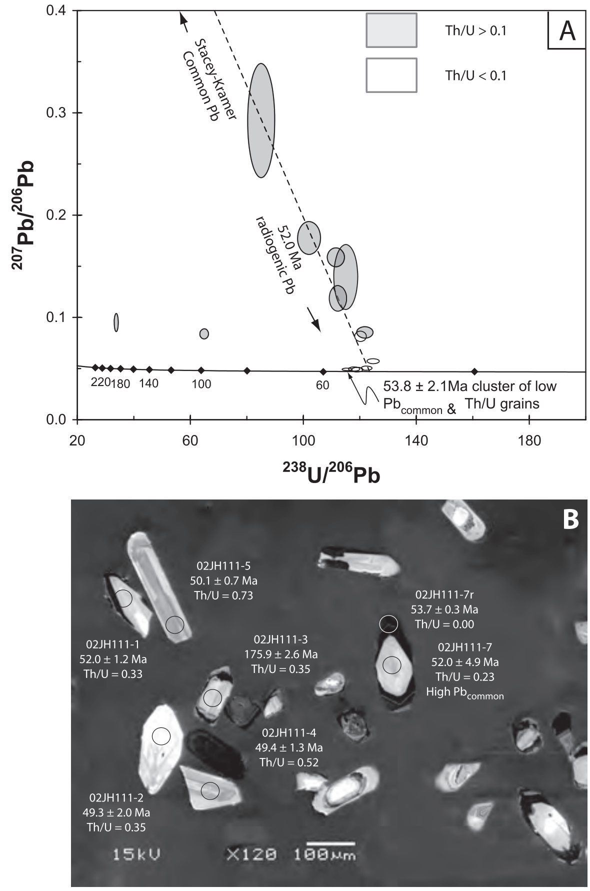

Fig. 16. Tera-Wasserburg concordia plot (panel A) and CL image (panel B) with ^{207}Pb-corrected ^{206}Pb/^{238}U grain-ages for analyzed representative zircons from granite intrusion (sample 02JH111) within the Kolpakova Gneiss in the Left Andrianovka region. The data exhibit considerable complexity and three populations can be identified: 1) a high common Pb, moderate Th/U population with a ~52 Ma weighted mean ^{207}Pb-corrected ^{206}Pb/^{238}U ages; 2) a low common Pb, low Th/U, high U rims with a 53.8 ± 2.1 Ma age; and 3) two zircon with low common Pb, moderate Th/U that plot off the radiogenic-common Pb mixing line interpreted as discordant xenocrystic cores (Appendix A.10).

Thirteen of 16 zircon spot analyses gave concordant results (fig. 19A) consistent with a single population of zircons with a ^{207}Pb-corrected ^{206}Pb*/^{238}U age of 51.5 ± 0.5 Ma (Appendix A.12). These new data demonstrate Early to Middle Eocene age for the base of the Baraba section, which is fully consistent with the metamorphic ages for the underlying Sredinnyi and Malka Complexes.

Detrital Zircon Reference Samples

U-Pb zircon grain-ages data from the Kolpakova Gneiss (samples 02JH48 and 02JH47/2) and Kamchatka Schist (samples 112/11 and 02AS07) suggest maximum stratigraphic ages of mid-to Late Cretaceous and Paleocene, respectively. Our working hypothesis is that the Sredinnyi Complex is made up of Cretaceous-Paleocene sediments derived from northeast Russian margin that were metamorphosed in the Eocene during arc-continent collision. To test this hypothesis, we compare our zircon grain-age distributions for the Sredinnyi Complex with new U-Pb zircon grain-age data

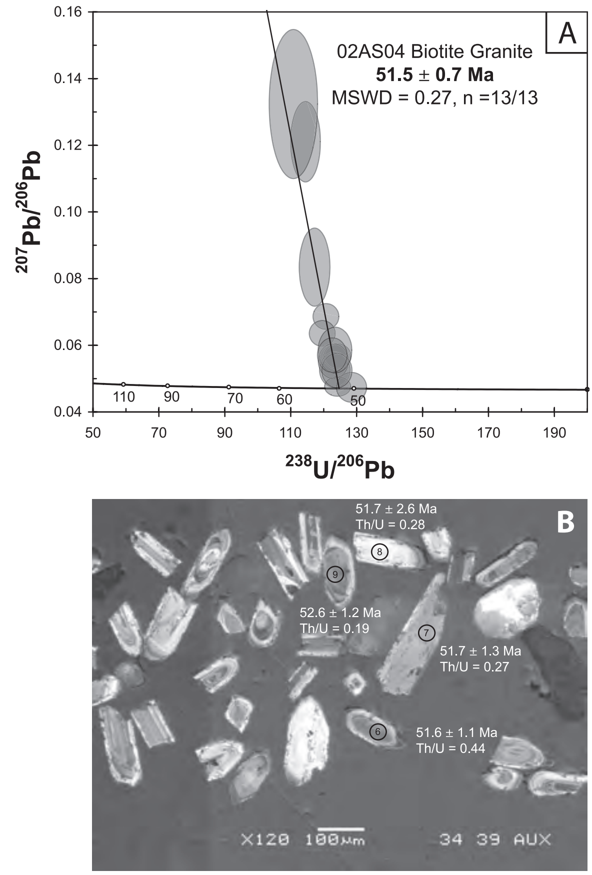

Fig. 17. Tera-Wasserburg concordia plot (panel A) and CL image (panel B) with ^{207}Pb-corrected ^{206}Pb/^{238}U grain-ages for analyzed representative zircons from a late syn-kinematic equigranular granite (Sample 02AS04) which stitches the Andrianovka Suture in the Krutogorova river region. Isotopic data are presented in Appendix A.11. The zircons yield a weighted mean ^{207}Pb-corrected ^{206}Pb/^{238}U age of 51.5 ± 0.7 Ma coeval with peak condition and anatexis at deeper structural levels.

from northeast Russian continental marginal sediments of similar inferred depositional age.

The Ukelayat Group, and its correlatives: the Lesnaya and Khozgon Groups, contain thick marine clastic sequences, mainly turbidites, that accumulated along the northeast Asian margin prior to the collision of the Olyutorsky island-arc terrane (Shantser and others, 1985; Garver and others, 2000a; Solov'ev and others, 2001). After the onset of collision this sedimentary sequence continued to accumulate in front of a west-vergent Olyutorsky thrust sheet. Sandstone petrography (Bullen, ms, 1997) and complementary detrital zircon fission-track (FT) grain-ages (Garver and others, 2000a; Solov'ev and others, 2001) show that Ukelayat sandstones were derived from a continental-arc source.

Khozgon and Ukelayat group detrital zircons.—We measured U-Pb ages for detrital zircons from two representative sandstone samples for comparison with Sredinnyi Complex detrital zircon ages. The first sandstone sample (sample 02JH87) was collected from a fault-bound sliver of the Khozgon Group on the eastern flank of the Sredinnyi Range (fig. 5). Thirty-two zircons were analyzed yielding ages from 52.7 ±

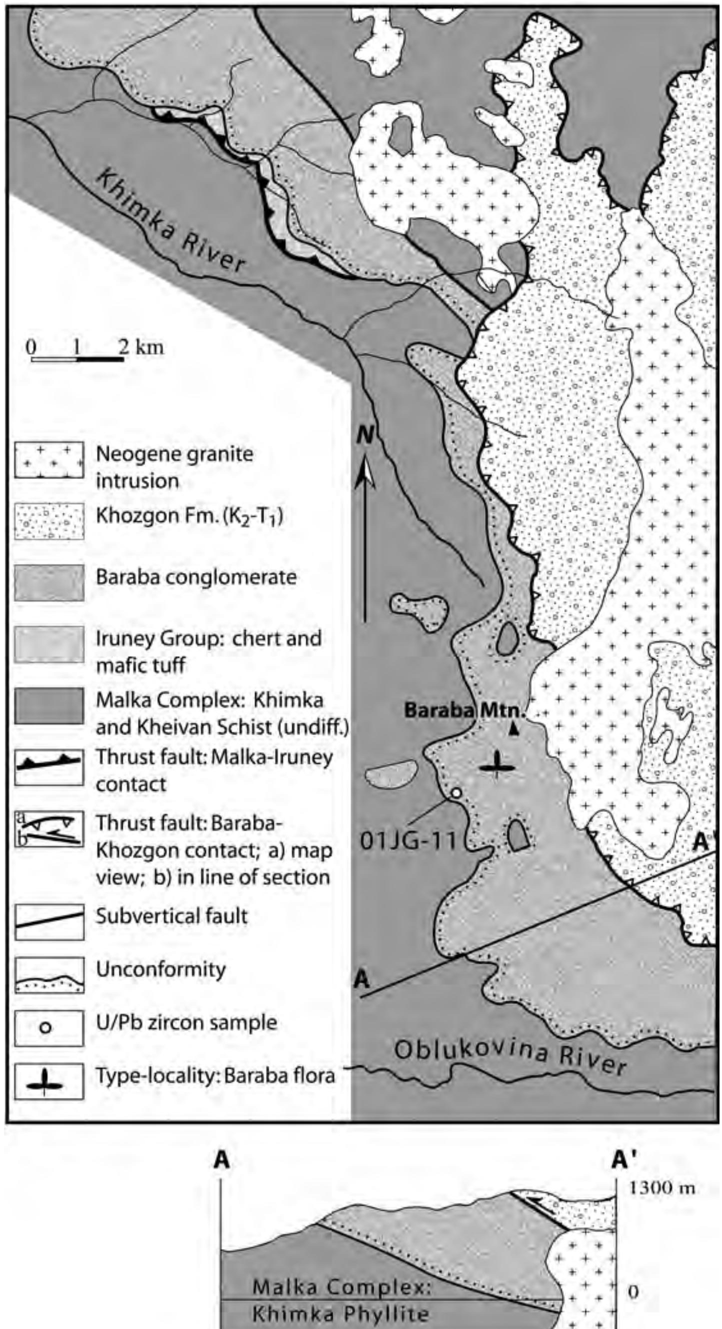

Fig. 18. Simplified geologic map and cross-section of the Baraba Mountain region (Soloviev and others, 2004). The unconformity between phyllites of the Malka Complex and the unroofing sequence of the Baraba conglomerate provides an important age constraint on metamorphism. Based on floral stratigraphy the Baraba conglomerate has traditionally been assigned a Campanian-Maastrichtian age (Shapiro and others, 1986). A 50.5 ± 1.2 Ma U-Pb zircon age from a basal tuff horizon indicates deposition occurred after the Early Eocene.

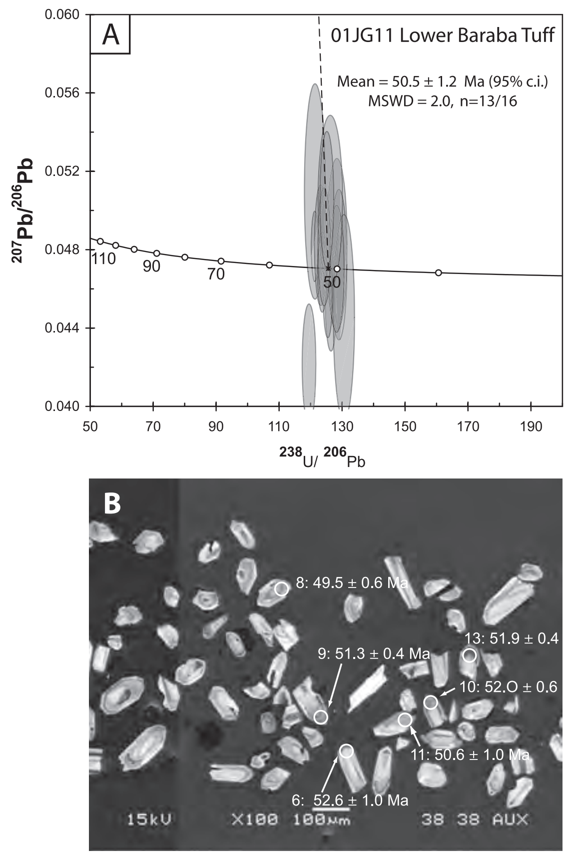

Fig. 19. Tera-Wasserburg concordia plot (panel A) and CL image (panel B) with ^{207}Pb-corrected ^{206}Pb/^{238}U grain-ages for analyzed representative zircons from the lower tuffaceous member of the Baraba Conglomerate (sample 01JG11) which unconformably overlies low greenschist facies rocks of the Malka Complex. Isotopic data are presented in Appendix A.12. The zircons yield a weighted mean ^{207}Pb-corrected ^{206}Pb/^{238}U age of 50.5 ± 1.2 Ma indicating that exhumation of Malka Complex rocks was nearly synchronous with peak conditions at depth.

5.4 to 1970.4 ± 21.9 Ma (Appendix A.13). The grain-age data are complicated by significant common Pb, which produced a high degree of discordance for most analyses (fig. 20A). We note that the R33 standard on this mount exhibited low ^{204}Pb count rates and good reproducibility suggesting that common Pb is intrinsic to the detrital sample and not related to surface contamination. The presence of common Pb, rather than inheritance-related discordance, is confirmed by higher-than-normal count rates on ^{204}Pb. ^{204}Pb-corrected data are largely concordant (fig. 20B); however precision of the ages is reduced because of the larger uncertainties associated with ^{204}Pb measurement.

The second sandstone sample is from the Ukelayat Group (sample 95JG-16), collected along the Matysken River in the Southern Koryak Highlands (fig. 1). Unreset detrital zircon FT ages for this sample constrain the maximum depositional age to be Paleocene or Eocene (Garver and others, 2000a). U-Pb SHRIMP ages from 50 detrital zircons yielded 45 concordant to near-concordant U-Pb grain-ages ranging from 56 Ma to 2077 Ma (fig. 21, Appendix A.14). An additional 5 grain-ages were rejected because of significant discordance.

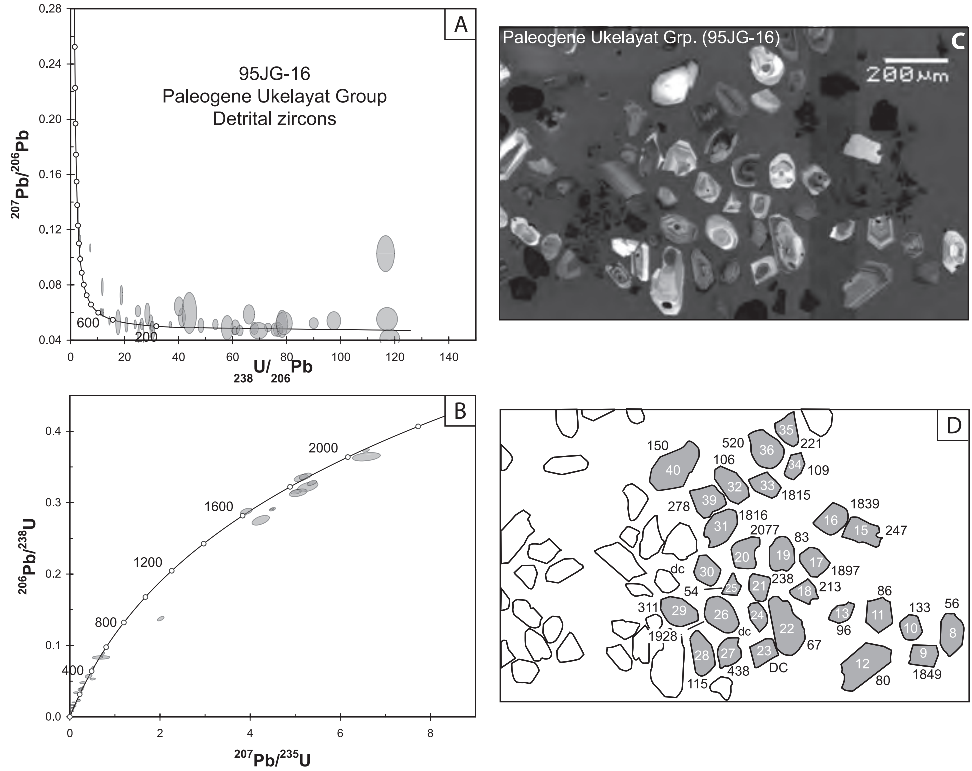

Fig. 20. Tera-Wasserburg (panel A) and Wetherill concordia (panel B) plots, CL images (panel C) and accompanying grain-age summary (panel D) for zircons from the Early Tertiary (Paleogene?) Khozgon Formation in the Left Andrianovka region (fig. 5). Zircons in this sample are complicated by high common Pb values not seen in the standard grains on the same mount indicating that the Pb is intrinsic to the sample. Uncorrected data appear highly discordant on Tera-Wasserburg (A) but plot as concordant ^{204}Pb-corrected analysis in Wetherill concordia space (B). All ages reported are ^{204}Pb-corrected $^{206}Pb/^{238}U$ ages because of the high common Pb. Grain-ages range from 53 to 1970 Ma. (Appendix A.13)

A detailed comparison of U-Pb grain-ages and textures from the Khozgon, Ukeleyat and Sredinniy Complex sample indicates striking similarity between these zircon populations. For instance, cathodoluminescence images of Kamchatka Schist (fig. 11), Khozgon sandstone (fig. 20) and the Ukelayat sandstone (fig. 21) zircon exhibit relatively simple, typically oscillatory internal zonation, and large grain-to-grain CL variability as would be expected for a detrital sample. The probability density plots shown in figure 22 are a useful comparison of the U-Pb grain-ages. In common, the Kamchatka Schist, and Ukelayat and Khozgon samples show a cluster of early Cenozoic (~55 Ma) through early Mesozoic (~150 Ma) ages and a broad Early Proterozoic peak at around 1.9 Ga. This 1.9 Ga peak shows up in all of the metamorphic rocks and sedimentary rocks.

Cumulative probability plots are shown for the two Kamchatka Schist and Ukelayat Group samples because these data sets contain the largest number of concordant grain-ages (fig. 23). The Kolmogorov-Smirnov (KS) test is used here to assess the similarity of the grain-age distributions (fig. 23) for the Kamchatka Schist and Ukelayat Group (95JG-16) samples; these samples were chosen because they have the largest number of grain-ages. The K-S statistic is a non-parametric method for comparing cumulative probability distributions (Press and others, 1992). The

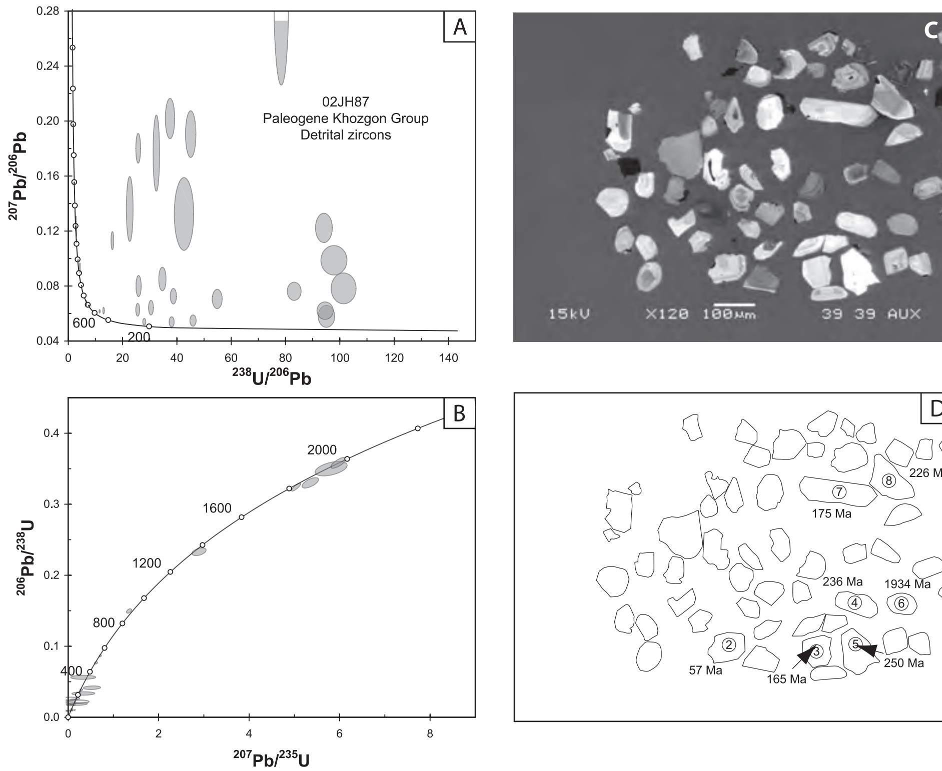

Fig. 21. Tera-Wasserburg (panel A) and Wetherill concordia (panel B) plots, CL images (panel C) and accompanying grain-age summary (panel D) for zircons from the early Tertiary (Paleogene?) Ukelayat flysch in the Koryak Highlands (fig. 1). This sample yields a texturally (C) and isotopically (Appendix A.14) heterogeneous suite of detrital zircons with concordant (A-B) grain-ages ranging from ~54 to 2077 Ma.

degree of misfit between the two distributions is measured by the maximum vertical separation (in percentage) between the cumulative probability plots. P(KS) gives the probability that the difference between samples are due to random sampling of the same parent populations. For our case, a P(KS) result of 46 percent suggests that the difference between Ukeleyat Group sandstone and Kamchatka Schist zircon grain-age distributions could be due to random chance alone.

In practical terms, the similarity of grain-age distributions suggests that the Kamchatka Schist and the Ukelayat Group shared a common sedimentary source region. The presence of Early Proterozoic zircons indicates that the source region likely included the Siberian Craton, which shows a distinctive peak in magmatic activity at 1900 Ma (Rosen, 2002). The northeast Russian margin has a long history island arc and continental margin arc magmatism that can account for the observed Mesozoic and Paleozoic zircon ages (see reviews in Zonenshain and others, 1990; Miller and others, 2002) In particular the Cretaceous-early Cenozic grain-ages can be explained by local sources. The Okhotsk-Chukotka Volcanic Belt was active from about 105 to 80 Ma (for example, Hourigan and Akinin, 2004). Magmatism within the Sikhote-Alin Arc to the south and scattered volcanic rocks in the Koryak Highlands (Ledneva and others, 2006) both show activity into the early Cenozoic. These sources may account for the zircons in the 150 to 55 Ma range.

Upper Cretaceous to early Cenozoic continental margin turbidites are exposed continuously along the western flank of the Kamchatka Peninsula and north into the

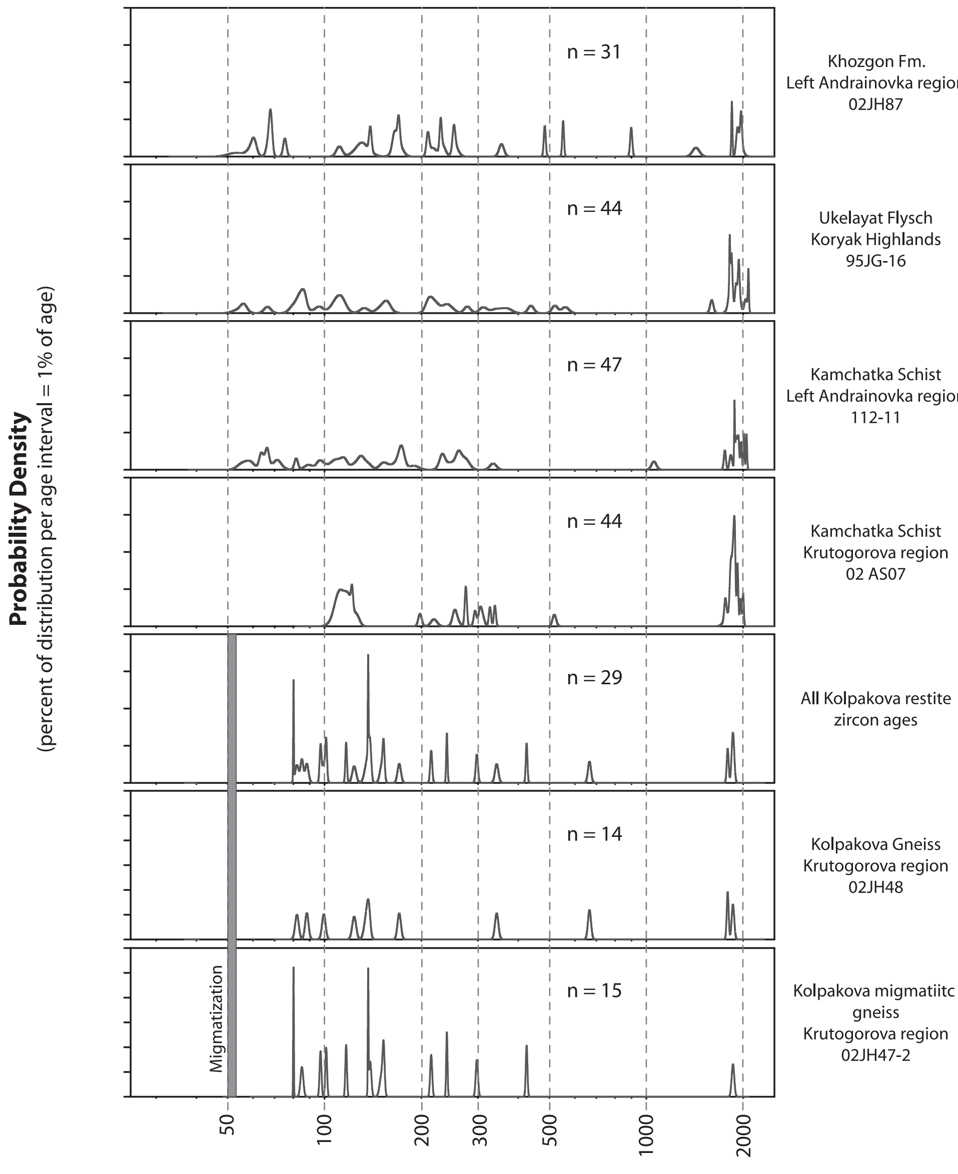

Fig. 22. Probability density plots for all detrital and metasedimentary zircon grain-ages. The age data are in log scale. A log-normal Gaussian kernel algorithm with an $\alpha = 0.6$ (Brandon, 1996) is used for the construction of grain-age probability density (PD) plots. PD plots are shown on log scale to accommodate the broad age range exhibited by these samples.

Koryak Highlands. The detrital zircon distribution in these units appear to be fairly uniform along the length of the basin (Garver and others, 2000a). Thus, the available evidence support the hypothesis that the Kolpakova and Kamchata units in the Serdinnyi Range represent metamorphosed sediments of the NE Asian continental margin.

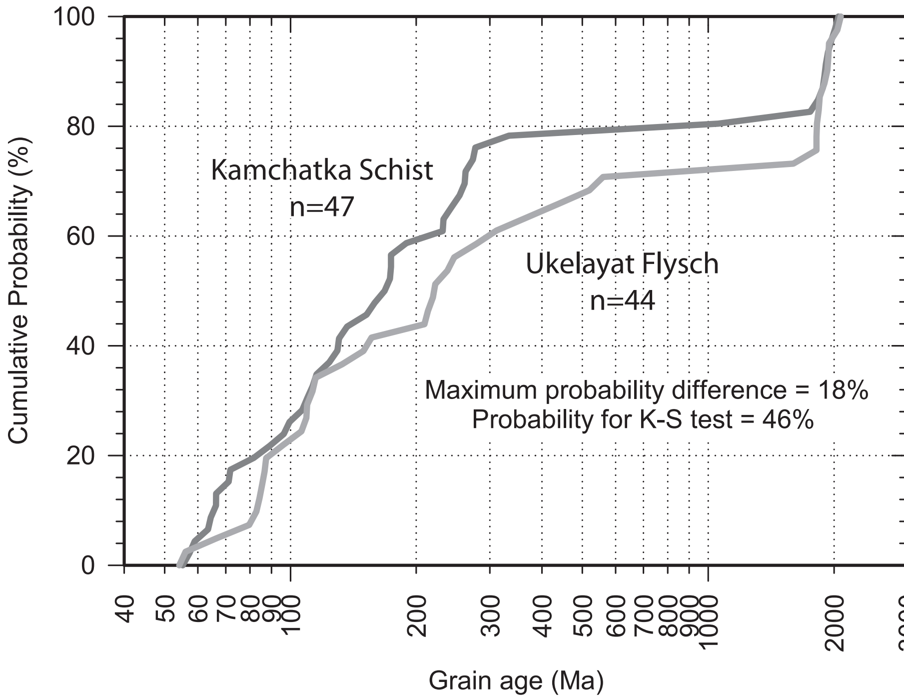

Fig. 23. Comparison of cumulative probability distributions for U-Pb grain-ages of the Kamchatka Schist and Ukelayat Group samples. The Kolmogorov-Smirnov statistic (P(KS)) is a nonparametric test of the degree of misfit of two independent populations. Here P(KS) = 46% indicates the probability that the difference between the two distributions might occur by chance alone.

These results are unexpected given that previous work had indicated a Precambrian age for the protolith and a Cretaceous age for metamorphism. A short discussion of this disparity is thus warranted. For example, Kuzmin and Chukhonin (1980) argued for a Proterozoic age for the Kolpakova Gneiss. They used ^{207}Pb/^{206}Pb results to date samples with multiple zircons. Thus, one would expect that their "bulk age" estimates should be equivalent to the weighted mean of our grain-age results. Consider a group of $i = 1$ to n U/Pb zircon grain ages, where all grains have similar mass. The bulk ^{207}Pb/^{206}Pb age is given by,

$$\frac{^{207}Pb}{^{206}Pb}_{bulk} = \sum_{i=1}^{n} \frac{(Pb_i^*)(^{207}Pb_i/^{206}Pb_i)}{\sum_{i=1}^{n}(Pb_i^*)},$$

where, for a given analysis, Pb^*_i and $^{207}Pb_i/^{206}Pb_i$ are a concentration of radiogenic lead and measured isotopic ratio, respectively. A "model" multigrain ^{207}Pb/^{206}Pb analyses of the Ukelayat (95JG16) sample and the Kamchatka Schist sample (112/11) would yield ages of 1.66 Ga and 1.73 Ga, respectively. While Early Proterozoic grains make up only a small fraction of the total grain-ages, their high concentration of radiogenic lead substantially biases multigrain analyses toward old ages. Thus old Pb-Pb and U-Pb data can be used to infer substantial inheritance, but do not reveal protolith ages.

Vinogradov and others (1988, 1991) and Vinogradov and Grigor'yev (1996) report many whole rock isochrons that suggest Cretaceous metamorphic ages for the Sredinnyi Range. These estimates are significantly older than our U-Pb zircon and Th-Pb monazite ages. We suspect that the Rb-Sr data yield "errorchrons" resulting from incomplete resetting of an isotopically evolved sedimentary protolith (Dickin, 1997). The applicability of the whole-rock isochron method for constraining metamorphic age of metasediments is predicated on complete Sr isotopic equilibration over the sampling volume during peak metamorphic conditions. However, the length-scale of Sr isotopic equilibrium is often significantly smaller than the volume over which sampling occurs, even under magmatic conditions (Roddick and Compston, 1977). Biotite-whole rocks pairs, however, yield Eocene ages (Vinogradov and others, 1991) that are consistent with our new results suggesting that isotopic equilibrium was achieved at the scale of a hand sample.

Bindeman and others (2002) argue for a Late Cretaceous metamorphic age based on a high frequency of 78 Ma grain-ages for euhedral, oscillatory-zoned rims enveloping texturally distinct cores. We argue that these ages may have been derived from the Krutogorova Granite, which yields a 78 Ma weighted-mean age for oscillatory zoned rim domains and exhibits abundant evidence for inherited cores. Given their sampling methodology, orthogneiss (foliated Krutogorova Granite) samples may have been included as Kolpakova Gneiss. The Krutogorova Granite sample has an order of magnitude more zircon grains per unit volume than Kolpakova Gneiss samples we have processed. This may account for the common occurrence 78 Ma grain-ages within the composite sample of Bindeman and others (2002).

Post Metamorphic Cooling

Published and new thermochronology are used to constrain the history of post-metamorphic cooling. Vinogradov and others (1991) and Vinogradov and Grigoriev (1996) present Rb/Sr mineral isochron data for the Sredinnyi Range. Unlike the whole-rock isochron method, which assumes complete isotopic re-equilibration over the entire sampling volume, the mineral isochron method requires equilibration at the hand sample scale. We recalculate isochrons from biotite-whole rock pairs using data reported by Vinogradov and others (1991); three samples yield isochron ages from 56.2 to 51.2 Ma. Vinogradov and Grigor'ev (1996) report a biotite-only isochron from a larger suite of hand samples ($n=7$) that yields a 47 ± 2 Ma isochron.

Bondarenko and others (1993) report a Rb-Sr mineral isochron age of 48 ± 3 Ma for a "garnet plagiogranite" hosted in the Kamchatka Schist, located about 35 km to the north of the Left Andrianovka study area. The rock is dominated by plagioclase with minor amphibole, garnet, and biotite. In this case, biotite exerts the largest control on the slope of the isochron. Where biotite is present in minor amounts, work by Jenkin and others (1995, 2001) suggests a closure temperature of 350 ± 50°C. We use this age in our time-temperature diagram (fig. 24; Bondarenko and others, 1993) because this sample is closest to our Left Andrianovka study area and was collected at a similar structural level.

Fleorov and Koloskov (1976) report a 48 ± 2 Ma biotite K-Ar age from a biotite pyroxenite of the Left Andrianovka Massif. This intrusion is restricted to the Malka Complex whereas the garnet plagiogranite of Bondarenko and others (1993) cuts the upper part of the Sredinnyi Complex.

One Kamchatka Schist sample (112-11) gives zircon and apatite FT ages of 23.5 ± 2.9 Ma and 14.6 ± 3.4 Ma, respectively. Apatite and zircons from syenite within the

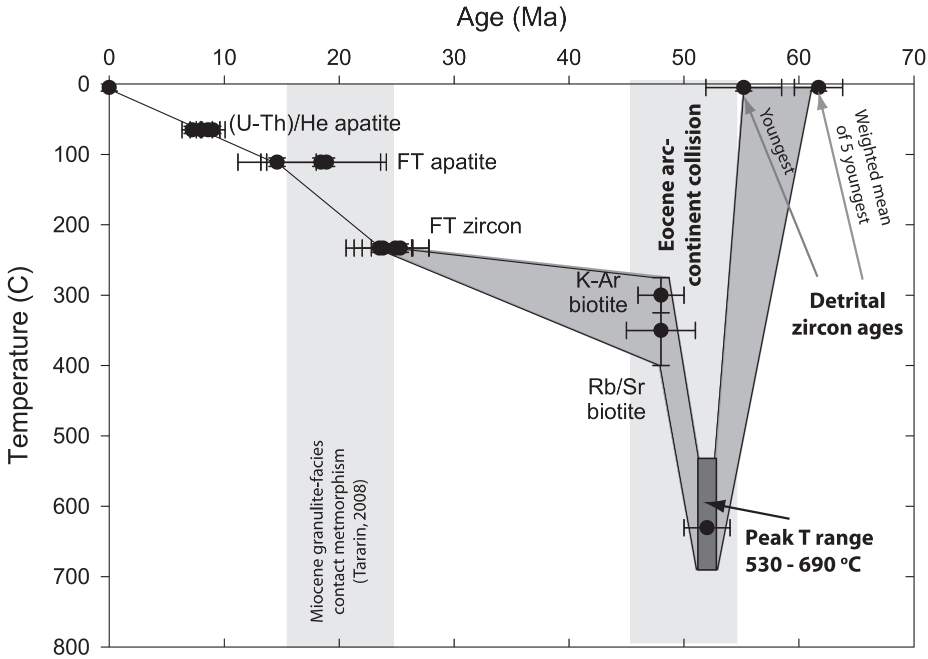

Fig. 24. Time-temperature history for Sredinnyi Complex. Data sources used for construction of this plot are given in table 3. Subduction and metamorphism of sediments as young as Paleocene in age resulted in high-grade metamorphism and migmatization at the deepest exposed structural levels. This high-grade event is well-constrained by monazite and zircon geochronology at ~52 Ma. Temperatures and pressures are from this study (after Khanchuk, 1985) and Tararin (2008). Cooling of core rocks to below ~300°C appears rapid. Low-temperature thermochronometry indicates that subsequent cooling proceeded more slowly.

Left-Andrianovka massif give 25.3 ± 2.5 Ma (LA-78), 24.9 ± 2.9 Ma (LA-90), and 23.8 ± 2.5 Ma (LA-90a) zircon FT ages and 18.9 ± 5.2 Ma (LA-78) and 18.4 ± 5.2 Ma (LA-78) apatite FT ages (table 3; fig. 24). Assuming ~10°C/m.y. cooling rate and typical annealing properties we estimate an effective FT closure temperature of 225 to 240°C for zircon (Brandon and Vance, 1992) and 105 to 117°C for apatite (Laslett and others, 1987). Apatites from the Left-Andrianovka intrusion yield (U-Th)/He ages ranging from 7.2 ± 0.9 Ma to 9.0 ± 1.1 Ma (table 3; fig. 24). Assuming cooling rates of ~10°C/m.y., we estimate an apatite (U-Th)/He closure temperature of 65 ± 5°C (Farley, 2000).

Discussion

Timing of Collision, Metamorphism and Exhumation

Geochronologic and thermochronologic data (table 3) are used to construct schematic sections (fig. 25) and a time-temperature path (fig. 24) for the Sredinnyi Complex on the east flank of the Sredinnyi Range. The youngest detrital zircons from metasedimentary rocks indicate Cenomanian and Paleocene maximum depositional ages for Kolpakova Gneiss and Kamchatka Schist, respectively. These estimates are consistent with the 78 Ma intrusive age of the Krutogorova Granite, which cross-cuts the Kolpakova Gneiss but is not observed in the Kamchatka Schist. Zircons with ~96 Ma grain-ages from the southern part of the Sredinnyi Range (Bindeman and others,

Table 3

Temperature-time plot data summary

Sample	Unit	Data Type	Date	Source	Temperature	Reference
LA-78--He$_1$	LA Massif (Andrianovka)	Apatite (U-Th)/He	7.2 ± 0.9 Ma	This study	65 ± 5 ºC	Farley, 2000
LA-78--He$_2$	LA Massif (Andrianovka)		8.0 ± 1.0 Ma			
LA-90--He$_2$	LA Massif (Andrianovka)		8.6 ± 1.0 Ma			
LA-90--He$_1$	LA Massif (Andrianovka)		9.0 ± 1.1 Ma			
LA78-FTA	LA Massif (Andrianovka)	Apatite FT	18.4 ± 5.2 Ma	This study	111 ± 6 ºC	Laslett and others, 1987
LA90-FTA	LA Massif (Andrianovka)		18.9 ± 5.2 Ma			
112-11-FTA	Kamchatka		14.6 ± 3.4 Ma			
LA90A-ab-FTZ	LA Massif (Andrianovka)	Zircon FT	23.8 ± 2.5 Ma	This study	233 ± 6 ºC	Brandon and Vance, 1992
LA90ab-FTZ	LA Massif (Andrianovka)		24.9 ± 2.9 Ma			
LA78ab-FTZ	LA Massif (Andrianovka)		25.3 ± 2.5 Ma			
112-11-FTZ	Kamchatka		23.5 ± 2.9 Ma			
LA Massif biotite pyroxenite	LA Massif (Andrianovka)	Biotite K-Ar	48.0 ± 2.0 Ma	Fleorov and Koloskov, 1976	300 ± 25 ºC	McDougall and Harrison, 1999
Garnet plagiogranite (w/biotite)	Kamchatka-Andrianovka contact	Rb-Sr mineral isochron	48.0 ± 3.0 Ma	Bondarenko and others, 1993	350 ± 50 ºC	Jenkin and others, 1995, 2001
112/11	Kamchatka	Youngest concordant grain-age	55.2 ± 3.3 Ma	This study	5 ± 5 ºC	This study
	Kamchatka	Youngest 5 grains-ages	61.7 ± 2.1 Ma	This study	5 ± 5 ºC	This study
Peak Conditions	Kolpakova	Metamorphic thermometry	52.0 ± 2.0 Ma	This study	530 -690 ºC	This study after Khanchuk, 1985; Tararin, 2008

Summary of geochronologic and thermochronologic data used to construct a time-temperature history plot shown in figure 25.

2002) also corroborate the Late Cretaceous depositional age that we assign to the Kolpakova Gneiss.

Metamorphism must be younger than the ~60 Ma age of the youngest detrital zircons in the Kamchatka Schist (sample 112-11). Zircon overgrowths from a leucosomal segregation, fine-scale rims on zircons from melanosomes, and monazite ages indicate that peak metamorphic conditions, including anatexis, were achieved by ~52 ± 2 Ma (fig. 24). Zircons from a cross-cutting pegmatite and a granite intrusion yield U-Pb data, indicating that magmatism and metamorphism were coeval. At higher structural levels, a late syn-kinematic granite (sample 02AS04) that stitches the Andrianovka suture yields a U-Pb zircon age of 51.5 ± 0.7 Ma.

A 50.5 ± 1.2 Ma zircon U-Pb age for a basal tuff horizon within the Baraba Conglomerate demonstrates that initial exhumation and surface exposure of low-

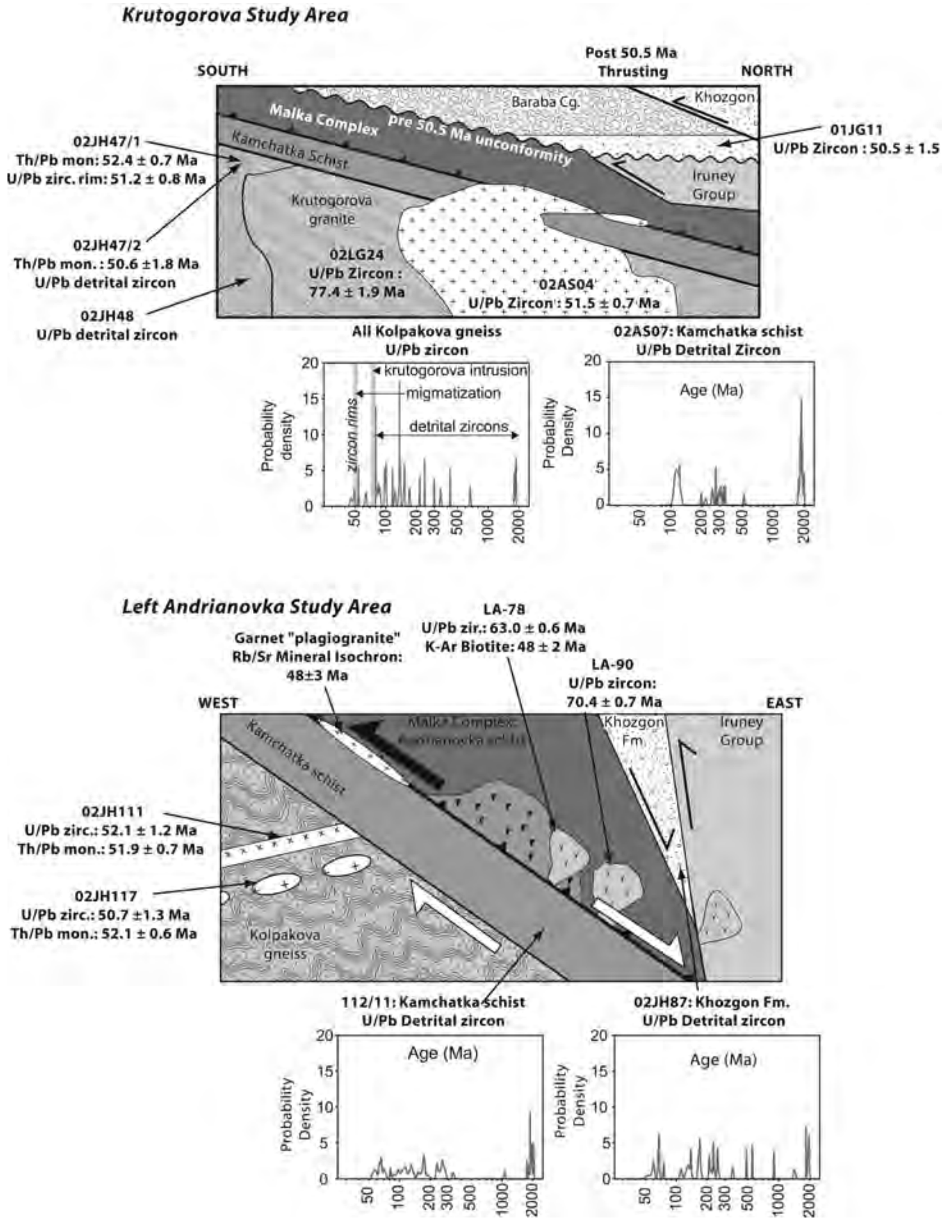

Fig. 25. Simplified schematic sections of the Krutogorova and Left Andrainovka study areas summarizing the geochronologic data in the context of important structural and tectono-stratigraphic relationships.

grade metamorphic rocks was synchronous with peak metamorphic conditions at deeper structural levels. While moderate temperature thermochronometry remains scarce, extant data are consistent with rapid exhumation through mid-crustal levels. The 48 Ma Rb-Sr age from a plagiogranite dike within the Andrainovka suture zone and the 48 Ma biotite K-Ar age from the Andrianovka Schist indicate that cooling from peak (amphibolite-facies) metamorphic conditions to below ~300°C was rapid (fig. 24). Together, these new data indicate that the root of the arc-continent collision zone evolved rapidly over ~12 m.y. period (from ~60 Ma to 48 Ma). During this time: (1) the protoliths for the Kamchatka Schist were deposited; (2) the Malka and Sredinnyi Complexes underwent structural burial and metamorphism with attendant crustal melting at deeper levels; and (3) the flanks of the structural culmination (gneiss dome) cooled rapidly to below ~300°C. These timing constraints demonstrate that heating and cooling were both rapid, with average rates of about ~80°C/m.y. and ~65°C/m.y., respectively (fig. 24). Rapid cooling of these rocks occurred presumably during ascent to mid-crustal depths. Compositional zoning in garnet from the Kamchatka Schist is also consistent with growth during decompression (fig. 6). Reconnaissance FT and (U-Th)/He data indicate that subsequent cooling and exhumation progressed at a much lower rate of about 7°C/m.y. (fig. 24).

A New Tectonic Model for the Origin of the Sredinnyi Range

Late Cretaceous continental margin arc.—During middle to Late Cretaceous time northwest-directed subduction beneath the northeast Russian margin created the Okhotsk-Chukotka Volcanic Belt (OCVB) and its southerly equivalent—the Sikhote-Alin arc. Arc-related magmatism ceased at ~81 Ma within the Okhotsk sector of the OCVB (Hourigan and Akinin, 2004). Following a possible brief hiatus, basaltic lavas with within-plate chemical affinities were erupted over a large part of the belt. $^{40}Ar/^{39}Ar$ data indicate that this activity spanned 78 to 73 Ma (Hourigan and Akinin, 2004). After 73 Ma, there is limited evidence for subduction-related activity in the northern Sea of Okhotsk region. Elsewhere, in the northwest Pacific basin subduction-related magmatism appears to continue uninterrupted. For instance, magmatism in the Sikhote-Alin arc to the south spans Late Cretaceous to Paleocene times (Zonenshain and others, 1990). To the northeast, subduction-related Late Cretaceous-early Cenozoic volcanic rocks are recognized within the Kuskokwin belt (Moll-Stalcup, 1994) and the Briston-Anadyr belt (Worrall, 1991; Ledneva and others, 2006).

The magmatic hiatus in the northern Sea of Okhotsk is typically ascribed to collision of a non-subducting microcontinent or oceanic plateau (Parfenov and Natal'in, 1977; Watson and Fujita, 1985; Bogdanov and Dobretsov, 2002). However, evidence of collision, including deformation and syn-orogenic sedimentation, are notably absent in the geologic record on land. Our new ages for the Krutogorova Granite demonstrate that volumetrically significant silicic magmatism was active at 80 to 78 Ma. Luchitskaya and others (2008) show that these meta-granites are likely arc-related; however, our understanding of the distribution of these granites outside of the Sredinnyi Range remains limited. These observations suggest that northeast Russian arc magmatism did not stop at 80 Ma, but instead may have migrated southeastward to Kamchatka. If correct, "within-plate" basaltic volcanism in the OCVB (Hourigan and Akinin, 2004) might represent back-arc volcanism (fig. 26).

Late Cretaceous island arc.—The Olyutorsky arc is built on a substrate of ophiolitic rocks with MORB affinities; this section is locally referred to as the Vatyna complex (Bogdanov and others, 1990). Overlapping volcanic and volcaniclastic rocks ascribed to the Achaivayam-Valagin sequence exhibit island-arc chemical affinities. The internal structure of the Olyutorsky arc was significantly disrupted during collision and obduction. As a result, there is little geologic evidence that can be used to resolve the subduction polarity of the arc. On the southeast flank, Olyutorsky arc volcanic rocks are in thrust contact with the Vetlovskiy terrane, which is interpreted as the accretionary wedge built in front of the Eocene Western Kamchatka-Kinkil volcanic arc

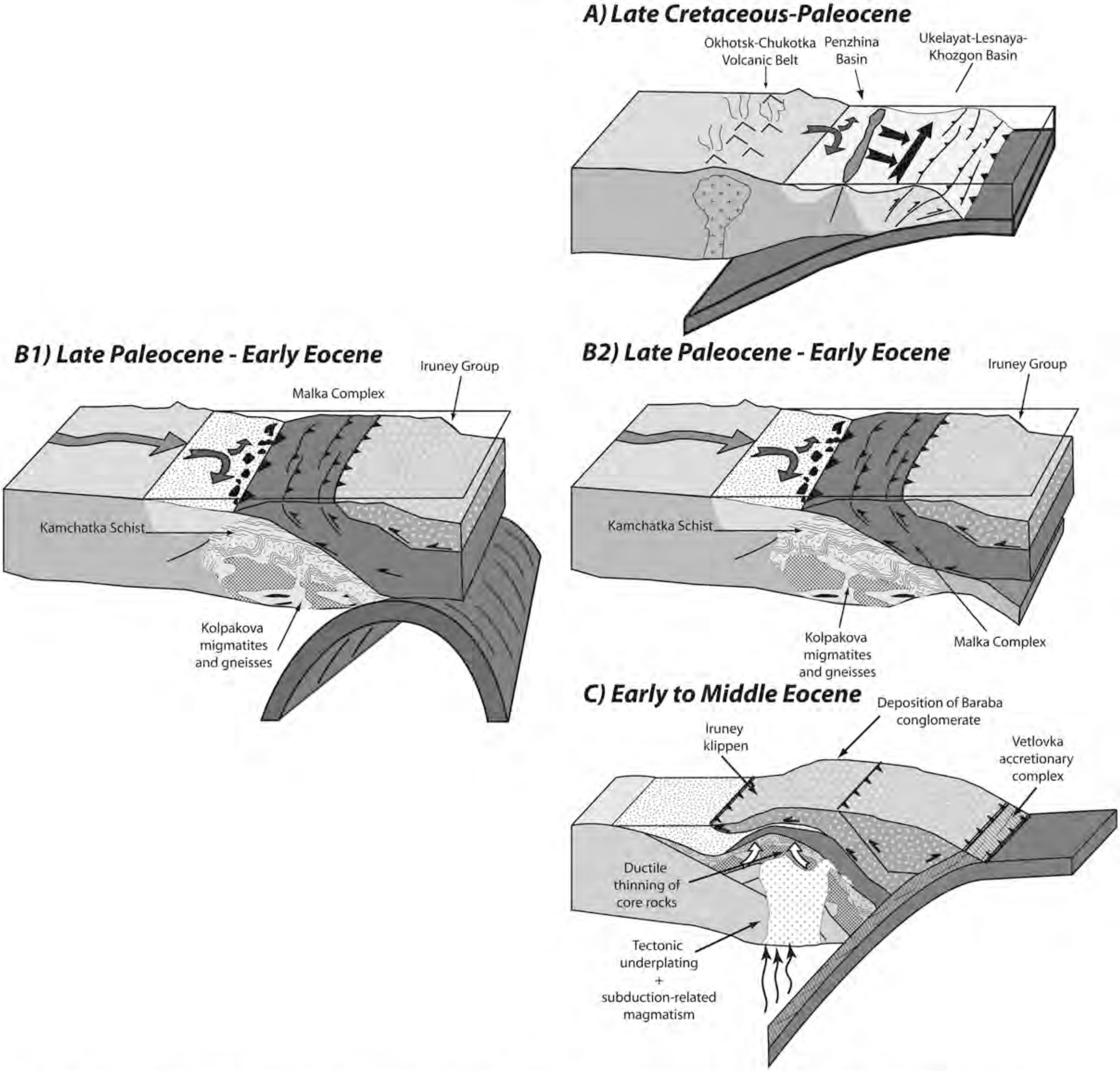

Fig. 26. Schematic model for the tectonic evolution of the Kamchatka Peninsula and the Sredinnyi Range in three time intervals.

(Solov'ev and others, 2004b). On its northwest margin, Olyutorsky ophiolitic and arc volcanic rocks are in thrust contact with continentally derived Paleogene flysch sequences (Garver and others, 2000a; Solov'ev and others, 2002).

In the Sredinnyi Range, Zinkevich and others (1994) describe a structural sequence comprising slices of arc volcanic rocks thrusted top-to-the-west over the Irunei Group basalt-chert assemblage, which they interpret as back-arc basin deposits. This tectonostratigraphic relationship suggests the existence of a back-arc basin in the west with the arc in a more easterly position. Zinkevich and others (1994) argue that the Olyutorsky Arc evolved as a southeast facing arc system with minimal separation from the continental margin (fig. 26). This model posits that arc-continent collision resulted as the arc "backed into" the northeast Russian margin during a brief reversal of subduction polarity or back thrusting (for example, Zonenshain and others, 1990; Geist and others, 1994). This model is consistent with an interpretation that a northwest dipping zone of tomographically imaged high P-wave velocity (Gorbatov and others, 2000) represents a remnant of the subducted slab beneath the back arc region of the Olyutorsky arc. However, this model is inconsistent with the regional evidence for absence of latest Cretaceous to Paleocene magmatism in the Okhotsk sector of the OCVB. The origin of 78 to 80 Ma granitoids in the Sredinniy Range in the context of this model has yet to be fully explained.

A more recent interpretation is that the Olyutorsky terrane evolved as northwest facing arc system (for example, Seliverstov, 1998; Konstantinovskaia, 2000, 2001). In these interpretations, the negative buoyancy of oceanic lithosphere, presumably forming the trailing (southeast) edge of the Okhotsk Sea plate, caused trench roll-back and associated northwestward arc migration. Paleomagnetic data from Cretaceous volcanic rocks indicate a paleolatitude of $49.7° \pm 5.6°$N (Levashova and others, 1998), $\sim 20°$ to the south of the expected latitudes for Eurasia and North America ($\sim 70°$N). Proponents of a northwest-facing Olyutorsky argue that south-directed subduction provides the most efficient mechanism for ~ 2000 km of northward transport while honoring the absence of late Cretaceous-Paleocene subduction-related magmatism within the OCVB.

Blueschist blocks occur in several localities in close association with the Olyutorsky terrane [for example, Kvakhona River in the western Sredinnyi Range and Tigil River in western Kamchatka (Sidorchuk and Khanchuk, 1981)]. In the Kvakhona river locality blueschist blocks occur in a serpentinite mélange zone that contains other blocks of ultramafic rocks (Sidorchuk and Khanchuk, 1981). Typically, the west-dipping fabrics preserved in these rocks have been used to argue for the accretion of an older, southeast-facing "Kvakhona Arc" (Bondarenko, 1997). Following Rikhter's (1995) interpretation that the mélange zones represent the Andrianov suture and Nekrasov's arguments for nappe tectonics (for example, Nekrasov, 2003), we argue that the west-dipping group of volcanic rocks are part of a continuous thrust sheet that was tilted westward during doming of the Sredinnyi Range core. If this is correct, the occurrence of low-temperature high-pressure blueschist-facies rocks on the western flank of the Sredinniy Range co-mingled with serpentinite mélange and ultramafic rocks suggests these rocks were formed in a subduction zone setting at the leading edge of the northwest-facing Olyutorsky arc.

Early Eocene arc-continent collision.—Metamorphic rocks of the Sredinnyi Range reached peak regional metamorphic conditions during the early Eocene (fig. 24). Irrespective of arc polarity, continental margin sediments were deeply buried beneath a mafic structural lid of the Olyutorsky Arc at this time. Structural burial and attendant heating rates were exceedingly rapid (up to 80°C/m.y.) as summarized in figure 24. Such a rapid temperature increase is somewhat unexpected given the tectonic position of these rocks at the leading edge of an active continental margin. Thermal modeling demonstrates that the time required to produce anatectic melts and mobilize the lower portions of a crustal section thickened by thrusting is on the order of ~10 to 20 m.y. assuming typical thermal conductivity values and boundary conditions (England and Thompson, 1984). We suggest that mantle-derived mafic melts may have provided additional heat during the arc-continent collision, allowing for faster onset of regional metamorphism.

Much work remains to characterize the age and petrogenesis of Eocene intrusive rocks in the Sredinnyi Range granitoids. Our field observations indicate that both anatectic (migmatite and equigranular peraluminous garnet-bearing two-mica granite) and mantle-derived (biotite tonalite) Eocene granitoids are present within our study areas in the northern Sredinnyi Range. Luchitskaya and others (2008) found a petrologically and geochemically diverse suite of Eocene intrusive rocks in the Kolpakova and Krutogorova drainages. The samples described in this study are generally strongly peraluminous granite (*sensu stricto*) but range from tonalitic to granitic in composition. Rare-earth element patterns suggest two distinct chemical groups: (1) enriched LREE and depleted HREE pattern that shares geochemical characteristics with Archean trondhjemite-tonalite-granodiorite and modern adakites (Drummond and others, 1996); and (2) less fractionated REE values that share chemical similarity with Himalayan leucogranite (Crawford and Windley, 1990). The latter are indistinguishable from their host gneiss and schist (Luchitskaya and others, 2008). These new geochemical data are consistent with the interpretation that these Eocene igneous units were derived by partial melting of a metabasaltic unit with residual garnet and a metasedimentary unit (Luchitskaya and others, 2008).

The southern part of the high-grade core of the Sredinnyi Range exposes a series of sill-like mafic and ultramafic intrusions collectively called the Kvinum Intrusive Suite (for example, Tararin and others, 2007), which shed further light on the role of magmatism in Eocene tectonic evolution of the Sredinnyi Range. Unlike the Late Cretaceous zoned mafic-ultramafic massifs in the Andrianovka that cross-cut only Malka Complex rocks, the Kvinum Intrusive Suite cross-cuts both the Sredinnyi and Malka complexes (Tararin and others, 2007). Konnikov and others (2006) report a SHRIMP U-Pb zircon age of 50.8 ± 1.4 Ma and 58 Ma $^{40}Ar/^{39}Ar$ ages from amphibole and biotite from the "Kuvalorog" prospect. These authors explain the apparent age discrepancy by suggesting that the amphibole and biotite ages date the main phase of the intrusion and the zircon data reflect crystallization of late differentiates (Konnikov and others, 2006). Bundtzen and others (2003) report a pair of hornblende $^{40}Ar/^{39}Ar$ ages from the Kuvalorog prospect that yield ~52 Ma inverse isochron ages (P. Layer, personal communication, 2008), which are more consistent with the zircon U-Pb age data of Konnikov and others (2006).

These new data indicate that the emplacement of mafic and ultramafic magmas in the lower and middle crust of the Sredinnyi Range was coeval with high-grade metamorphism and anatexis at higher (?) structural levels.

Middle Eocene continental margin arc.—A new east-facing subduction zone was initiated along Kamchatka margin, almost immediately after the start of collision of the Olyutorsky arc. The arc and subduction complex for this new subduction zone are represented by the Western Kamchatka-Koryak magmatic belt and Vetlovka Complex (Konstantinovskaia, 2000; Solov'ev and others, 2002, 2004). Stratigraphic work by Gladenkov and others (1997) indicates that volcanic rocks of the Kinkil Group started accumulating in the middle Eocene. Northeast of the Sredinnyi Range, in the Kamchatka Isthumus, this volcanic belt and associated plutons overlap and cut the Olyutorsky suture zone, indicating that the arc was initiated after collision at 45 Ma

(Soloviev and others, 2002). Furthermore, biostratigraphic (Gladenkov, 1998) and FT detrital zircon age evidence (Solov'ev and others, 2004a) indicate that Vetlovka subduction complex started to accrete trench-fill turbidites in the middle Eocene. On the western flank of the southern Sredinniy Range, Kinkil Group volcanic rocks unconformably overlie klippen of the Irunei Group. Furthermore, the 50.5 Ma zircon U-Pb age for the lower tuffaceous unit of the Baraba Conglomerate suggests active volcanism prior to the unroofing of the Sredinnyi Range core; however, it is unknown whether these units are early deposits of the subduction-related Kinkil Group or represent extrusive equivalents of the crustal melts at deeper structure levels.

Our new data suggest that the Sredinnyi Range is a gneiss dome that was exhumed rapidly following high-grade metamorphism and generation of its granite + migmatite core. The apparent rates at which prograde heating and syn-collisional exhumation occurred raise important questions about the mechanics of gneiss dome formation. Initially we considered that underplating at the base of an orogenic wedge, balanced by erosion at the surface, could explain the observed depths of exhumation. However, these types of settings are not typically associated with high heat flow and thus are inconsistent with the high temperatures of metamorphism observed in the Sredinnyi Range. Subduction-related magmatism likely plays an essential role in high-grade of metamorphism and generation of a low-viscosity lower crust. While a low-viscosity middle and lower crustal layer is required for gneiss dome formation, the mechanisms by which the lower crust returns to the surface are debated. Many workers argue that gneiss dome initiation and growth result from "gravitational collapse" of orogenically thickened crust (Teyssier and Whitney, 2002; Vanderhaeghe and others, 2003a, 2003b). However, for the Sredinnyi Range case, the inference that Kamchatka was likely a low-standing orogen in the Eocene (Gladenkov and others, 1997) suggests that large horizontal gradients in gravitational potential energy required for gravitational collapse were not present (see review by Rey and others, 2001). Alternatively, workers have argued that density inversions (dense mafic crust over low density, low viscosity lower crust) in the absence of significant topography can contribute to dome initiation in the form of diapirs (Fletcher, 1972; Martinez and others, 2001; Fletcher and Hallet, 2004). In both cases, the addition of mantle-derived melts (Gans, 1987; Hill and others, 1995) or generation of melts (*in situ*) by decompression (Norlander and others, 2002; Teyssier and Whitney, 2002) may accelerate the rise of the domal culmination. We argue that a model of magmatically enhanced diapirism driven by a density instability set-up during the obduction of mafic arc crust of the Malka Complex over siliclastic sedimentary rocks of the northeast Russian margin is most consistent with our growing understanding of the evolution of the Sredinnyi Range.

CONCLUSIONS

This investigation is the first to document the nature and timing of metamorphism and the age of protoliths of the Sredinnyi Range by integrating field observations with metamorphic petrology, structural geology and modern high-precision geo- and thermochronology. Our data provide dramatically different estimates for the age of protoliths and the timing of crustal consolidation within the Sredinnyi Range. High-grade gneiss and schist were derived, in part, from young (Cretaceous to Paleocene) sediments that are "native" to the northeast Russian margin. The timing of high-grade metamorphism is now well-constrained by monazite Th-Pb ages and U-Pb zircon overgrowth ages from leucosomes in the Kolpakova gneiss as well as cross-cutting syn- to late syn-kinematic intrusions at a variety of structural levels. The weighted mean age of all data that bear on the timing of peak metamorphism is 51.6

± 1.4 Ma (2σ) (fig. 13). At the regional scale, the age of obduction of the Olyutorsky arc onto the northeast Russian margin spans 10 m.y. from 55 Ma to 45 Ma (fig. 24) (Garver and others, 2000a; Soloviev and others, 2001, 2002). Our data demonstrate that arc-continent collision and high-grade metamorphism in the Sredinnyi range were synchronous. We conclude, therefore, that crustal consolidation occurred as a result of structural burial and metamorphism of young sediments of the northeast Russian margin during arc-continent collision in the Early Eocene.

Rates of exhumation of the Sredinnyi Range were initially rapid and coeval with peak metamorphism at depth (fig. 26). Outstanding questions remain regarding the mode of exhumation. Presently, we find no evidence for major discontinuities in metamorphic grade within the Sredinnyi Range that would indicate excision of metamorphic section accompanying exhumation by low-angle normal faulting. However, qualitative field observations indicate a dramatic decrease in metamorphic grade from upper amphibolite-facies to sub-greenschist facies over <5 km at the flanks of the dome. This apparent attenuation of metamorphic section suggests that ductile thinning was an important process in the exhumation of high-grade core of the range.

Obduction of dense, mafic Olyutorsky arc crust over low-density sediments of the northeast Russian margin may have generated a crustal-scale density instability. The addition of mantle-derived melts into the arc-continent collision zone is a likely cause of high-grade metamorphism including lower crustal anatexis. Thermal weakening produced by heat advection and ultimately crustal melting would have contributed to this density instability. Thus, we argue that density inversion and thermal weakening of the lower density lower crust caused the initiation of diapiric ascent and the rapid exhumation of the high-grade core of Sredinnyi Range.

ACKNOWLEDGMENTS

We appreciate critical reviews by Donna Whitney and George Gehrels that helped us to improve the final product. We thank Aleksandr Khanchuk, Mikhail Shapiro, Igor Tararin, Gelena Ledneva, Marina Luchitskaya, Grisha Bondarenko, Paul Layer and Thomas Bundtzen for informative discussions about their research in the Sredinnyi Range. Joe Wooden, Anders Meibom, and Harold Persing of the Stanford-USGS MicroAnalytical Center provided invaluable support with SHRIMP data collection and interpretation. Emily Peterman provided a thorough review of the revised manuscript. Akinori Takeuchi helped with zircon (U-Th)/He dating of the Left Andrianovka massif. Finally, we are grateful to Sergei Kuzmenko for delivering us safely to and from the field in his track vehicle. The research was partially supported by NSF grants EAR 9911925 and EAR 9911910 to Brandon and Garver, respectively, and RFBR N 05-05-64066 to Soloviev.

Appendix

METHODOLOGY

Thermobarometry

For our samples, we performed standard petrography on multiple thin sections to locate equilibrium assemblages appropriate for usage with published geothermobarometers. Mineral analyses for our samples were done on the JEOL JXA-8600 electron microprobe at Yale University, using standard operating procedures (wavelength-dispersive spectrometers, 20 nA Faraday cup current, 15 kV accelerating voltage, natural and synthetic standards, off-peak and fluorescence-corrected, non-linear mean atomic number background corrections, and matrix corrections). Individual thermobarometric estimates were calculated only on rim compositions for neighboring grains where equilibrium textures were observed.

Zircon Geochronometry

Zircons were separated using standard crushing, hydro-dynamic, heavy-liquid and magnetic separation techniques (for example, Garver and others, 2000c). Approximately 100 zircons per sample were mounted in epoxy and polished to their mid-sections. We used transmitted and reflected light microscopy at 20X magnification to identify crack- and inclusion-free regions for subsequent SHRIMP analysis. A custom-built cathodoluminescence (CL) detector mounted on a JEOL JSM 5600 scanning electron microscope was used to image the fine-scale trace element zonation and illuminate the internal structure of each crystal, which is known to convey petrogenetic significance (Hanchar and others, 1992, 1993).

Zircons were analyzed on the Stanford-USGS SHRIMP-RG following standard operating procedures (Muir and others, 1996; Ireland and Gibson, 1998). Individual $^{206}Pb^*/^{238}U$ age determinations have analytical precision of ~2 percent, with better precision for older grain where the $^{207}Pb^*/^{206}Pb^*$ is more precisely measured. Low U concentration and large variations in count rates, however, result in larger uncertainties. Low abundance of ^{207}Pb in young samples results in a large uncertainty in the $^{207}Pb^*/^{206}Pb^*$ ratio; therefore ^{207}Pb-corrected $^{206}Pb^*/^{238}U$ ages are reported here for grain-ages less that 1.0 Ga. The ^{207}Pb-correction assumes that the measured isotopic ratios represent simple mixtures of radiogenic and common lead at the time of crystallization (T_1) with measured $^{207}Pb/^{206}Pb$ used to monitor common lead. Slightly discordant data are extrapolated along a line projected from an estimate of $^{207}Pb/^{206}Pb$ at T_1 (Stacey and Kramers, 1975) through the measured data point onto concordia. For old grains (>1Ga) we present ^{204}Pb-corrected $^{207}Pb^*/^{206}Pb^*$ ages. Highly discordant data were rejected from data sets for the purposes of calculating weighted mean ages or grain-age probability density.

Monazite Thermochronometry

Monazite (Ce, La, Th)PO_4 is a commonly used accessory phase for U-Pb and Th-Pb dating of crustal rocks. Monazites typically contain <0.5 percent U and from 1 to 30 percent Th (Overstreet, 1967). Monazites sustain little radiation damage and are unlikely to lose Pb at under typical metamorphic conditions. However, grains with very high Th content and Th/U ratios are known to suffer from excess ^{206}Pb derived from ^{230}Th incorporated during crystallization causing primary disequilibrium (Scharer, 1984; Parrish, 1990).

Monazite grains were separated using standard crushing, hydro-dynamic, heavy-liquid and magnetic separation techniques. Thirty to forty grains per sample were mounted in epoxy with WEN-1 (StanfordUSGS SHRIMP-RG Laboratory age standard 301 Ma; Wooden, personal communication) and polished to their mid sections. We used transmitted and reflected light microscopy at 20X magnification to identify crack- and inclusion-free regions for subsequent SHRIMP analysis. Back scatter electron images produced at 15kV using the high-gain setting on a JEOL JXA-733A Superprobe failed to illuminate significant internal zonation or growth domains within the monazite fractions analyzed in this study.

Monazites were analyzed on the Stanford-USGS SHRIMP-RG using a run table consisting of mass stations 156($^{140}Ce^{16}O$), 204 (^{204}Pb), 204.5(background), 206 (^{206}Pb),207(^{207}Pb), 208(^{208}Pb), 232(^{232}Th), 238(^{238}U), 248($^{232}Th^{16}O$), 254($^{238}U^{16}O$), to allow for calculation of Th-Pb and U-Pb ages using both Th/Pb vs. Th/ThO and U/Pb vs. U/UO calibrations. Monazite data were reduced using Squid v. 2.0 for the U/UO calibration and the ANU-produced PRAWN and LEAD data reduction programs for the Th/ThO calibration.

Both U/Pb and Th/Pb ratios and ages are reported in this study. U-Pb ages presented here are ^{207}Pb-corrected $^{206}Pb^*/^{238}U$ ages. Since monazites can contain several weight percent thorium, significant ^{230}Th, an member of the ^{238}U-^{206}Pb decay chain, may be incorporated at the time of crystallization. The effect is the production of excess ^{206}Pb, unsupported by the existing ^{238}U and resulting in $^{206}Pb^*/^{238}Pb$ ages that are too old (for example, Scharer, 1984; Parrish, 1990). A correction for excess ^{206}Pb is outlined by Parrish (1990) but requires knowledge of the whole-rock $^{230}Th/^{232}Th$ ratio, and thus was impractical for the purposes of this study. The $^{207}Pb^*/^{235}U$ system is not hampered by excess radiogenic Pb; however in young samples, low count rates on ^{207}Pb preclude precise age determination. Additionally, an isobaric interference at m/e =204 ($ThNdO_2^{2+}$) introduces inaccuracies in the ^{204}Pb-corrected isotopic ratios (T. Ireland, personal communication). The $^{208}Pb/^{232}Th$ system, on the other hand affords high count rates in parent and daughter isotopes yielding precise ratio measurements and the ^{207}Pb correction allows for subtraction of common Pb independent of measurements of ^{204}Pb and other isobars at mass 204. Thus, we favor the reported ^{207}Pb-corrected $^{208}Pb/^{232}Th$ ages in this paper.

Apatite and Zircon Fission Track Thermochronometry

Fission track dating is based on the decay of trace ^{238}U in zircon and apatite by spontaneous nuclear fission resulting in crystal lattice damage trails or fission tracks. Above a compositionally- and cooling rate-dependent effective closure temperature the tracks are completely annealed. Below the effective closure temperature the number of fission tracks is a function of uranium concentration and elapsed time. By counting the number of fission spontaneous tracks for a known uranium concentration, it is possible to date the timing of cooling below the effective closure temperature. Zircons and apatites were analyzed using the external detector method (see reviews by Bernet and Garver, 2005; Tagami and O'Sullivan, 2005).

(U-Th)/He Thermochronometry

(U-Th)/He dating is based on the α-decay of ^{235}U, ^{238}U and ^{232}Th nuclides producing daughter ^{4}He. Like the fission track system, a compositionally and cooling rate dependent closure temperature daughter ^{4}He atoms diffuse out the crystal lattice. Helium was extracted by CO_2 laser heating of optically-pure single and multiple crystal aliquots in ~1 mm Pt foil packets at ~1000°C (House and others, 2000). Degassesd helium was measured by ^{3}He isotope dilution with a Balzers quadropole mass spectrometer following cryogenic purification. Foil packets containing the apatite crystals were then dissolved in ^{229}Th- and ^{233}U-spiked HCl in Teflon bombs. U and Th concentrations were then measured by isotope dilution on a Finnegan Element2 high-resolution magnetic sector ICP-MS (analytical uncertainties of 1-2% for U-Th content). Grain size measurements were used to correct for α-emission following Farley and others (1996).

DATA TABLES

Tables A.1–A.6, A.8–A.14.—U, Th and Pb concentration, isotopic and age data for SHRIMP spot analyses of zircons and monazite. Data tables are presented in a standardized format. Sample locality coordinates are given and sites can be found in figures 1, 4 and 5. For grain age less than 1.0 Ga Tera-Wasserburg concordia data and ^{207}Pb-corrected ^{206}Pb/^{238}U ages are given. For ages > 1.0 Ga Wetherill concordia data and ^{204}Pb-corrected ^{207}Pb/^{206}Pb ages are reported. Notes: †—discordant analysis not used in calculation of weighted mean age; r—rim analysis; c—core analysis.

Table A.7.—U-Th-Pb isotopic data for five monazite samples from the Kolpakova Gneiss. Ages cited in figures are weighted-mean ^{207}Pb-corrected ^{206}Pb/^{238}U ages. The preferred (see text and Appendix—methodology) ^{207}Pb-corrected ^{208}Pb/^{232}Th ages are given table A.7.

TABLE A.1

Sample 02JH47/2—Zircon from melanosome in the Kolpakova Gneiss, Krutogorova region (54° 50.120 N, 157° 23.096 E, 1320 m)

Analysis	$\%^{206}Pb_{comm}$	U_{ppm}	Th_{ppm}	Th/U	Uncorrected $^{238}U/^{206}Pb$	Uncorrected $^{207}Pb/^{206}Pb$		^{207}Pb Corrected $^{238}U/^{206}Pb$ Age
02JH47/2-1	0.76	397	241	0.63	65.34 ± 0.70	0.0540 ± 0.0023		97.2 ± 1.1
02JH47/2-2	1.09	198	141	0.73	45.51 ± 0.64	0.0575 ± 0.0030		138.6 ± 2.0
02JH47/2-3	0.36	9695	15642	1.67	79.69 ± 0.27	0.0504 ± 0.0016		80.1 ± 0.3
02JH47/2-3R	3.88	259	61	0.24	72.36 ± 1.11	0.0785 ± 0.0046		85.1 ± 1.5
02JH47/2-4	0.32	454	263	0.60	54.55 ± 0.52	0.0509 ± 0.0020		116.7 ± 1.1
02JH47/2-5	-0.06	2159	762	0.36	46.71 ± 0.19	0.0483 ± 0.0008		136.6 ± 0.6
02JH47/2-7	-0.01	1296	29	0.02	118.05 ± 1.08	0.0470 ± 0.0017		54.4 ± 0.5
02JH47/2-8	1.14	176	139	0.82	29.22 ± 0.35	0.0596 ± 0.0024		214.5 ± 2.6
02JH47/2-9	0.04	183	145	0.82	14.67 ± 0.15	0.0557 ± 0.0017		424.9 ± 4.2
02JH47/2-9A	0.80	256	81	0.33	41.41 ± 0.47	0.0555 ± 0.0024		152.6 ± 1.8
02JH47/2-10	1.15	115	86	0.78	20.92 ± 0.28	0.0615 ± 0.0027		297.6 ± 4.1
02JH47/2-11	0.62	570	521	0.94	26.21 ± 0.20	0.0559 ± 0.0013		239.9 ± 1.9
02JH47/2-12	5.18	76	39	0.54	40.15 ± 0.84	0.0903 ± 0.0056		150.5 ± 3.5
02JH47/2-13	0.99	447	157	0.36	62.57 ± 0.62	0.0559 ± 0.0022		101.2 ± 1.1
					^{204}Pb Corrected $^{207}Pb/^{235}U$	^{204}Pb Corrected $^{206}U/^{238}Pb$	^{204}Pb Corrected $^{207}Pb/^{206}Pb$	^{204}Pb Corrected $^{207}Pb/^{206}Pb$ Age
02JH47/2-6	0.22	79	36	0.48	5.24 ± 0.10	0.3341 ± 0.0038	0.1137 ± 0.0018	1859.0 ± 29.1

Table A.2

Sample 02JH48—Zircon from melanosome in Kolpakova Gneiss, Krutogorova region (54° 50.128 N, 157° 23.106 E, 1380 m)

					Uncorrected			^{207}Pb Corrected
Analysis	**%^{206}Pb$_{comm}$**	**U$_{ppm}$**	**Th$_{ppm}$**	**Th/U**	**^{238}U/^{206}Pb**	**^{207}Pb/^{206}Pb**		**^{238}U/^{206}Pb Age**
02JH48-1	0.96	197	48	0.25	77.29 ± 1.71	0.0552 ± 0.0026		82.1 ± 1.8
02JH48-2	0.73	108	17	0.16	99.44 ± 2.62	0.0531 ± 0.0041		64.0 ± 1.7
02JH48-3	1.19	203	63	0.32	63.53 ± 1.36	0.0575 ± 0.0023		99.5 ± 2.2
02JH48-4	0.95	53	17	0.34	46.91 ± 1.23	0.0563 ± 0.0038		134.7 ± 3.6
02JH48-5	0.11	614	121	0.20	46.45 ± 0.92	0.0496 ± 0.0010		137.2 ± 2.7
02JH48-7	0.43	552	502	0.94	9.14 ± 0.18	0.0653 ± 0.0006		666.2 ± 12.4
02JH48-8C	0.47	90	88	1.01	51.40 ± 1.23	0.0522 ± 0.0031		123.6 ± 3.0
02JH48-8R	3.86	222	1	0.01	125.05 ± 2.96	0.0776 ± 0.0040		49.4 ± 1.2
02JH48-9C	0.09	157	115	0.76	37.25 ± 0.78	0.0502 ± 0.0018		170.6 ± 3.6
02JH48-9R	19.15	70	3	0.04	113.11 ± 3.65	0.1985 ± 0.0102		45.9 ± 2.1
02JH48-10A	0.18	91	3	0.03	18.27 ± 0.39	0.0548 ± 0.0019		343.0 ± 7.2
02JH48-11	1.18	414	24	0.06	71.81 ± 1.48	0.0572 ± 0.0024		88.1 ± 1.8
						^{204}Pb Corrected		
					^{207}Pb/^{235}U	**^{206}U/^{238}Pb**	**^{207}Pb/^{206}Pb**	**^{207}Pb/^{206}Pb Age**
02JH48-10B	4.66	231	36	0.16	2.58 ± 0.06	0.1711 ± 0.0033	0.1094 ± 0.0012	1790.2 ± 20.5
02JH48-6	4.07	38	20	0.55	3.19 ± 0.10	0.2053 ± 0.0048	0.1128 ± 0.0022	1859.0 ± 29.1

Table A.3

Sample 02LG24—Zircon from the foliated Krutogorova Granite, Krutogorova region (54° 50.564 N, 157° 22.754 E, 1091 m)

					Uncorrected		^{207}Pb corrected	
Analysis	**%^{206}Pb$_{comm}$**	**U$_{ppm}$**	**Th$_{ppm}$**	**Th/U**	**^{238}U/^{206}Pb**	**^{207}Pb/^{206}Pb**	**^{206}Pb/^{238}U Age**	
02LG24-1	4.97	80	22	0.29	81.23 ± 2.28	0.0869 ± 0.0082	74.7 ± 2.8	
02LG24-2	0.80	282	94	0.34	83.77 ± 1.24	0.0539 ± 0.0040	75.9 ± 1.2	
02LG24-3	0.25	778	33	0.04	80.25 ± 0.70	0.0496 ± 0.0018	79.7 ± 0.7	
02LG24-4	3.64	269	55	0.21	85.38 ± 1.26	0.0763 ± 0.0039	73.1 ± 1.2	†
02LG24-5	4.78	124	19	0.16	78.62 ± 2.06	0.0855 ± 0.0064	79.3 ± 2.2	
02LG24-6	18.94	87	28	0.33	79.23 ± 2.24	0.1974 ± 0.0110	67.2 ± 3.0	†
02LG24-6R	2.90	475	33	0.07	78.40 ± 0.84	0.0706 ± 0.0027	79.6 ± 0.9	
02LG24-7	1.95	161	43	0.28	81.83 ± 1.58	0.0630 ± 0.0046	76.6 ± 1.8	
02LG24-8	5.20	231	81	0.36	5.54 ± 0.16	0.1166 ± 0.0022	1049.2 ± 30.1	†
02LG24-8R	1.14	503	44	0.09	86.11 ± 2.65	0.0565 ± 0.0029	73.5 ± 2.3	
02LG24-9	4.45	171	121	0.73	80.62 ± 2.70	0.0829 ± 0.0075	77.6 ± 3.1	
02LG24-10	1.73	140	67	0.50	81.14 ± 3.22	0.0613 ± 0.0049	78.0 ± 3.4	

Weighted Mean ^{206}Pb/^{238}U Age
78.5 ± 1.5 Ma (95% c.i.)
n=9/12
MSWD = 2.1, probability = 0.033

† Discordant analysis not used in calculation of weighted mean age

Table A.4

Sample 02AS07—Kamchatka Schist zircon grain-age data, Krutogorova region (N 54°53.16′, E157°17.21)

Analysis	$\%^{206}Pb_{comm}$	U_{ppm}	Th_{ppm}	Th/U	$^{238}U/^{206}Pb$	$^{207}Pb/^{206}Pb$	$^{238}U/^{206}Pb$ Age
02AS07-1	5.82	26	11	0.45	47.56 ± 1.51	0.0949 ± 0.0071	126.4 ± 4.3
02AS07-2	0.60	85	58	0.70	53.21 ± 1.28	0.0532 ± 0.0032	119.3 ± 2.9
02AS07-5	0.14	140	67	0.50	32.02 ± 0.68	0.0511 ± 0.0018	198.0 ± 4.2
02AS07-6	1.31	47	58	1.28	24.56 ± 0.60	0.0618 ± 0.0048	253.9 ± 6.3
02AS07-7	1.89	17	6	0.38	52.80 ± 2.12	0.0634 ± 0.0085	118.7 ± 4.9
02AS07-8	0.03	329	218	0.69	20.69 ± 0.41	0.0527 ± 0.0011	304.2 ± 5.9
02AS07-10	12.22	12	4	0.34	46.54 ± 1.91	0.1456 ± 0.0152	120.5 ± 6.0
02AS07-11	9.32	62	28	0.47	54.24 ± 1.78	0.0720 ± 0.0075	114.3 ± 3.9
02AS07-12	0.00	199	192	1.00	22.92 ± 0.30	0.0533 ± 0.0024	274.8 ± 3.7
02AS07-15	0.00	55	21	0.39	56.98 ± 2.09	0.0701 ± 0.0084	109.1 ± 4.2
02AS07-17	0.72	122	112	0.94	21.30 ± 0.36	0.0577 ± 0.0031	293.8 ± 5.0
02AS07-19	0.00	38	16	0.42	51.59 ± 2.21	0.0591 ± 0.0091	122.1 ± 5.4
02AS07-20	0.00	496	502	1.05	52.41 ± 0.62	0.0489 ± 0.0023	121.8 ± 1.5
02AS07-22	0.00	112	72	0.67	54.25 ± 1.33	0.0566 ± 0.0051	116.5 ± 2.9
02AS07-23	0.00	25	29	1.17	24.15 ± 0.94	0.0671 ± 0.0082	256.5 ± 10.2
02AS07-24	0.00	45	16	0.37	58.24 ± 2.39	0.0373 ± 0.0066	111.3 ± 4.6
02AS07-26	7.95	32	12	0.40	56.49 ± 2.82	0.0520 ± 0.0098	112.6 ± 5.8
02AS07-27	0.00	208	127	0.63	18.49 ± 0.23	0.0554 ± 0.0023	338.6 ± 4.2
02AS07-29	0.00	191	136	0.74	19.30 ± 0.26	0.0500 ± 0.0023	326.8 ± 4.4
02AS07-30	0.00	39	14	0.38	57.04 ± 2.56	0.0493 ± 0.0090	111.9 ± 5.1
02AS07-33	0.00	34	13	0.38	28.42 ± 1.03	0.0656 ± 0.0076	218.8 ± 8.2
02AS07-34	0.00	44	13	0.31	58.58 ± 2.52	0.0528 ± 0.0084	108.5 ± 4.8
02AS07-35	0.00	64	51	0.82	20.28 ± 0.48	0.0550 ± 0.0059	309.4 ± 7.6
02AS07-36	0.00	231	85	0.38	22.83 ± 0.29	0.0548 ± 0.0024	275.3 ± 3.5
02AS07-40	1.05	47	36	0.79	11.96 ± 0.27	0.0572 ± 0.0039	518.0 ± 11.7
02AS07-41	0.00	26	6	0.26	59.68 ± 3.21	0.0550 ± 0.0110	106.2 ± 5.9
02AS07-42	4.41	41	21	0.54	56.17 ± 2.00	0.0542 ± 0.0071	112.9 ± 4.1

					^{204}Pb Corrected				
					$^{207}Pb/^{235}U$	$^{206}U/^{238}Pb$	$^{207}Pb/^{206}Pb$	$^{207}Pb/^{206}Pb$ Age	
02AS07-4	1.13	12	5	0.43	4.86 ± 0.24	0.3239 ± 0.0088	0.1088 ± 0.0045	1779.3 ± 76.0	
02AS07-9	0.26	73	56	0.80	5.84 ± 0.13	0.3516 ± 0.0072	0.1205 ± 0.0013	1964.0 ± 18.7	
02AS07-13	0.00	71	37	0.54	4.78 ± 0.12	0.3022 ± 0.0042	0.1147 ± 0.0023	1874.8 ± 36.8	
02AS07-14	0.07	278	100	0.37	5.71 ± 0.07	0.3510 ± 0.0024	0.1179 ± 0.0011	1925.0 ± 17.4	
02AS07-16	0.22	48	22	0.48	5.08 ± 0.16	0.3268 ± 0.0056	0.1128 ± 0.0029	1845.1 ± 47.3	
02AS07-18	0.10	274	117	0.44	3.75 ± 0.05	0.2524 ± 0.0019	0.1077 ± 0.0013	1760.1 ± 22.5	†
02AS07-21	0.04	373	257	0.71	4.97 ± 0.05	0.2933 ± 0.0018	0.1230 ± 0.0011	2000.0 ± 15.8	†
02AS07-25	0.08	293	169	0.60	4.81 ± 0.06	0.3124 ± 0.0021	0.1116 ± 0.0012	1825.4 ± 19.2	
02AS07-28	0.00	117	44	0.39	5.16 ± 0.10	0.3296 ± 0.0036	0.1136 ± 0.0018	1858.5 ± 28.6	
02AS07-31	2.82	247	73	0.31	5.05 ± 0.23	0.3279 ± 0.0034	0.1118 ± 0.0050	1828.4 ± 80.5	
02AS07-32	0.12	419	151	0.37	2.20 ± 0.04	0.1401 ± 0.0010	0.1137 ± 0.0016	1859.3 ± 26.1	†
02AS07-37	0.00	145	62	0.44	5.14 ± 0.09	0.3321 ± 0.0032	0.1123 ± 0.0016	1837.4 ± 25.3	
02AS07-38	0.02	429	67	0.16	5.22 ± 0.05	0.3225 ± 0.0018	0.1175 ± 0.0009	1918.6 ± 14.3	
02AS07-39	0.00	69	46	0.69	11.87 ± 0.23	0.4794 ± 0.0063	0.1796 ± 0.0024	2648.9 ± 22.6	
02AS07-3C	4.47	179	59	0.34	3.12 ± 0.07	0.1980 ± 0.0039	0.1144 ± 0.0011	1870.4 ± 17.2	†
02AS07-3R	0.52	143	44	0.32	5.18 ± 0.11	0.3260 ± 0.0064	0.1152 ± 0.0009	1883.6 ± 14.2	
02AS07-43	0.00	205	92	0.46	4.96 ± 0.06	0.3117 ± 0.0023	0.1153 ± 0.0013	1885.3 ± 19.7	

† Discordant analysis not used in calculation of weighted mean age.

TABLE A.5

Sample 112-11—Kamchatka Schist zircon grain-age data, Left Andrianovka region (N 54°30′40″, E 157°38′50″, 1500 m)

Analysis	U/ppm	Th/ppm	Th/U	Isotopic Ratios (± 1σ)				Age (Ma, ± 1σ)	
Grain-ages <1.0 Ga									
					^{207}Pb / ^{206}Pb	^{238}U / ^{206}Pb		^{206}Pb / ^{238}U Age	
112-11-2	160	94	0.59		0.0454 ± 0.0043	46.88 ± 2.07		136.7 ± 6.0	
112-11-5	306	347	1.13		0.0498 ± 0.0030	55.27 ± 2.05		115.4 ± 4.3	
112-11-6	747	237	0.32		0.0529 ± 0.0013	24.03 ± 1.05		262.5 ± 11.2	
112-11-7	642	465	0.72		0.0470 ± 0.0020	51.64 ± 2.43		123.9 ± 5.8	
112-11-8	149	86	0.58		0.0618 ± 0.0034	29.46 ± 1.29		212.2 ± 9.2	†
112-11-9	107	56	0.52		0.0478 ± 0.0068	108.71 ± 5.30		59.0 ± 2.9	
112-11-10	154	56	0.36		0.0509 ± 0.0028	22.82 ± 1.16		276.8 ± 13.8	
112-11-11	76	49	0.65		0.0466 ± 0.0047	40.18 ± 3.22		159.0 ± 12.6	
112-11-12	361	167	0.46		0.0541 ± 0.0020	23.05 ± 1.06		273.1 ± 12.4	
112-11-14	581	367	0.63		0.0488 ± 0.0019	58.24 ± 3.44		109.7 ± 6.4	
112-11-15	377	156	0.41		0.0519 ± 0.0022	24.90 ± 1.46		253.7 ± 14.6	
112-11-16	153	46	0.30		0.0474 ± 0.0030	36.67 ± 1.46		173.9 ± 6.9	
112-11-17	79	40	0.51		0.0531 ± 0.0037	25.98 ± 1.51		242.8 ± 13.9	
112-11-19	890	377	0.42		0.0512 ± 0.0011	27.36 ± 1.17		231.3 ± 9.7	
112-11-22	330	157	0.47		0.0503 ± 0.0030	59.80 ± 3.10		106.6 ± 5.5	
112-11-25	8	0	0.01		0.1367 ± 0.0483	108.80 ± 12.67		52.3 ± 7.1	†
112-11-26	407	169	0.42		0.0469 ± 0.0034	112.05 ± 7.85		57.3 ± 4.0	
112-11-27	190	145	0.76		0.0520 ± 0.0047	88.80 ± 5.43		71.8 ± 4.4	
112-11-28	837	429	0.51		0.0502 ± 0.0030	115.82 ± 6.83		55.2 ± 3.3	
112-11-18c	1037	21	0.02		0.0477 ± 0.0017	37.98 ± 1.83		167.9 ± 8.0	
112-11-18r	387	397	1.03		0.0478 ± 0.0019	33.63 ± 2.10		189.4 ± 11.7	
112-11-23c	616	233	0.38		0.0487 ± 0.0018	49.29 ± 1.94		129.5 ± 5.1	
112-11-23r	1141	730	0.64		0.0474 ± 0.0015	56.64 ± 3.31		113.0 ± 6.5	
112-11-1.1	362	230	0.63		0.0487 ± 0.0030	66.31 ± 2.54		96.4 ± 3.7	
112-11-2.1	184	107	0.58		0.0584 ± 0.0035	74.69 ± 2.47		84.6 ± 2.8	†
112-11-4.1	1276	294	0.23		0.0492 ± 0.0013	71.65 ± 3.66		89.2 ± 4.5	
112-11-5.1	368	178	0.48		0.0512 ± 0.0018	41.77 ± 2.00		152.1 ± 7.2	
112-11-6.1	1278	175	0.14		0.0532 ± 0.0009	35.82 ± 1.96		176.7 ± 9.5	†
112-11-7.1	530	285	0.54		0.0485 ± 0.0022	100.92 ± 2.36		63.5 ± 1.5	
122-11-8.1	1312	413	0.32		0.0487 ± 0.0014	90.00 ± 3.84		71.1 ± 3.0	
122-11-9.1	58	48	0.83		0.0504 ± 0.0037	27.27 ± 0.82		232.3 ± 7.0	
112-11-10.1	195	87	0.45		0.1483 ± 0.0075	59.80 ± 4.31		93.4 ± 6.8	†
112-11-13.1	262	205	0.78		0.0440 ± 0.0028	78.83 ± 1.71		81.6 ± 1.8	
112-11-14.1	691	254	0.37		0.0524 ± 0.0010	24.17 ± 0.74		261.0 ± 7.9	
112-11-15.1	212	149	0.70		0.0480 ± 0.0038	99.41 ± 3.79		64.5 ± 2.5	
112-11-16.1	880	301	0.34		0.0494 ± 0.0015	36.55 ± 1.26		174.0 ± 6.0	
112-11-17.1	258	124	0.48		0.0505 ± 0.0026	48.75 ± 2.08		130.6 ± 5.5	
112-11-18.1	306	258	0.84		0.0494 ± 0.0028	64.21 ± 3.78		99.5 ± 5.8	
112-11-19.1	1108	108	0.10		0.1137 ± 0.0009	6.71 ± 0.32		848.3 ± 37.4	†
112-11-20.1	1868	543	0.29		0.0500 ± 0.0008	36.76 ± 1.20		172.9 ± 5.6	
112-11-21.1	948	842	0.89		0.0478 ± 0.0017	96.67 ± 3.72		66.3 ± 2.5	
112-11-22.1	189	177	0.94		0.0506 ± 0.0019	18.84 ± 0.76		334.4 ± 13.1	
112-11-23.1	836	54	0.06		0.1453 ± 0.0011	6.13 ± 0.41		890.6 ± 55.9	†
112-11-24.1	1052	832	0.79		0.0476 ± 0.0015	96.57 ± 1.95		66.4 ± 1.3	
Grain-ages >1.0 Ga									
				206%	^{206}Pb / ^{238}U	^{207}Pb / ^{235}U	^{207}Pb / ^{206}Pb	^{207}Pb / ^{206}Pb Age	
112-11-1	1184	204	0.17	0.02	0.3368 ± 0.0139	5.338 ± 0.223	0.1150 ± 0.0005	1879.4 ± 7.7	
112-11-3	159	124	0.78	0.14	0.3031 ± 0.0116	4.678 ± 0.203	0.1119 ± 0.0019	1831.0 ± 30.6	
112-11-4	348	298	0.86	0.02	0.3690 ± 0.0278	6.432 ± 0.494	0.1264 ± 0.0010	2048.9 ± 14.1	
112-11-13	301	160	0.53	0.06	0.3188 ± 0.0155	5.210 ± 0.265	0.1185 ± 0.0012	1934.3 ± 17.9	
112-11-20	255	76	0.30	0.01	0.3288 ± 0.0120	5.486 ± 0.214	0.1210 ± 0.0012	1971.0 ± 17.1	
112-11-21	156	81	0.52	0.32	0.3399 ± 0.0190	5.487 ± 0.327	0.1171 ± 0.0017	1912.1 ± 26.8	
112-11-24	420	54	0.13	0.14	0.3181 ± 0.0205	5.094 ± 0.343	0.1161 ± 0.0015	1897.5 ± 23.1	
112-11-3.1	192	44	0.23	0.02	0.1759 ± 0.0072	1.808 ± 0.082	0.0745 ± 0.0012	1056.1 ± 31.3	
112-11-11.1	236	134	0.57	-0.05	0.2910 ± 0.0098	4.306 ± 0.160	0.1073 ± 0.0013	1754.3 ± 22.0	
112-11-12.1	242	95	0.39	0.02	0.3422 ± 0.0130	5.842 ± 0.232	0.1238 ± 0.0009	2012.2 ± 13.4	

† Discordant analysis not used in calculation of weighted mean age.

Table A.6

U-Pb isotopic data for Left Andrianovka massif zircon samples

Analysis	**U** ppm	**Th** ppm	Th/U	Uncorrected Ratios ^{207}Pb / ^{206}Pb	Uncorrected Ratios ^{238}U / ^{206}Pb	^{207}Pb corrected ^{206}Pb/ ^{238}Pb Age
LA-78-KAM: Left-Andrianovka syenite (N 54º35.900', E 157º37.60', 1100 m)						
LA-78-1	1703	1945	1.14	0.0468 ± 0.0015	91.98 ± 6.16	70.8 ± 4.7
LA-78-2	438	184	0.42	0.0504 ± 0.0030	103.28 ± 4.59	62.8 ± 2.8
LA-78-3	1046	973	0.93	0.0494 ± 0.0019	102.28 ± 2.72	63.5 ± 1.7
LA-78-4	4566	3260	0.71	0.0464 ± 0.0011	95.74 ± 2.30	68.0 ± 1.6†
LA-78-5	303	184	0.61	0.0475 ± 0.0035	104.53 ± 5.78	62.2 ± 3.4
LA-78-6	620	457	0.74	0.0463 ± 0.0025	104.96 ± 3.16	62.1 ± 1.9
LA-78-7	283	105	0.37	0.0597 ± 0.0047	103.82 ± 3.29	61.8 ± 2.0
LA-78-8	238	108	0.45	0.0486 ± 0.0040	107.85 ± 3.96	60.3 ± 2.2
LA-78-9	95	37	0.38	0.0538 ± 0.0107	95.54 ± 4.29	67.6 ± 3.1
LA-78-10	242	152	0.63	0.0472 ± 0.0047	100.49 ± 2.95	64.8 ± 1.9
LA-78-11	426	215	0.50	0.0451 ± 0.0037	102.33 ± 3.38	63.8 ± 2.1
LA-78-12	256	154	0.60	0.0489 ± 0.0045	100.81 ± 4.16	64.4 ± 2.7
LA-78-13	397	181	0.46	0.0501 ± 0.0039	110.23 ± 5.30	58.9 ± 2.8
LA-78-14	1417	957	0.68	0.0464 ± 0.0018	100.56 ± 4.99	64.8 ± 3.2
LA-78-15	197	75	0.38	0.0443 ± 0.0042	106.27 ± 4.13	61.5 ± 2.4
					^{206}Pb/ ^{238}Pb Age Mean = 63.0 ± 1.2 95% conf. n=14/15 MSWD = 0.86, probability = 0.59	
LA-90-KAM: Left-Andrianovka syenite (N 54º34.20', E157º38.70, 1400 m)						
LA-90-1	2010	967	0.48	0.0490 ± 0.0012	91.81 ± 3.12	70.7 ± 2.4
LA-90-2	2543	1175	0.46	0.0496 ± 0.0010	88.20 ± 3.21	73.5 ± 2.7
LA-90-3	1300	711	0.55	0.0508 ± 0.0021	87.04 ± 7.75	74.4 ± 6.6
LA-90-4	616	177	0.29	0.0487 ± 0.0027	97.16 ± 2.88	66.9 ± 2.0
LA-90-5	1166	315	0.27	0.0456 ± 0.0018	98.37 ± 8.36	66.3 ± 5.6
LA-90-6	722	180	0.25	0.0459 ± 0.0023	90.20 ± 2.37	72.2 ± 1.9
LA-90-7	1640	537	0.33	0.0467 ± 0.0016	96.20 ± 5.29	67.7 ± 3.7
LA-90-8	3533	1597	0.45	0.0473 ± 0.0008	91.14 ± 3.08	71.4 ± 2.4
LA-90-9	702	117	0.17	0.0474 ± 0.0023	93.74 ± 2.81	69.4 ± 2.1
LA-90-10	1750	1111	0.63	0.0500 ± 0.0015	89.08 ± 4.17	72.8 ± 3.4
LA-90-11	642	182	0.28	0.0506 ± 0.0040	94.40 ± 5.01	68.6 ± 3.6
LA-90-12	2939	1001	0.34	0.0499 ± 0.0012	92.13 ± 2.95	70.4 ± 2.3
LA-90-13	1499	798	0.53	0.0493 ± 0.0015	93.03 ± 7.96	69.8 ± 5.9
LA-90-14	2459	2862	1.16	0.0468 ± 0.0012	90.04 ± 6.90	72.3 ± 5.5
LA-90-15	1075	648	0.60	0.0491 ± 0.0018	93.37 ± 2.81	69.5 ± 2.1
					^{206}Pb/ ^{238}Pb Age Mean = 70.2 ± 1.4 95% conf. n=15/15 MSWD = 0.60, probability = 0.87	

TABLE A.7

Monazite U-Th-Pb isotopic data for all Kolpakova Gneiss samples

	%				Uncorrected		^{207}Pb corrected		
Analysis	$^{206}Pb_{comm}$	U_{ppm}	Th_{ppm}	**Th/U**	$^{238}U/^{206}Pb$	$^{207}Pb/^{206}Pb$	$^{238}U/^{206}Pb$ Age	$^{208}Pb/^{232}Th$	$^{232}Th/^{208}Pb$ Age
02JH47/1: *Leucosome from migmatites of the Kolpakova Gneiss, Krutogorova-Kvakhona Pass (54º 50.120 N, 157º 23.096 E, 1320 m)*									
02JH47/1-1	0.51	227	1856	8.44	117.64 ± 1.91	0.0512 ± 0.0007	54.3 ± 0.9	0.00265 ± 0.00004	**53.4 ± 0.9**
02JH47/1-2	0.34	249	1231	5.11	119.61 ± 1.97	0.0498 ± 0.0007	53.5 ± 0.9	0.00253 ± 0.00006	**51.0 ± 1.2**
02JH47/1-3	0.26	186	1837	10.18	116.41 ± 1.91	0.0492 ± 0.0007	55.0 ± 0.9	0.00263 ± 0.00006	**53.1 ± 1.1**
02JH47/1-4	0.39	224	1202	5.54	116.86 ± 1.90	0.0502 ± 0.0006	54.7 ± 0.9	0.00261 ± 0.00007	**52.7 ± 1.5**
02JH47/1-5	0.29	211	1369	6.69	116.55 ± 1.91	0.0494 ± 0.0007	54.9 ± 0.9	0.00263 ± 0.00006	**53.2 ± 1.2**
02JH47/1-6	0.28	201	1362	7.01	117.88 ± 1.92	0.0493 ± 0.0007	54.3 ± 0.9	0.00254 ± 0.00006	**51.2 ± 1.2**
02JH47/1-7	0.18	256	1236	4.98	118.54 ± 1.92	0.0485 ± 0.0006	54.1 ± 0.9	0.00257 ± 0.00008	**51.8 ± 1.6**
02JH47/1-8	0.20	252	1406	5.76	118.04 ± 1.92	0.0487 ± 0.0007	54.3 ± 0.9	0.00259 ± 0.00006	**52.2 ± 1.1**
02JH47/1-9	0.12	475	1107	2.41	122.64 ± 1.96	0.0480 ± 0.0005	52.3 ± 0.8	0.00258 ± 0.00006	**52.1 ± 1.2**
02JH47/1-10	0.39	207	1597	7.99	117.60 ± 1.96	0.0502 ± 0.0007	54.4 ± 0.9	0.00252 ± 0.00006	**50.9 ± 1.2**
02JH47/1-11	0.58	160	1230	7.96	115.71 ± 1.91	0.0517 ± 0.0008	55.2 ± 0.9	0.00259 ± 0.00005	**52.4 ± 1.0**
02JH47/1-12	0.44	240	1703	7.35	120.13 ± 1.96	0.0506 ± 0.0007	53.2 ± 0.9	0.00262 ± 0.00005	**52.9 ± 1.0**
					$^{206}Pb/^{238}Pb$ Age Mean = 54.1 ± 0.5 Ma 95% c.i. n=12/12 MSWD = 0.92, probability = 0.52			**$^{208}Pb/^{232}Th$ Age** Mean = **52.4 ± 0.7 Ma** 95% c.i. n =12/12 MSWD = 0.59, probability = 0.84	
02JH47/2: *Melanosome from migmatites of the Kolpakova Gneiss, Krutogorova-Kvakhona Pass (54º 50.120 N, 157º 23.096 E, 1320 m)*									
02JH47/2-1B	0.68	106	691	6.71	116.40 ± 2.02	0.0525 ± 0.0011	54.8 ± 1.0	0.00225 ± 0.00004	**45.5 ± 0.9**
02JH47/2-2	0.52	212	1153	5.62	118.59 ± 2.01	0.0512 ± 0.0007	53.9 ± 0.9	0.00250 ± 0.00006	**50.5 ± 1.1**
02JH47/2-3	0.19	209	1014	5.02	116.89 ± 1.91	0.0486 ± 0.0007	54.8 ± 0.9	0.00257 ± 0.00005	**52.0 ± 1.0**
02JH47/2-5	0.39	202	1204	6.15	120.37 ± 1.97	0.0502 ± 0.0007	53.1 ± 0.9	0.00256 ± 0.00005	**51.8 ± 1.0**
02JH47/2-6	0.48	206	1279	6.40	123.00 ± 2.03	0.0508 ± 0.0007	51.9 ± 0.9	0.00247 ± 0.00007	**49.9 ± 1.4**
02JH47/2-7A	0.28	204	1104	5.59	120.33 ± 1.97	0.0493 ± 0.0007	53.2 ± 0.9	0.00257 ± 0.00005	**51.8 ± 1.0**
02JH47/2-8	0.47	171	1089	6.57	118.65 ± 1.96	0.0508 ± 0.0008	53.8 ± 0.9	0.00256 ± 0.00006	**51.6 ± 1.1**
02JH47/2-9	0.48	149	901	6.26	117.68 ± 1.95	0.0509 ± 0.0008	54.3 ± 0.9	0.00259 ± 0.00004	**52.2 ± 0.9**
02JH47/2-10	0.36	196	1338	7.05	113.15 ± 1.85	0.0500 ± 0.0007	56.5 ± 0.9	0.00259 ± 0.00004	**52.3 ± 0.9**
02JH47/2-11	1.50	157	1140	7.49	126.44 ± 2.11	0.0589 ± 0.0031	50.0 ± 0.9	0.00232 ± 0.00007	**46.8 ± 1.3**
					$^{206}Pb/^{238}Pb$ Age Mean = 54.0 ± 1.0 Ma 95% c.i. n=9/10 MSWD = 2.1, probability = 0.3			**$^{208}Pb/^{232}Th$ Age** Mean = **51.7 ± 0.7 Ma** 95% c.i. n=8/10 MSWD = 0.53, probability =0. 81	
02JH14: *Kolpakova Gneiss, Krutogorova watershed (54º 49.288', N 157º 13.258', 1555m)*									
02JH14-1	0.92	185	1696	9.50	133.62 ± 2.22	0.0542 ± 0.0009	47.6 ± 0.8	0.00222 ± 0.00005	**44.8 ± 1.0**
02JH14-2	0.94	127	1519	12.37	125.19 ± 2.11	0.0544 ± 0.0010	50.8 ± 0.9	0.00247 ± 0.00007	**49.9 ± 1.4**
02JH14-3	0.93	128	1415	11.38	123.76 ± 2.10	0.0544 ± 0.0010	51.4 ± 0.9	0.00241 ± 0.00006	**48.7 ± 1.2**
02JH14-4	0.83	169	1592	9.72	123.62 ± 2.05	0.0536 ± 0.0009	51.5 ± 0.9	0.00246 ± 0.00005	**49.7 ± 1.0**
02JH14-5	0.97	138	1591	11.94	119.51 ± 2.01	0.0547 ± 0.0010	53.2 ± 0.9	0.00250 ± 0.00006	**50.4 ± 1.3**
02JH14-6	0.61	193	1486	7.96	122.97 ± 2.02	0.0518 ± 0.0008	51.9 ± 0.9	0.00249 ± 0.00008	**50.2 ± 1.7**
02JH14-7	0.99	94	1193	13.10	121.53 ± 2.11	0.0549 ± 0.0012	52.3 ± 0.9	0.00252 ± 0.00005	**51.0 ± 1.1**
02JH14-8	0.67	180	1557	8.92	118.91 ± 2.00	0.0524 ± 0.0008	53.6 ± 0.9	0.00253 ± 0.00005	**51.2 ± 1.0**
02JH14-9	0.79	196	1558	8.23	123.02 ± 2.04	0.0533 ± 0.0009	51.8 ± 0.9	0.00248 ± 0.00004	**50.1 ± 0.9**
02JH14-10	0.68	227	1744	7.94	120.04 ± 1.97	0.0525 ± 0.0008	53.1 ± 0.9	0.00252 ± 0.00006	**51.0 ± 1.1**
02JH14-11	0.71	190	1394	7.58	121.42 ± 2.00	0.0527 ± 0.0008	52.5 ± 0.9	0.00260 ± 0.00005	**52.4 ± 0.9**
02JH14-12	0.51	114	1332	12.08	119.44 ± 2.05	0.0512 ± 0.0011	53.5 ± 0.9	0.00248 ± 0.00007	**50.2 ± 1.3**
					$^{206}Pb/^{238}Pb$ Age Mean = 52.3 ± 0.5 Ma 95% c.i. n =11/12 MSWD = 1.13, probability = 0.34			**$^{208}Pb/^{232}Th$ Age** Mean = **50.5 ± 0.7** Ma 95% c.i. n=11/12 MSWD = 0.89, probability = 0.55	
02JH111: *Sheeted granite intrusion within the Kolpakova Gneiss, Left Andrianovka area (54º 37.547' N, 157º 35.049' E, 1040m)*									
02JH111-1	0.55	139	1792	13.28	117.70 ± 1.95	0.0514 ± 0.0008	54.2 ± 0.9	0.00259 ± 0.00006	**52.3 ± 1.3**
02JH111-2	0.33	400	1235	3.19	121.23 ± 1.94	0.0497 ± 0.0005	52.8 ± 0.8	0.00258 ± 0.00004	**52.1 ± 0.9**
02JH111-3	0.28	384	1062	2.86	119.82 ± 1.92	0.0493 ± 0.0005	53.4 ± 0.9	0.00257 ± 0.00007	**51.9 ± 1.5**
02JH111-4	0.25	180	1027	5.88	120.44 ± 1.98	0.0491 ± 0.0008	53.2 ± 0.9	0.00253 ± 0.00005	**51.1 ± 1.0**
02JH111-5	0.36	148	807	5.64	120.23 ± 1.99	0.0499 ± 0.0008	53.2 ± 0.9	0.00254 ± 0.00005	**51.4 ± 1.0**
02JH111-6	0.36	236	931	4.07	115.73 ± 1.89	0.0500 ± 0.0006	55.3 ± 0.9	0.00260 ± 0.00004	**52.5 ± 0.9**
02JH111-7	0.23	233	1072	4.76	119.79 ± 1.95	0.0489 ± 0.0006	53.5 ± 0.9	0.00257 ± 0.00005	**51.9 ± 1.0**
02JH111-8	0.45	102	1994	20.27	118.74 ± 2.07	0.0507 ± 0.0010	53.8 ± 0.9	0.00257 ± 0.00004	**51.9 ± 0.9**
					$^{206}Pb/^{238}Pb$ Age Mean = 53.6 ± 0.6 Ma 95% c.i. n=8/8 MSWD = 0.77, probability = 0.62			**$^{208}Pb/^{232}Th$ Age** Mean = 51.9 ± 0.7 Ma 95% c.i. n=8/8 MSWD = 0.25, probability = 0.9	

Table A.7

(continued)

Spot Name	% $^{206}Pb_{comm}$	U_{ppm}	Th_{ppm}	Th/U	Uncorrected $^{238}U/^{206}Pb$	Uncorrected $^{207}Pb/^{206}Pb$	^{207}Pb corrected $^{238}U/^{206}Pb$ Age	^{207}Pb corrected $^{208}Pb/^{232}Th$	^{207}Pb corrected $^{232}Th/^{208}Pb$ Age
02JH117: Boudinaged garnet-muscovite-Kspar pegmatite within the Kolpakova Gneiss, Left Andrianovka area (54º 37.017', 157º 34.935', 1070m)									
02JH117-1	0.29	186	1770	9.84	115.62 ± 1.89	0.0494 ± 0.0007	55.4 ± 0.9	0.00255 ± 0.00007	**51.5 ± 1.4**
02JH117-2	0.71	152	1849	12.55	115.71 ± 1.95	0.0527 ± 0.0015	55.1 ± 0.9	0.00256 ± 0.00006	**51.7 ± 1.1**
02JH117-3	0.25	198	2270	11.84	114.75 ± 1.87	0.0491 ± 0.0007	55.8 ± 0.9	0.00259 ± 0.00005	**52.3 ± 1.0**
02JH117-4	0.38	182	2461	13.94	114.68 ± 1.91	0.0502 ± 0.0008	55.8 ± 0.9	0.00260 ± 0.00007	**52.5 ± 1.4**
02JH117-5	0.39	163	2174	13.74	114.32 ± 1.88	0.0502 ± 0.0008	55.9 ± 0.9	0.00261 ± 0.00005	**52.6 ± 1.0**
02JH117-6	0.11	135	1209	9.23	111.77 ± 1.85	0.0480 ± 0.0008	57.4 ± 1.0	0.00257 ± 0.00005	**51.8 ± 1.1**
02JH117-7	0.15	134	1176	9.10	113.97 ± 1.89	0.0483 ± 0.0008	56.2 ± 0.9	0.00259 ± 0.00005	**52.3 ± 0.9**
02JH117-8	0.57	119	1309	11.40	112.67 ± 1.88	0.0516 ± 0.0009	56.6 ± 0.9	0.00258 ± 0.00006	**52.1 ± 1.1**
02JH117-9	0.55	150	2143	14.74	114.39 ± 1.90	0.0515 ± 0.0008	55.8 ± 0.9	0.00260 ± 0.00005	**52.5 ± 1.0**
02JH117-10	0.16	144	1191	8.55	111.40 ± 1.84	0.0484 ± 0.0008	57.5 ± 1.0	0.00259 ± 0.00008	**52.2 ± 1.6**
02JH117-11	0.66	136	1551	11.83	114.05 ± 1.93	0.0524 ± 0.0008	55.9 ± 0.9	0.00259 ± 0.00005	**52.3 ± 1.0**
02JH117-12	0.04	199	1249	6.50	113.58 ± 1.86	0.0475 ± 0.0007	56.5 ± 0.9	0.00255 ± 0.00005	**51.5 ± 0.9**

$^{206}Pb/^{238}Pb$ Age	$^{208}Pb/^{232}Th$ Age
Mean = 56.1 ± 0.53 Ma 95% c.i.	Mean = **52.1 ± 0.6** Ma 95% c.i.
n=12/12	n=12/12
MSWD = 0.62, probability = 0.82	MSWD = 0.12, probability = 1

Table A.8

Sample 02JH47/1—Zircon from leucosome of Kolpakova Gneiss, Krutogorova R. (54° 50.120 N, 157° 23.096 E, 1320 m)

Analysis	% $^{206}Pb_{comm}$	U_{ppm}	Th_{ppm}	Th/U	Uncorrected $^{238}U/^{206}Pb$	Uncorrected $^{207}Pb/^{206}Pb$	^{207}Pb Corrected $^{238}U/^{206}Pb$ Age	
02JH47/1-1	5.86	977	15	0.02	36.96 ± 1.08	0.0960 ± 0.0053	162.1 ± 5.0	c
02JH47/1-2	0.42	1063	6	0.01	128.29 ± 4.08	0.0504 ± 0.0026	49.8 ± 1.6	r
02JH47/1-3R	2.46	1093	5	0.00	121.06 ± 3.64	0.0665 ± 0.0028	51.7 ± 1.6	r
02JH47/1-3C	0.40	205	124	0.62	25.45 ± 0.76	0.0544 ± 0.0021	247.5 ± 7.3	c
02JH47/1-4	0.54	1463	13	0.01	133.71 ± 3.89	0.0512 ± 0.0019	47.8 ± 1.4	r †
02JH47/1-5	-0.13	1113	5	0.00	137.28 ± 4.05	0.0459 ± 0.0021	46.9 ± 1.4	r †
02JH47/1-6	0.18	608	217	0.37	12.28 ± 0.35	0.0587 ± 0.0009	504.0 ± 13.9	c
02JH47/1-7	0.37	2440	11	0.00	124.04 ± 3.65	0.0500 ± 0.0013	51.6 ± 1.5	r
02JH47/1-8	0.62	1092	4	0.00	125.93 ± 3.69	0.0519 ± 0.0021	50.7 ± 1.5	r
02JH47/1-9	0.54	1161	6	0.01	124.63 ± 3.66	0.0513 ± 0.0021	51.2 ± 1.5	r
02JH47/1-10	0.55	1313	7	0.01	123.01 ± 3.57	0.0514 ± 0.0018	51.9 ± 1.5	r
02JH47/1-11	0.42	1353	7	0.01	123.23 ± 3.56	0.0504 ± 0.0017	51.9 ± 1.5	r
02JH47/1-12	1.41	1142	8	0.01	125.74 ± 3.90	0.0582 ± 0.0025	50.3 ± 1.6	r
02JH47/1-13	0.05	1515	6	0.00	118.79 ± 3.51	0.0475 ± 0.0019	54.0 ± 1.6	r †
02JH47/1-14	2.29	937	10	0.01	109.58 ± 3.22	0.0653 ± 0.0025	57.2 ± 1.7	r †

$^{206}Pb/^{238}Pb$ Age

Mean = 51.2 ± 0.5 Ma 95% c.i.

n = 8/12 rim analyses

MSWD = 0.97, probability = 0.45

† Discordant analysis not used in calculation of weighted mean age. r = rim analysis, c = core analysis.

TABLE A.9

Sample 02JH117—Zircon from pegmatite within the Kolpakova Gneiss, Left Andrianovka area (54° 37.017′, 157° 34.935′, 1070m)

Analysis	$\%^{206}Pb_{comm}$	U_{ppm}	Th_{ppm}	Th/U	Uncorrected $^{238}U/^{206}Pb$	Uncorrected $^{207}Pb/^{206}Pb$	^{207}Pb Corrected $^{238}U/^{206}Pb$ Age	
02JH117-1	35.43	72	12	0.17	78.78 ± 2.33	0.3276 ± 0.0167	52.6 ± 4.3	†
02JH117-2	0.30	3003	26	0.01	122.89 ± 1.32	0.0494 ± 0.0011	52.1 ± 0.6	
02JH117-3	0.70	5306	96	0.02	123.64 ± 1.26	0.0526 ± 0.0009	51.6 ± 0.5	
02JH117-4	2.86	8125	99	0.01	124.98 ± 1.28	0.0697 ± 0.0024	49.9 ± 0.6	
02JH117-5	0.76	10860	100	0.01	133.27 ± 1.31	0.0530 ± 0.0007	47.8 ± 0.5	
02JH117-6	1.34	3330	37	0.01	126.87 ± 1.40	0.0576 ± 0.0012	49.9 ± 0.6	
02JH117-7	0.74	734	85	0.12	99.14 ± 1.41	0.0531 ± 0.0024	64.2 ± 0.9	†
02JH117-8	0.27	2123	30	0.01	127.92 ± 1.46	0.0492 ± 0.0014	50.1 ± 0.6	

$^{206}Pb/ ^{238}Pb$ Age
Mean = 50.1 ± 1.7 Ma 95% conf.
Wtd by data-pt errs only, 7/9 analyses
MSWD = 8.4, probability = 0.0

† Discordant analysis not used in calculation of weighted mean age.

TABLE A.10

Sample 02JH111—Zircon from granite within the Kolpakova Gneiss, Left Andrianovka area (54° 37.547′ N, 157° 35.049′ E, 1040m)

Analysis	$\%^{206}Pb_{comm}$	U_{ppm}	Th_{ppm}	Th/U	Uncorrected $^{238}U/^{206}Pb$	Uncorrected $^{207}Pb/^{206}Pb$	^{207}Pb corrected $^{238}U/^{206}Pb$ Age	
02JH111-2	11.77	143	48	0.35	115.04 ± 2.53	0.1402 ± 0.0207	49.3 ± 2.0	
02JH111-3C	5.78	288	98	0.35	34.05 ± 0.34	0.0957 ± 0.0058	175.9 ± 2.6	†
02JH111-4	14.20	320	161	0.52	111.59 ± 1.69	0.1594 ± 0.0061	49.4 ± 1.3	
02JH111-5	4.96	529	374	0.73	121.84 ± 1.51	0.0863 ± 0.0036	50.1 ± 0.7	
02JH111-6	4.48	1900	56	0.03	120.35 ± 0.79	0.0825 ± 0.0034	51.0 ± 0.5	
02JH111-7	30.98	43	9	0.23	85.24 ± 3.08	0.2924 ± 0.0366	52.0 ± 4.9	
02JH111-7R	0.36	4206	20	0.00	119.14 ± 0.63	0.0500 ± 0.0015	53.7 ± 0.3	
02JH111-8	0.41	5615	314	0.06	115.51 ± 0.43	0.0503 ± 0.0008	55.3 ± 0.2	
02JH111-98	0.44	2114	121	0.06	117.98 ± 0.74	0.0506 ± 0.0014	54.2 ± 0.4	
02JH111-10	0.57	3628	81	0.02	122.47 ± 0.58	0.0516 ± 0.0014	52.1 ± 0.3	
02JH111-11	16.53	108	54	0.52	102.07 ± 2.47	0.1779 ± 0.0105	52.5 ± 2.0	
02JH111-12	1.41	1768	229	0.13	124.72 ± 0.86	0.0582 ± 0.0016	50.8 ± 0.4	
02JH111-12C	4.65	380	106	0.29	65.04 ± 0.75	0.0848 ± 0.0032	93.8 ± 1.3	†

$^{206}Pb/ ^{238}Pb$ Age
Mean = 52.6 ± 1.2 [2.3%] 95% conf.
n= 12/12
MSWD = 6.0, probability = 0.000

† Discordant analysis not used in calculation of weighted mean age.

TABLE A.11

Sample 02AS04—Zircon from a late syn-kinematic granite, Krutogorova River (N 54°53.15′, E157°17.20′)

Analysis	$\%^{206}Pb_{comm}$	U_{ppm}	Th_{ppm}	Th/U	Uncorrected $^{238}U/^{206}Pb$	Uncorrected $^{207}Pb/^{206}Pb$	^{207}Pb corrected $^{238}U/^{206}Pb$ Age
02AS04-1	0.71	156	74	0.49	123.37 ± 3.03	0.0526 ± 0.0035	51.7 ± 1.3
02AS04-2	1.21	346	330	0.99	124.18 ± 2.69	0.0566 ± 0.0025	51.1 ± 1.1
02AS04-3	4.60	134	37	0.28	117.24 ± 3.05	0.0834 ± 0.0077	52.2 ± 1.5
02AS04-4	2.73	347	493	1.47	120.69 ± 2.57	0.0686 ± 0.0025	51.7 ± 1.1
02AS04-7	1.04	174	45	0.27	122.94 ± 2.99	0.0553 ± 0.0034	51.7 ± 1.3
02AS04-5	9.35	136	46	0.35	114.48 ± 2.96	0.1211 ± 0.0079	50.8 ± 1.6
02AS04-6	0.07	470	199	0.44	124.24 ± 2.59	0.0476 ± 0.0019	51.6 ± 1.1
02AS04-8	10.78	22	6	0.28	110.81 ± 4.83	0.1324 ± 0.0147	51.7 ± 2.6
02AS04-9	2.08	392	71	0.19	119.57 ± 2.57	0.0636 ± 0.0025	52.6 ± 1.2
02AS04-10	0.05	218	85	0.40	128.44 ± 3.00	0.0474 ± 0.0029	50.0 ± 1.2
02AS04-11	0.68	166	53	0.33	124.02 ± 3.00	0.0524 ± 0.0034	51.4 ± 1.3
02AS04-12	1.45	109	45	0.43	123.44 ± 3.35	0.0585 ± 0.0045	51.3 ± 1.4
02AS04-13	1.26	201	83	0.43	122.60 ± 2.94	0.0571 ± 0.0034	51.7 ± 1.3

$^{206}Pb/^{238}Pb$ Age
Mean = 51.5 ± 0.7 95% conf.
n=13/13
MSWD = 0.27, probability = 0.993

Table A.12

Sample 01JG11—Zircon from lower tuffaceous member of the Eocene Baraba Conglomerate (N 55°04′25″, E157°18′35″, 1260 m)

Analysis	$\%^{206}Pb_{comm}$	U (ppm)	Th(ppm)	Th/U	$^{206}Pb^*$ (ppm)	Uncorrected $^{238}U/^{206}Pb$ (±%)	Uncorrected $^{207}Pb/^{206}Pb$ (±%)	Age (Ma, ± 1σ)	
JG11-1	0.00	427	199	0.48	2.82	130.4 ± 3.1	0.0443 ± 4.1	**49.4 ±1.5**	
JG11-2	0.00	497	277	0.58	3.34	128.0 ± 3.1	0.0455 ± 3.8	**50.3 ±1.5**	
JG11-3	0.18	210	59	0.29	1.37	131.7 ± 3.4	0.0484 ± 7.0	**48.7 ±1.7**	
JG11-4	0.05	290	118	0.42	1.94	128.3 ± 3.3	0.0474 ± 5.4	**50.0 ±1.7**	
JG11-5	0.00	146	52	0.37	0.968	129.6 ± 3.4	0.0445 ± 7.7	**49.7 ±1.7**	
JG11-6	0.49	110	32	0.31	0.769	122.6 ± 3.5	0.0510 ± 7.1	**52.1 ±1.8**	
JG11-7A	0.07	937	107	0.12	6.81	118.2 ± 3.0	0.0477 ± 2.5	**54.3 ±1.6**	
JG11-8	0.00	377	87	0.24	2.40	134.9 ± 3.1	0.0469 ± 4.5	**47.6 ±1.5**	
JG11-9	0.00	647	283	0.45	4.40	126.5 ± 3.0	0.0457 ± 3.2	**50.8 ±1.5**	
JG11-10	0.14	394	105	0.27	2.67	126.8 ± 3.1	0.0482 ± 4.2	**50.6 ±1.6**	
JG11-11	0.43	197	97	0.51	1.35	126.1 ± 3.3	0.0505 ± 5.7	**50.7 ±1.7**	
JG11-12A	2.67	126	48	0.39	2.81	38.5 ± 3.1	0.0705 ± 3.7	**161.0 ±5.0**	†
JG11-13	0.00	790	163	0.21	5.38	126.1 ± 3.0	0.0469 ± 2.9	**50.9 ±1.5**	
JG11-14	0.00	327	93	0.29	2.23	126.2 ± 3.2	0.0422 ± 4.7	**51.2 ±1.6**	
JG11-15	0.14	391	112	0.30	2.65	127.1 ± 3.1	0.0481 ± 4.1	**50.5 ±1.6**	
JG11-16	0.44	333	93	0.29	2.29	124.9 ± 3.1	0.0505 ± 4.5	**51.2 ±1.6**	

$^{206}Pb/^{238}Pb$ Age
Mean = 50.5 ± 1.2 95% conf.
n=15/16
MSWD = 0.90

† Discordant analysis not used in calculation of weighted mean age.

Table A.13

Sample 02JH87—Detrital zircon from Paleocene (?) Khozgon Formation sandstone (54° 32.178′ N, 157° 41.531′ E, 1220 m

Analysis	% Pb_{com}	U/ppm	Th/ppm	Th/U	Isotopic Ratios (± 1σ)		Age (Ma, ± 1σ)	
Grain-ages <1.0 Ga					^{207}Pb Corrected Ratios		^{207}Pb Corrected	^{204}Pb Corrected
					$^{207}Pb/^{206}Pb$	**$^{238}U/^{206}Pb$**	**$^{206}Pb/^{238}U$ Age**	**$^{206}Pb/^{238}U$ Age**
02JH87-02	30.8	211	91	0.45	0.2913 ± 0.0430	78.45 ± 1.77	**52.7 ± 5.4**	**53.2 ± 5.4**
02JH87-03	16.0	100	79	0.82	0.1767 ± 0.0182	32.43 ± 0.76	**161.2 ± 9.4**	**168.6 ± 9.7**
02JH87-04	3.6	84	99	1.21	0.0800 ± 0.0050	25.89 ± 0.61	**230.8 ± 8.1**	**232.9 ± 7.8**
02JH87-05	10.6	29	60	2.11	0.1361 ± 0.0156	22.63 ± 0.79	**262.8 ± 9.9**	**255.4 ± 9.8**
02JH87-07	4.5	93	48	0.53	0.0851 ± 0.0056	34.66 ± 0.87	**167.4 ± 8.3**	**170.0 ± 2.5**
02JH87-08	0.4	658	490	0.77	0.0540 ± 0.0016	27.98 ± 0.35	**226.6 ± 2.8**	**229.5 ± 2.9**
02JH87-09	2.9	199	88	0.46	0.0726 ± 0.0037	38.70 ± 0.73	**156.9 ± 4.1**	**164.8 ± 4.1**
02JH87-10	7.4	107	62	0.60	0.1130 ± 0.0043	16.24 ± 0.31	**353.0 ± 11.0**	**355.0 ± 10.7**
02JH87-11	16.3	106	103	1.01	0.1802 ± 0.0071	25.75 ± 0.56	**212.2 ± 9.5**	**217.1 ± 9.5**
02JH87-12	17.9	94	54	0.59	0.1905 ± 0.0112	45.09 ± 1.25	**120.9 ± 8.5**	**125.9 ± 8.7**
02JH87-13	9.5	338	129	0.39	0.1223 ± 0.0070	94.14 ± 2.03	**58.8 ± 3.0**	**59.2 ± 3.0**
02JH87-15	3.6	369	155	0.43	0.0762 ± 0.0043	83.19 ± 1.67	**74.6 ± 1.7**	**75.3 ± 1.6**
02JH87-16	0.7	367	112	0.31	0.0621 ± 0.0016	12.99 ± 0.17	**475.8 ± 5.9**	**483.8 ± 5.8**
02JH87-17	6.5	211	113	0.56	0.0987 ± 0.0070	97.84 ± 3.15	**65.6 ± 2.1**	**66.9 ± 1.8**
02JH87-19	-0.2	343	57	0.17	0.0677 ± 0.0012	6.66 ± 0.09	**899.0 ± 11.2**	**897.8 ± 11.5**
02JH87-20	10.5	20	0	0.01	0.1324 ± 0.0174	42.61 ± 2.34	**128.2 ± 7.6**	**130.8 ± 7.0**
02JH87-21	3.9	166	105	0.65	0.0783 ± 0.0074	101.40 ± 3.02	**61.5 ± 2.1**	**60.4 ± 1.8**
02JH87-22	0.8	367	368	1.04	0.0549 ± 0.0027	45.94 ± 0.75	**138.1 ± 2.3**	**135.9 ± 10.0**
02JH87-23	0.4	1086	151	0.14	0.0616 ± 0.0008	11.54 ± 0.12	**534.5 ± 5.4**	**551.6 ± 5.7**
02JH87-25	19.2	100	93	0.96	0.2018 ± 0.0096	37.47 ± 1.12	**139.6 ± 10.6**	**138.8 ± 2.1**
02JH87-26	1.3	349	182	0.54	0.0579 ± 0.0052	95.08 ± 2.00	**66.6 ± 1.5**	**68.0 ± 1.3**
02JH87-27	1.8	182	93	0.53	0.0642 ± 0.0035	30.45 ± 0.57	**205.2 ± 3.9**	**209.4 ± 3.6**
02JH87-28	2.8	203	122	0.62	0.0706 ± 0.0046	54.85 ± 1.19	**110.3 ± 4.2**	**111.2 ± 4.1**
02JH87-29	1.5	218	74	0.35	0.0627 ± 0.0030	25.57 ± 0.45	**244.7 ± 4.3**	**252.6 ± 4.1**
02JH87-30	1.9	462	222	0.50	0.0621 ± 0.0042	94.58 ± 1.96	**67.8 ± 1.4**	**68.1 ± 1.4**
02JH87-32	0.6	429	323	0.78	0.0539 ± 0.0025	38.06 ± 0.59	**166.4 ± 2.6**	**169.5 ± 8.2**
Grain-ages >1.0 Ga					^{204}Pb Corrected Ratios			^{204}Pb Corrected
					$^{206}Pb/^{238}U$	**$^{207}Pb/^{235}U$**	**$^{207}Pb/^{206}Pb$**	**$^{207}Pb/^{206}Pb$ Age**
02JH87-06	1.0	52	34	0.67	0.3501 ± 0.0067	5.81 ± 0.23	0.1204 ± 3.5315	**1962.8 ± 63.0**
02JH87-14	0.8	120	78	0.67	0.2331 ± 0.0035	2.89 ± 0.10	0.0900 ± 3.1761	**1426.3 ± 60.7**
02JH87-18	0.8	117	34	0.30	0.3301 ± 0.0048	5.35 ± 0.12	0.1176 ± 1.7148	**1920.1 ± 30.7**
02JH87-24	0.3	686	79	0.12	0.3240 ± 0.0036	5.04 ± 0.07	0.1128 ± 0.6856	**1844.7 ± 12.4**
02JH87-31	0.1	217	95	0.45	0.3583 ± 0.0050	5.98 ± 0.11	0.1210 ± 1.2258	**1970.4 ± 21.9**

Table A.14

Sample 95JG16—Detrital zircon from a Paleocene Ukelayat Group sandstone, Koryak Highlands (61° 41.947′ N, 171° 47.844′ E, 430 m)

Analysis	U/ppm	Th/ppm	Th/U	Isotopic Ratios (± 1σ)				Age (Ma, ± 1σ)
Grain-ages <1.0 Ga								
					$^{207}Pb / ^{206}Pb$	$^{238}U / ^{206}Pb$		$^{206}Pb / ^{238}U$ Age
95JG16-1	110	113	1.03		0.0472 ± 0.0050	30.74 ± 1.22		**209.3 ± 8.3**
95JG16-3	192	174	0.91		0.0621 ± 0.0060	49.06 ± 4.88		**129.6 ± 12.8†**
95JG16-4	90	69	0.77		0.0491 ± 0.0058	57.26 ± 2.48		**113.0 ± 4.9**
95JG16-6	353	213	0.60		0.0486 ± 0.0033	76.90 ± 2.95		**84.4 ± 3.2**
95JG16-8	247	120	0.49		0.0409 ± 0.0042	116.87 ± 4.45		**56.2 ± 2.2**
95JG16-10	222	93	0.42		0.0517 ± 0.0031	48.44 ± 2.52		**132.9 ± 6.9**
95JG16-11	365	147	0.40		0.0476 ± 0.0029	75.92 ± 3.22		**85.6 ± 3.6**
95JG16-12	323	133	0.41		0.0501 ± 0.0055	81.30 ± 3.70		**79.7 ± 3.6**
95JG16-13	400	684	1.71		0.0471 ± 0.0025	67.45 ± 3.14		**96.3 ± 4.5**
95JG16-15	33	37	1.14		0.0433 ± 0.0072	26.16 ± 1.42		**246.5 ± 13.3**
95JG16-18	259	184	0.71		0.0496 ± 0.0021	30.06 ± 1.20		**213.4 ± 8.4**
95JG16-19	120	50	0.42		0.0538 ± 0.0050	77.74 ± 3.22		**82.9 ± 3.5**
95JG16-21	165	220	1.33		0.0505 ± 0.0027	26.91 ± 1.26		**237.7 ± 11.0**
95JG16-22	247	110	0.44		0.0515 ± 0.0038	97.35 ± 4.01		**66.5 ± 2.7**
95JG16-23	851	48	0.06		0.1088 ± 0.0020	7.39 ± 0.62		**771.0 ± 61.8†**
95JG16-24	105	45	0.42		0.0721 ± 0.0080	12.01 ± 0.72		**507.7 ± 29.6†**
95JG16-25	207	125	0.60		0.0520 ± 0.0049	119.39 ± 8.78		**54.2 ± 4.0**
95JG16-27	173	86	0.50		0.0531 ± 0.0022	14.32 ± 0.52		**438.3 ± 15.4**
95JG16-28	435	525	1.21		0.0517 ± 0.0023	56.12 ± 3.01		**114.9 ± 6.1**
95JG16-29	69	104	1.51		0.0517 ± 0.0032	20.39 ± 0.95		**311.3 ± 14.3**
95JG16-30	118	116	0.98		0.0666 ± 0.0042	40.47 ± 2.73		**155.9 ± 10.4†**
95JG16-32	526	243	0.46		0.0485 ± 0.0025	60.98 ± 4.02		**106.2 ± 7.0**
95JG16-34	475	198	0.42		0.0480 ± 0.0023	59.30 ± 2.74		**109.3 ± 5.0**
95JG16-35	73	54	0.74		0.0568 ± 0.0045	28.61 ± 1.34		**222.1 ± 10.3**
95JG16-36	206	117	0.57		0.0584 ± 0.0017	11.92 ± 0.43		**519.8 ± 18.2**
95JG16-37	179	87	0.48		0.0501 ± 0.0051	73.99 ± 8.56		**87.5 ± 10.1**
95JG16-38	248	67	0.27		0.0611 ± 0.0015	10.99 ± 0.50		**560.3 ± 24.5**
95JG16-39	194	145	0.75		0.0521 ± 0.0019	22.88 ± 0.92		**278.1 ± 11.0**
95JG16-40	19	16	0.84		0.0590 ± 0.0117	42.61 ± 2.48		**149.6 ± 8.9**
95JG16-41	117	55	0.47		0.0697 ± 0.0046	18.12 ± 1.21		**342.0 ± 22.3**
95JG-16-1.1	579	162	0.28		0.0493 ± 0.0019	73.76 ± 2.03		**86.7 ± 2.4**
95JG-16-2.1	494	317	0.64		0.0517 ± 0.0023	88.35 ± 4.83		**72.2 ± 3.9†**
95JG-16-3.1	271	86	0.32		0.0975 ± 0.0081	113.16 ± 2.58		**53.1 ± 1.3†**
95JG-16-4.1	507	702	1.39		0.0591 ± 0.0039	21.86 ± 1.24		**285.9 ± 16.0†**
95JG-16-5.1	112	156	1.40		0.0525 ± 0.0034	28.86 ± 1.92		**219.1 ± 14.4**
95JG-16-7.1	172	100	0.58		0.0493 ± 0.0045	58.23 ± 4.19		**109.6 ± 7.9**
95JG-16-8.1	148	91	0.62		0.0575 ± 0.0049	63.79 ± 3.74		**99.1 ± 5.8†**
95JG-16-9.1	850	111	0.13		0.0506 ± 0.0014	40.66 ± 1.69		**156.3 ± 6.4**
95JG-16-10.1	31	31	1.00		0.0528 ± 0.0054	16.98 ± 1.04		**369.4 ± 22.2**
Grain-ages >1.0 Ga								
				%f206	$^{206}Pb / ^{238}U$	$^{207}Pb / ^{235}U$	$^{207}Pb / ^{206}Pb$	$^{207}Pb / ^{206}Pb$ Age
95JG16-2	59	22	0.38	0.02	0.3172 ± 0.0162	5.218 ± 0.307	0.1193 ± 0.0028	**1945.7 ± 42.7**
95JG16-5	107	79	0.74	0.02	0.2866 ± 0.0136	3.895 ± 0.204	0.0986 ± 0.0017	**1597.5 ± 32.2**
95JG16-7	122	99	0.81	0.07	0.3322 ± 0.0156	5.097 ± 0.267	0.1113 ± 0.0020	**1820.3 ± 32.3**
95JG16-9	144	73	0.51	0.02	0.3356 ± 0.0121	5.233 ± 0.209	0.1131 ± 0.0015	**1849.4 ± 24.3**
95JG16-14	218	39	0.18	0.02	0.3291 ± 0.0114	5.393 ± 0.201	0.1188 ± 0.0012	**1938.9 ± 17.4**
95JG16-16	673	82	0.12	0.02	0.2899 ± 0.0102	4.493 ± 0.168	0.1124 ± 0.0010	**1838.6 ± 16.2**
95JG16-17	270	388	1.44	0.14	0.3158 ± 0.0137	5.056 ± 0.236	0.1161 ± 0.0014	**1897.1 ± 22.2**
95JG16-20	589	300	0.51	0.01	0.3807 ± 0.0126	6.742 ± 0.234	0.1284 ± 0.0009	**2076.6 ± 13.0**
95JG16-26	80	89	1.10	0.02	0.3153 ± 0.0149	5.136 ± 0.272	0.1181 ± 0.0022	**1928.3 ± 33.9**
95JG16-31	1403	56	0.04	0.04	0.2976 ± 0.0151	4.556 ± 0.236	0.1110 ± 0.0006	**1816.2 ± 9.1**
95JG16-33	56	11	0.19	0.02	0.2917 ± 0.0115	4.463 ± 0.228	0.1110 ± 0.0031	**1815.2 ± 51.7**
95JG-15-6.1	78	33	0.42	0.02	0.3690 ± 0.0129	6.391 ± 0.277	0.1256 ± 0.0027	**2037.8 ± 38.3**

† Discordant analysis not used in calculation of weighted mean age.

References

Batanova, V. G., Pertsev, A. N., Kamenetsky, V. S., Ariskin, A. A., Mochalov, A. G., and Sobolev, A. V., 2005, Crustal Evolution of Island-Arc Ultramafic Magma: Galmoenan Pyroxenite-Dunite Plutonic Complex, Koryak Highland (Far East Russia): Journal of Petrology, v. 46, p. 1345–1366, doi:10.1093/petrology/egi018.

Belyatskiy, B. V., Landa, E. A., Markovskiy, B. A., and Siderov, E. G., 2002, Perviye danniye isotopnogo datirovaniya dunit-klinopyroxenit zonal’nogo massiva tsentral’noi Kamchatki (First data of isotopic dating of a dunite-clinopyroxenite zoned massif of central Kamchatka): Doklady (Transactions) Russian Academy of Sciences, v. 382, p. 235–237.

Bernet, M., and Garver, J. I., 2005, Fission-track analysis of detrital zircon, Low-Temperature Thermochronology: Techniques, Interpretations, and Applications: Reviews in Mineralogy and Geochemistry, v. 58, p. 205–237, doi: 10.2138/rmg.2005.58.8.

Bindeman, I. N., Vinogradov, V. I., Valley, J. W., Wooden, J. L., and Natal'in, B. A., 2002, Archean Protolith and Accretion of Crust in Kamchatka: SHRIMP Dating of Zircons from Sredinny and Ganal massifs: The Journal of Geology, v. 110, p. 271–289, doi:10.1086/339532.

Bogdanov, N. A., and Chekhovich, V. D., 2002, On the Collision between the West Kamchatka and Sea of Okhotsk Plates: Geotectonics, v. 36, p. 63–76.

Bogdanov, N. A., and Dobretsov, N. L., 2002, The Okhotsk Volcanic Plateau: Russian Geology and Geophysics (English Translation), v. 43, p. 87–99.

Bogdanov, N. A., Til'man, S. M., and Chekhovich, V. D., 1990, Geology of the western Bering Sea region; Chapter 3, Late Cretaceous-Cenozoic history of the Koryak-Kamchatka region and the Commander Basin of the Bering Sea [modified]: International Geology Review, v. 32, p. 1185–1201.

Bondarenko, G. Y., ms, 1992, The Jurassic-Valangin Stage of the Evolution of Kamchatka (in Russian): Moscow, Russia, Moscow State University and Geological Institute, Moscow, Ph. D. thesis.

——— 1997, Ul'traosnovnyye i osnovnyye metavulkanity sredinnogo khrebta kamchatki; polozheniye v razreze i obstanovka formirovaniya. Ultramafic and mafic metavolcanic rocks of Sredinny Ridge, Kamchatka; sequential development and formation conditions: Byulleten' Moskovskogo Obshchestva Ispytateley Prirody, Otdel Geologicheskiy, v. 72, p. 32–40.

Bondarenko, G. Y., Kuznetsov, N. B., Savostin, L. A., Smolyar, M. I., and Sokolov, S. Y., 1993, Izontopnyy vozrast granatovykh plagiogranioidov sredinnogo khrebet, Kamchatki. Isotopic age of garnet plagiogranites in the Central Kamchatka Range: Doklady, RAN, v. 330, p. 233–236.

Brandon, M. T., 1996, Probability density plots for fission-track grain-age samples: Radiation Measurements, v. 26, p. 663–676, doi:10.1016/S1350-4487(97)82880-6.

Brandon, M. T., and Vance, J. A., 1992, Tectonic evolution of the Cenozoic Olympic subduction complex, Washington State, as deduced from fission track ages for detrital zircons: American Journal of Science, v. 292, p. 565–636.

Bullen, M. E. ms, 1997, Fission-track dating of detrital zircons used to constrain the collision of the Olyutorsky Island Arc, Koryak Highlands, Northern Kamchatka: Schenectady, New York, Union College, 126 p.

Bundtzen, T. K., Layer, P. W., Sidorov, E., and Anonymous, 2003, Geology, geochemistry, and new isotopic ages of PGE-Ni-Cu bearing, mafic/ultramafic rocks of the Farewell and Sredinny terranes, Alaska, USA, and Kamchatka, Russia: Geological Society of America, Abstracts with Programs, v. 35, p. 60.

Burk, C. A., and Gnibidenko, H. S., 1977, The structure and age of acoustic basement in the Okhotsk Sea, *in* Talwani, M., and Pitman, W. C., III, editors, Island arcs, deep sea trenches and back-arc basins: Washington, American Geophysical Union, p. 451–461.

Catlos, E. J., Gilley, L. D., and Harrison, T. M., 2002, Interpretation of monazite ages obtained via in situ analysis: Chemical Geology, v. 188, p. 193–215, doi:10.1016/S0009-2541(02)00099-2.

Cherniak, D. J., Watson, E. B., Grove, M., and Harrison, T. M., 2004, Pb diffusion in monazite: A combined RBS/SIMS study: Geochimica et Cosmochimica Acta, v. 68, p. 829–840, doi:10.1016/j.gca.2003.07.012.

Crawford, M. B., and Windley, B. F., 1990, Lecograntites of the Himalaya/Karakoram: Implications for magmatic evolution within collisional belts and the study of collision-related leucogranite petrogenesis: Journal of Volcanology and Geothermal Research, v. 44, p. 1–19, doi:10.1016/0377-0273(90)90008-4.

Dickin, A. P., 1997, Radiogenic Isotope Geology: Cambridge, United Kingdom, Cambridge University Press, 490 p.

Drummond, M. S., Defant, M. J., and Kepezhinskas, P. K., 1996, Petrogenesis of slab-derived trondhjemite-tonalite-dacite/adakite magmas, *in* Walker, J. R., Candela, P. A., Peck, D. L., Stephens, W. E., Brown, M., and Zen, E-An, editors, Origin of Granites and Related Rocks, The Third Hutton Symposium: Transactions of the Royal Society of Edinburgh: Earth Sciences, v. 87, p. 205–215.

England, P. C., and Thompson, A. B., 1984, Pressure-temperature-time paths of regional metamorphism I. Heat transfer during the evolution of regions of thickened continental crust: Journal of Petrology, v. 25, p. 894–928, doi: 10.1093/petrology/25.4.894.

Farley, K. A., 2000, Helium diffusion from apatite: General behavior as illustrated by Durango fluorapatite: Journal of Geophysical Research, v. 105(B2), Solid Earth and Planets, v. 105, p. 2903–2914, doi:10.1029/1999JB900348.

Farley, K. A., Wolf, R. A., and Silver, L. T., 1996, The effects of long alpha-stopping distances on (U-Th)/He ages: Geochimica et Cosmochimica Acta, v. 60, p. 4223–4229, doi:10.1016/S0016-7037(96)00193-7.

Fleorov, G. B., and Koloskov, A. V., 1976, Schelochnoi basaltovoi magmatism Sredinno-Kamchatskogo massiva (Alkalic basaltic magmatism in the Central-Kamchatka massif): Moscow, Nauka, 147 p.

Fletcher, R. C., 1972, Application of a mathematical model to the emplacement of mantled gneiss domes: American Journal of Science, v. 272, p. 197–216.

Fletcher, R. C., and Hallet, B., 2004, Initiation of gneiss domes by necking, density instability, and erosion: Geological Society of America, Special Paper, v. 380, p. 79–95.

Gans, P. B., 1987, An open-system, two-layer crustal stretching model for the eastern Great Basin: Tectonics, v. 6, p. 1–12, doi:10.1029/TC006i001p00001.

Garver, J. I., Soloviev, A. V., Bullen, M. E., and Brandon, M. T., 2000a, Towards a more complete record of magmatism and exhumation in continental arcs using detrital fission track thermochronometry: Physics and Chemistry of the Earth, Part A, v. 25, p. 565–570.

Garver, J. I., Brandon, M. T., and Soloviev, A. V., 2000b, Eocene Collision of the Olutorsky terrane, Kamchatka, Russia: American Geophysical Union, EOS Transactions, p. F1243.

Garver, J. I., Brandon, M. T., Bernet, M., Brewer, I., Soloviev, A. V., Kamp, P. J. J., and Meyer, N., 2000c, Practical consideration for using detrital zircon fission track thermochronology for provenance, exhumation studies, and dating sediments, *in* Noble, W. P., O'Sullivan, P. B., and Brown, R. W., editors, The 9th International Conference of Fission-track dating and Thermochronology, Lorne, Australia, February 6–11, 2000: Geological Society of Australia Abstracts, v. 58, p. 109–111.

Geist, E. L., Vallier, T. L., and Scholl, D. W., 1994, Origin, transport, and emplacement of an exotic island-arc terrane exposed in eastern Kamchatka, Russia: Geological Society of America Bulletin, v. 106, p. 1182–1194, doi:10.1130/0016-7606(1994)106⟨1182:OTAEOA⟩2.3.CO;2.

German, L. L., 1978, Drevneyshiye kristallicheskiye kompleksy Kamchatki: Moscow, Izd. Nedra, 124 p.

Gladenkov, Y. B., 1998, Resolutions of Interdepartmental Working Conferences on Paleogene and Neogene Stratigraphy of Eastern Russia: Kamchatka, Koryak Upland, Sakhalin, and Kurile Islands, Explanatory Note to Stratigraphic Schemes [in Russian]: Moscow, GEOS.

Gladenkov, Y. B., Shantser, A. Y., Chelebayeva, A. I., Sinel'nikova, V. N., Antipov, M. P., Ben'yamovskiy, V. N., Brattseva, G. M., Polyanskiy, B. V., Stupin, S. I., and Fedorov, P. I., 1997, Nizhniy paleogen Zapadnoy Kamchatki; stratigrafiya, paleogeografiya, geologicheskiye sobytiya. Lower Paleogene of western Kamchatka; stratigraphy, paleogeography, geological events: Trudy—Rossiyskaya Akademiya Nauk, Geologicheskiy Institut, v. 488, p. 367.

Gnibidenko, H. S., and Khvedchuk, I. I., 1982, The tectonics of the Okhotsk Sea: Marine Geology, v. 50, p. 155–198, doi:10.1016/0025-3227(82)90138-4.

Gorbatov, A., Widiyantoro, S., Fukao, Y., and Gordeyev, Y., 2000, Signature of remnant slabs in the North Pacific from P-wave tomography: Geophysical Journal International, v. 142, p. 27–36, doi:10.1046/j.1365-246x.2000.00122.x.

Hanchar, J. M., and Miller, C. F., 1992, Zircon zonation patterns as revealed by cathodoluminescence and backscattered electron images: Implications for interpretation of complex crustal histories, *in* Watson, E. B., Harrison, T. M., Miller, C. F., and Ryerson, F. J., editors, Geochemistry of Accessory Minerals, Third V. M. Goldschmidt Conference, Reston, Virginia, 08–10 May 1992: Elsevier, Chemical Geology, v. 110, n. 1–3, p. 1–13.

Hanchar, J. M., Rudnick, R. L., and Hensen, B. J., 1993, Revealing hidden structures; the application of cathodoluminescence and back-scattered electron imaging to dating zircons from lower crustal xenoliths, *in* O'Reilly, S. Y., and Hensen, B. J., editors, International workshop: The xenolith window to the lower crust: Lithos, v. 36 p. 289–303.

Harrison, T. M., Catlos, E. J., and Montel, J.-M., 2002, U-Th-Pb dating of Minerals, *in* Kohn, M. J., Rakovan, J., and Hughes, J. M., editors, Phosphates: Geochemical, Geobiological and Materials Importance: Reviews in Mineralogy and Geochemistry, v. 48, p. 524–558, doi: 10.2138/rmg.2002.48.14.

Harrison, T. M., Lovera, O. M., and Grove, M., 1997, New insights into the origin of two contrasting Himalayan granite belts: Geology, v. 25, p. 899–902, doi:10.1130/0091-7613(1997)025⟨0899:NIITOO⟩2.3.CO;2.

Hill, E. J., Baldwin, S. L., and Lister, G. S., 1995, Magmatism as an essential driving force for formation of active metamophic core complexes in eastern Papua New Guinea: Journal of Geophysical Research, v. 100(B6), p. 10,441–10,541, doi:10.1029/94JB03329.

Hourigan, J. K., and Akinin, V. V., 2004, Tectonic and chronostratigraphic implications of new $^{40}Ar/^{39}Ar$ geochronology and geochemistry of the Arman and Maltan-Ola volcanic fields, Okhotsk-Chukotka volcanic belt, northeastern Russia: GSA Bulletin, v. 116, p. 637–654, doi:10.1130/B25340.1.

Hourigan, J. K., Solov'ev, A. V., Ledneva, G. V., Garver, J. I., Brandon, M. T., and Reiners, P. W., 2004, Dating of syenite intrusions on the eastern flank of the Sredinniy Range: rates of exhumation of accretionary complexes: Geochemistry International, v. 42, n. 2, p. 97–105.

House, M. A., Farley, K. A., and Stockli, D., 2000, Helium chronometry of apatite and titanite using Nd-YAG laser heating: Earth and Planetary Science Letters, v. 183, p. 365–368, doi:10.1016/S0012-821X(00)00286-7.

Ireland, T. R., and Gibson, G. M., 1998, SHRIMP monazite and zircon geochronology of high-grade metamorphism in New Zealand: Journal of Metamorphic Geology, v. 16, p. 149–167, doi: 10.1111/j.1525-1314.1998.00112.x.

Jenkin, G. R. T., Rogers, G., Fallick, A. E., and Farrow, C. M., 1995, Rb-Sr closure temperatures in bi-mineralic rocks: a mode effect and test for different diffusion models: Chemical Geology, v. 122, p. 227–240, doi:10.1016/0009-2541(95)00013-C.

Jenkin, G. R. T., Ellam, R. M., Rogers, G., and Stuart, F. M., 2001, An investigation of closure temperature of the biotite Rb-Sr system: The importance of cation exchange: Geochimica et Cosmochimica Acta, v. 65, p. 1141–1160, doi:10.1016/S0016-7037(00)00560-3.

Jolivet, L., Cadet, J. P., and Lalevee, F., 1988, Mesozoic evolution of Northeast Asia and the collision of the Okhotsk microcontinent: Tectonophysics, v. 149, p. 89–109, doi:10.1016/0040-1951(88)90120-5.

Khanchuk, A. I., 1985, Evolutsiya Drevnoy Sialicheskoy Kory v Octrovoduzhnoy Sisteme Vostochnoy Asii (Evolution of ancient sialic crust in Island Arc systems of East Asia, In Russian): Vladivostok, Nauka, 135 p.

Kirmasov, A. B., Soloviev, A. V., and Hourigan, J. K., 2004, Collision and Postcollision Structural Evolution of the Andrianovka Suture, Sredinny Range, Kamchatka: Geotectonics, v. 38, p. 294–316.

Kohn, M. J., and Spear, F. S., 1990, Two new geobarometers for garnet amphibolites, with applications to southeastern Vermont: American Mineralogist, v. 75, p. 89–96.

Konnikov, E. G., Chubarov, V. M., Travin, A. V., Matukov, D. I., and Sidorov, E. G., 2006, Formation time of the Ni-bearing norite-cortlandite association of East Asia: Geochemistry International, v. 44, p. 516–521, doi:10.1134/S0016702906050090.

Konstantinovskaia, E. A., 2000, Geodynamics of an Early Eocene Arc-Continent Collision reconstructed from the Kamchatka Orogenic Belt, NE Russia: Tectonophysics, v. 325, p. 87–105, doi:10.1016/S0040-1951(00)00132-3.

——— 2001, Arc-continent collision and subduction reversal in the Cenozoic evolution of the Northwest Pacific; an example from Kamchatka (NE Russia), *in* Lallemand, S., Liu, C.-S., Angelier, J., and Tsai, Y. B., editors, Active subduction and collision in Southeast Asia (SEASIA): Amsterdam, Elsevier, Tectonophysics, v. 333, 10 April 2001, p. 75–94, doi: 10.1016/S0040-1951(00)00268-7.

—— 2002, The mechanism of continental crust accretion: an example of Western Kamchatka: Geotectonics, v. 36, p. 67–87.
Kuzmin, M. I., and Chukhonin, A. P., 1980, Precambrian age of gneisses of the Kamchatka Pluton: Doklady, Earth Science sections AN USSR, v. 251, p. 61–63.
Kuzmin, V. K., Belaytskii, B. V., and Puzankov, U. M., 2003, Noviye danniye o dokambriskom vozraste gneisovogo komplexa Kamchatskogo massiva (New data about Precambrian age of the gneiss complex of the Kamchatka massif), Geodynamics, magmatism and mineragenesis of the North Pacific continental margin: Magadan, p. 162–165 (in Russian).
L'vov, A. B., Neelov, A. N., Bogomolov, E. S., and Mikhailova, N. S., 1985, Age of metamorphic rocks of Ganalsk Range of Kamchatka: Soviet Geology and Geophysics, v. 26, p. 42–49.
Laslett, G. M., Green, P. F., Duddy, I. R., and Gleadow, A. J. W., 1987, Thermal annealing of fission tracks in apatite 2. A quantitative analysis: Chemical Geology: Isotope Geoscience Section, v. 65, p. 1–13, doi:10.1016/0168-9622(87)90057-1.
Lebedev, M. M., Tararin, I. A., and Lagovskaya, Y. A., 1967, Metamorphic zones of Kamchatka as an example of the metamorphic assemblages of the inner part of the Pacific belt: Tectonophysics, v. 4, p. 445–461, doi:10.1016/0040-1951(67)90010-8.
Ledneva, G. V., Soloviev, A. V., and Garver, J. I., 2000, Massifs of the Heterogeneous Mafic-Ultramafic Complex of the Olyutorsky Zone, Koryak Mountains: Petrology and Geodynamic Aspects: Petrology, v. 8, p. 428–454.
Ledneva, G. V., Nosova, A. A., and Soloviev, A. V., 2006, "Calc-Alkaline" Magmatism of the Omgon Range: Evidence for Early Paleogene Extension in the Western Kamchatka Segment of the Eurasian Continental Margin: Petrology, v. 14, p. 154–186, doi:10.1134/S0869591106020020.
Levashova, N. M., Bazhenov, M. L., and Shapiro, M. N., 1997, Late Cretaceous paleomagnetism of the East Ranges island arc complex, Kamchatka: Implications for terrane movements and kinematics of the northwest Pacific: Journal of Geophysical Research-Solid Earth, v. 102, p. 24,843–24,857, doi:10.1029/97JB00780.
Levashova, N. M., Shapiro, M. N., and Bazhenov, M. L., 1998, Late Cretaceous paleomagnetic data from the Median Range of Kamchatka, Russia: tectonic implications: Earth and Planetary Science Letters, v. 163, p. 235–246, doi:10.1016/S0012-821X(98)00190-3.
Levashova, N. M., Shapiro, M. N., Beniamovsky, V. N., and Bazhenov, M. L., 2000, Paleomagnetism and geochronology of the Late Cretaceous-Paleogene island arc complex of the Kronotsky Peninsula, Kamchatka, Russia: Kinematic implications: Tectonics, v. 19, p. 834–851, doi:10.1029/1998TC001087.
Litvinov, A. F., Patoka, M. G., and Markovskii, B. A., 1999, Map of the mineral resources of Kamchatka Region: St. Petersburg, VSEGEI, Scale 1:500 000.
Luchitskaya, M. V., Solov'ev, A. V., and Hourigan, J. K., 2008, Two stages of granite formation in the Sredinny Range, Kamchatka: Tectonic and geodynamic setting of granitic rocks: Geotectonics, v. 42, p. 286–304, doi:10.1134/S0016852108040031.
Marchenko, A. F., 1967, Geological map of USSR, Western Kamchatka series, Sheet N-57-XIV: Leningrad, VSEGEI.
—— 1975, O tektonicheskoi prirode, vozraste i strukturnom polozhenie metamorficheskikh kompleksov Kamchatki, On the tectonic nature, age and structural position of metamorphic complexes of Kamchatka, Voprosi magmatizma i tektoniki Dal'nevo Vostoka, Questions of Magmatism and Tectonics of the Far East: Vladivostok, Nauka, p. 234–246.
Martinez, F., Goodliffe, A. M., and Taylor, B., 2001, Metamorphic core complex formation by density inversion and lower crustal extrusion: Nature, v. 411, p. 930–934, doi:10.1038/35082042.
McDougall, I., and Harrison, T. M., 1999, Geochronology and Thermochronolgy by the ^{40}Ar/^{39}Ar Method: Oxford, Oxford University Press, 269 p.
Meldrum, A., Boatner, L. A., Weber, W. J., and Ewing, R. C., 1998, Radiation damage in zircon and monazite: Geochimica et Cosmochimica Acta, v. 62, p. 2,509–2,520, doi:10.1016/S0016-7037(98)00174-4.
Miller, E. L., Gelman, M., Parfenov, L., and Hourigan, J., 2002, Tectonic setting of Mesozoic magmatism: A comparison between northeastern Russia and the North American Cordillera: Geological Society of America, Special Paper, v. 360, p. 313–332, doi: 10.1130/0-8137-2360-4.313
Moll-Stalcup, E. J., 1994, Latest Cretaceous and Cenozoic magmatism in mainland Alaska, *in* Plafker, G., and Berg, H. C., editors, The Geology of Alaska: Boulder, Colorado, Geological Society of America, Geology of North America, v. G-1, p. 589–619.
Muir, R. J., Ireland, T. R., Weaver, S. D., and Bradshaw, J. D., 1996, Ion microprobe dating of Paleozoic granitoids; Devonian magmatism in New Zealand and correlations with Australia and Antarctica: Chemical Geology, v. 127, p. 191–210, doi:10.1016/0009-2541(95)00092-5.
Nekrasov, G. E., 2003, Tectonics of the Koryak-Kamchatka region and the general geodynamics of the northern Pacific Rim: Geotectonics, v. 37, p. 480–503.
Nokleberg, W. J., Parfenov, L. M., Monger, J. W. H., Norton, I. O., Khanchuk, A. I., Stone, D. B., Scholl, D. W., and Fujita, K., 1998, Phanerozoic tectonic evolution of the Circum-North Pacific: Reston, Virginia, U. S. Geological Survey, Open-File Report—OF 98-0754, 125 p.
Norlander, B. H., Whitney, D. L., Teyssier, C., and Vanderhaeghe, O., 2002, Partial melting and decompression of the Thor-Odin dome, Shuswap metamorphic core complex, Canadian Cordillera: Lithos, v. 61, p. 103–125
North American Commission on Stratigraphic Nomenclature, 2005, North American Stratigraphic Code: AAPG Bulletin, v. 89, p. 1547–1591, doi:10.1306/07050504129.
Overstreet, 1967, The geologic occurrence of monazite: Geological Survey Professional Paper 530, p. 1–327.
Parfenov, L. M., 1984, Kontinental'niye okraini i ostrovniye dugi mezozoid severo-vostoka azii, Continental Margins and Island Arcs of the Mesozoid of North-East Asia: Novosibirsk, Nauka, 183 p.

Parfenov, L. M., and Natal'in, B. A., 1977, Mesozoic-Cenozoic tectonic evolution of northeastern Asia: Transactions (Doklady) of the U.S.S.R. Academy of Sciences: Earth Science Sections, v. 235, p. 89–91.
Parrish, R. R., 1990, U-Pb dating of monazite and its application to geological problems: Canadian Journal of Earth Sciences = Journal Canadien des Sciences de la Terre, v. 27, p. 1431–1450.
Pechersky, D. M., Levashova, N. M., Shapiro, M. N., Bazhenov, M. L., and Sharonova, Z. V., 1997, Palaeomagnetism of Palaeogene volcanic series of the Kamchatsky Mys peninsula, east Kamchatka: The motion of an active island arc: Tectonophysics, v. 273, p. 219–237, doi:10.1016/S0040-1951(97)00002-4.
Powell, R., and Holland, T. J. B., 1988, An Internally Consistent Dataset with Uncertainties and Correlations:3. Applications to Geobarometry, Worked Examples and a Computer-Program: Journal of Metamorphic Geology, v. 6, p. 173–204, doi:10.1111/j.1525-1314.1988.tb00415.x.
Press, W. H., Teukolsky, S. A., Vetterling, W. T., and Flannery, B. P., 1992, Numerical Recipes in Fortran: The Art of Scientific Computing: Cambridge, England, Cambridge University Press, 963 p.
Rey, P., Vanderhaeghe, O., and Teyssier, C., 2001, Gravitational collapse of the continental crust: definition, regimes and modes: Tectonophysics, v. 342, p. 435–449, doi:10.1016/S0040-1951(01)00174-3.
Rikhtyer, A. V., 1995, Structure of the metamorphic complex of the central Kamchatka Massif: Geotectonics, v. 29, p. 65–72.
Roddick, J. C., and Compston, W., 1977, Strontium isotopic equilibration: A solution to a paradox: Earth and Planetary Science Letters, v. 34, p. 238–246, doi:10.1016/0012-821X(77)90008-5.
Rosen, 2002, Siberian craton—a fragment of a Paleoproterozoic supercontinent: Russian Journal of Earth Sciences, v. 4, p. 103–119.
Rotman, V. K., 1981, Geological Map of the USSR, Sheet N-56,57: Leningrad, VSEGEI, scale 1:1000000.
Salvador, A., 1994, International Stratigraphic Guide—A guide to stratigraphic classification, terminology, and procedure, 2nd edition: The International Union of Geological Sciences and The Geological Society of America, p. 214.
Savostin, L. A., Kuznetsov, N. B., Bondarenko, G. Y., Perchuk, A. L., and Gerya, T. V., 1994, New data on the relations between the Kamchatka and Andrianov complexes, central Kamchatka: Transactions (Doklady) of the U.S.S.R. Academy of Sciences: Earth Science Sections, v. 327A, p. 53–58.
Scharer, U., 1984, The effect of initial ^{230}Th disequilibrium on young U-Pb ages: the Makalu case, Himalaya: Earth and Planetary Science Letters, v. 67, p. 93–105.
Seliverstov, N. I., 1998, Evolution of a junction zone between the Kuril-Kamchatka and Aleutian island arcs; a geodynamic model: Volcanology and Seismology, v. 19, p. 269–275.
Sengor, A. M. C., and Natalin, B. A., 1996, Paleotectonics of Asia: Fragments of a synthesis, *in* Yin, A., and Harrison, M., editors, The Tectonic Evolution of Asia: London, Cambridge University Press, p. 486–641.
Shanster, A. E., and Chelebaeva, A. I., 2004, Stratigraphy, geological events, and a new model of Late Cretaceous-Early Paleogene rifting in central Kamchatka: Stratigraphy and Geological Correlation (English translation), v. 12, p. 394–405.
——— 2005, The Late Cretaceous of Central Kamchatka (In Russian): Moscow, Geos, p. 116.
Shantser, A. Y., Shapiro, M. N., Koloskov, A. V., Chelebayeva, A. I., and Sinel'nikova, V. N., 1985, Evolyutsiya struktury Lesnovskogo podnyatiya i yego obramleniya v kaynozoye (Severnaya Kamchatka). Evolution of Lesnovsk Rise structure and its frame in the Cenozoic, northern Kamchatka: Tikhookeanskaya Geologiya = Pacific Geology, v. 1985, p. 66–74.
Shapiro, M. N., 1995, The Upper Cretaceous Achaivayamian-Valginian volcanic arc and kinematics of the North Pacifc plates: Geotectonics, v. 29, p. 52–64.
Shapiro, M. N., Raznitsyn, Y. N., Shanster, A. E., and Lander, A. V., 1986, Struktura severo-vostochnogo obramleniya massiva metamorficheskikh porod sredinnigo khrebta Kamchatki (Structure of the northeastern framing of the Kamchatka's Sredinniy Ridge metamorphic massif), Ocherki po Geologii Vostoka SSSR (Articles on the Geology of Eastern USSR): Moscow, Nauka, p. 5–21.
Shapiro, M. N., Soloviev, A. V., Garver, J. I., and Brandon, M. T., 2001, Sources of zircons from Cretaceous and lower Paleogene terrigenous sequences from the southern Koryak upland and western Kamchatka: Lithology and Mineral Resources, v. 36, p. 322–336.
Sidorchuk, I. A., and Khanchuk, A. I., 1981, Mesozoic glaucophane schist complex on the western slope of the central ridge of Kamchatka: Soviet Geology and Geophysics, v. 22, p. 144–148.
Sivertseva, I. A., and Smirnova, A. N., 1974, O nakhodke paleozoyskikh spor v metamorfizovannykh otlozheniyakh Kamchatki. Paleozoic spore finds recovered from the metamorphic rocks of Kamchatka: Geologiya i Geofizika, v. 1974, p. 126–128.
Slyadnev, B. I., Sokolov, V. A., and Markovskiy, B. A., 1997, Barabskie Konglomerati: Osobennosti stroyeniya, sostava i problema proizkhozhdeniuya. (Baraba Conglomerate: Details of the structure, composition and problem of provenance): Tikhookeanskaya geologia (Pacific Geology), v. 16, p. 83–88.
Smith, H. A., and Barreiro, B., 1990, Monazite U-Pb dating of staurolite grade metamorphism in pelitic schists: Contributions to Mineralogy and Petrology, v. 105, p. 602–615.
Smith, H. A., and Giletti, B. J., 1997, Lead diffusion in monazite: Geochimica et Cosmochimica Acta, v. 61, p. 1047–1055.
Solov'ev, A. V., Garver, J. I., and Shapiro, M. N., 2001, Fission-Track Dating of Detrital Zircons from Sandstone of the Lesnaya Group, Northern Kamchatka: Stratigraphy and Geological Correlations, v. 9, p. 293–303.
Solov'ev, A. V., Shapiro, M. N., and Garver, J. I., 2002, Lesnaya Nappe, northern Kamchatka: Geotectonics, v. 36, p. 469–482.
Solov'ev, A. V., Shapiro, M. N., Garver, J. E., and Lander, A. V., 2004a, Formation of the east Kamchatkan accretionary prism according to fission-track dating of zircons from terrigene rocks: Geologiya i Geofizika, v. 45, p. 1292–1302.

——— 2004b, Formation of the east Kamchatkan accretionary prism based on fission-track dating of detrital zircons from terrigene rocks: Russian Geology and Geophysics, v. 45, p. 1237–1247.
Solov'ev, A. V., Palechek, T. N., Shapiro, M. N., Johnston, S. A., Garver, J. I., and Ol'shanetskii, D. M., 2007, New data on the Baraba Formation age (the Sredinnyi Range of Kamchatka): Stratigraphy and Geological Correlation, v. 15, p. 112–119.
Soloviev, A. V., and Palechek, T. N., 2004, New data about age of the Andrianovka Unit (Sredinny Range, Kamchatka): structure of the metamorphic complex at convergent setting, Evolution of the tectonic processes in Earth history: Moscow, GEOS, p. 86–89.
Soloviev, A. V., Brandon, M. T., Garver, J. I., and Shapiro, M. N., 2001, Kinematics of the Vatyn-Lesnaya thrust fault (Southern Koryakia): Geotectonics, v. 35, p. 471–489.
Soloviev, A. V., Shapiro, M. N., Garver, J. I., Shcherbinina, E. A., and Kravchenko-Berezhnoy, I. R., 2002, New age data from the Lesnaya Group: a key to understanding the timing of arc-continent collision, Kamchatka, Russia: The Island Arc, v. 11, p. 79–90.
Soloviev, A. V., Hourigan, J. K., Brandon, M. T., Garver, J. I., and Grigorenko, E. S., 2004, The Age of the Baraba Formation Inferred from the U/Pb (SHRIMP) Dating (Sredinnyi Range, Kamchatka): Geological Consequences: Stratigraphy and Geological Correlations, v. 12, p. 418–424.
Stacey, J. S., and Kramers, J. D., 1975, Approximation of terrestrial lead isotope evolution by a two-stage model: Earth and Planetary Science Letters, v. 26, p. 207–221, doi:10.1016/0012-821X(75)90088-6.
Tagami, T., and O'Sullivan, P. B., 2005, Fundamentals of fission-track thermochronology: Reviews in Mineralogy and Geochemistry, v. 58, p. 19–47, doi:10.2138/rmg.2005.58.2.
Tararin, I. A., 2008, Granulites of the Kolpakovskaya Series in the Sredinny range, Kamchatka: A Myth or Reality?: Petrology, v. 16, p. 193–209.
Tararin, I. A., Chubarov, V. M., Ignat'yev, E. K., and Moskaleva, S. V., 2007, The geological position, mineralogy, and platinoid mineralization of copper-nickel occurrences of the Kvinum ore field, Sredinnyy Ridge of Kamchatka: Pacific Geology, v. 26, p. 94–110.
Teyssier, C., and Whitney, D. L., 2002, Gneiss domes and orogeny: Geology, v. 30, p. 1139–1142, doi:10.1130/0091-7613(2002)030⟨1139:GDAO⟩2.0.CO;2.
Tilman, S. M., and Bogdanov, N. A., 1992, Tectonic Map of Northeast Asia: Moscow, Institute of the Lithosphere, RAS and Circum-Pacific Council for Energy and Mineral Resources.
Vanderhaeghe, O., Medvedev, S., Fullsack, P., Beaumont, C., and Jamieson, R. A., 2003a, Evolution of orogenic wedges and continental plateaux: insights from crustal thermal-mechanical models overlying subducting mantle lithosphere: Geophysical Journal International, v. 153, p. 27–51, doi:10.1046/j.1365-246X.2003.01861.x
Vanderhaeghe, O., Teyssier, C., MacDougall, I., and Dunlap, W. J., 2003b, Cooling and exhumation of the Shuswap Metamorphic Core Complex constrained by $^{40}Ar/^{39}Ar$ thermochronology: GSA Bulletin, v. 115, p. 200–216, doi:10.1130/0016-7606(2003)115⟨0200:CAEOTS⟩2.0.CO;2.
Vavra, G., Schmid, R., and Gebauer, D., 1999, Internal morphology, habit and U-Th-Pb microanalysis of amphibolite-to-granulite facies zircons: geochronology of the Ivrea Zone (Southern Alps): Contributions to Mineralogy and Petrology, v. 134, p. 380–404, doi:10.1007/s004100050492.
Vinogradov, V. I., and Grigor'yev, V. S., 1994, Rb-Sr ages of middle metamorphic block on Kamchatka: Transactions (Doklady) of the Russian Academy of Sciences, Earth Science Section, v. 339, p. 645–649.
——— 1996, Rb-Sr ages of rocks in the Median Ridge of Kamchatka: Transactions (Doklady) of the Russian Academy of Sciences, Earth Science Section, v. 343A, p. 80–86.
Vinogradov, V. I., Grigor'yev, V. S., and Leytes, A. M., 1988, Vozrast metamorfizma porod Sredinnogo khrebta Kamchatki: Izvestiya Akademii Nauk SSSR, Seriya Geologicheskaya, v. 1988, p. 30–38.
Vinogradov, V. I., Grigor'yev, V. S., and Kastrykina, V. M., 1991, Vosrast metamorficheskikh porod fundamenta Kamchatki: Sovetskaya Geologiya, v. 1991, p. 58–65.
Watson, B. F., and Fujita, K., 1985, Tectonic evolution of Kamchatka and the Sea of Okhotsk implications for the Pacific Basin, *in* Howell, D. G., editor, Tectonostratigraphic terranes of the Circum-Pacific region: Houtson, Texas, Circum-Pacific Council for Energy and Mineral Resources, p. 333–348.
Watson, E. B., Cherniak, D. J., Hanchar, J. M., Harrison, T. M., and Wark, D. A., 1997, The incorporation of Pb into zircon: Chemical Geology, v. 141, p. 19–31, doi:10.1016/S0009-2541(97)00054-5.
Wendt, I., and Carl, C., 1991, The statistical distribution of the mean squared weighted deviation: Chemical Geology, v. 86, p. 275–285.
Worrall, D. M., 1991, Tectonic history of the Bering Sea and the evolution of Tertiary strike-slip basins of the Bering shelf: Geological Society of America, Special Paper, v. 257, p. 120.
Zinkevich, V. P., Rikhter, A. V., and Fugzan, M. M., 1993, $^{40}Ar/^{39}Ar$ dating of East Kamchatka metamorphic rocks: Transactions, v. 335, p. 78–82.
Zinkevich, V. P., Kolodyazhny, S. Y., Bragina, L. G., Konstantinovskaya, Y. A., and Fedorov, P. I., 1994, Tectonics of the eastern edge of Kamchatka's Sredinny metamorphic massif: Geotectonics, v. 28, p. 75–90.
Zinkevich, V. P., Rikhter, A. V., and Tsukanov, N. V., 1998, Accretion tectonics and geodynamics of Kamchatka-Sakhalin region: Virtual Geology, p. http://geo.tv-sign.ru/virtugeo/articles/tsukanov/articl.htm.
Zonenshain, L. P., Kuzmin, M. I., Natapov, L. M., and Page, B. M., 1990, Geology of the USSR; a plate-tectonic synthesis: Washington D.C., American Geophysical Series, v. 21, 242 p.